

Wave Tank Studies on Dispersant Effectiveness as a Function of Energy Dissipation Rate and Particle Size Distribution

**A Final Report Submitted to
The Coastal Response Research Center**

Submitted by

K. Lee and Z. Li¹, A.D. Venosa², M. C. Boufadel³ and S.M. Miles⁴

¹ Bedford Institute of Oceanography
Centre for Offshore Oil and Gas Environmental Research
1 Challenger Drive, Dartmouth, Nova Scotia, B2Y 4A2

² National Risk Management Research Laboratory
US Environmental Protection Agency
26 W. Martin Luther King Drive, Cincinnati, OH 45268

³ Department of Civil and Environmental Engineering
Temple University
1947 North 12th Street, Philadelphia, PA 19122

⁴ 1261 Energy, Coast and Environment Building
Louisiana State University
Baton Rouge, LA 70803

Project Period: January, 2006 – January, 2009

Report Date: April 30, 2009



This project was funded by a grant from NOAA/UNH Coastal Response Research Center.
NOAA Grant Number: NA04NOS4190063. UNH Agreement No.: 06-085



Abstract

The use of chemical dispersants can be an effective means to combat oil spills at sea. There has been renewed interest in the use of chemical dispersants due to escalated oil spill incidents, logistical constraints of traditional spill response options, and the development of new generation, low-toxicity, high efficiency dispersant formulations for potential use on oils covering a greater viscosity range. For the assessment of chemical dispersant effectiveness under realistic sea states, test protocols are required to produce hydrodynamic conditions close to the mixing, transport and dilution effects found in the natural environment. To meet this requirement, a wave tank has been designed and constructed at the Bedford Institute of Oceanography (BIO) to evaluate chemical dispersant effectiveness under different wave conditions with energy levels ranging from regular non-breaking waves to plunging breakers. The hydrodynamics of these wave conditions were characterized using an autocorrelation function method applied to *in-situ* velocity measurements. Quantification of oil dispersant effectiveness was based on observed changes in dispersed oil concentrations and oil-droplet size distribution using a laser *in-situ* scattering and transmissometry particle size analyzer.

Evaluation of chemical dispersant effectiveness in a batch mode established quantitative relationships between dispersant effectiveness and energy dissipation rate under a variety of simulated wave conditions. The results indicated that 53% to 90% of the test crude oils have been dispersed in the presence of chemical dispersants and only 10% to 20% were dispersed under control conditions in the absence of chemical dispersant. The characterization of the *in-situ* dispersed oil droplet size distributions indicated that the physical dispersion generated mono-modal lognormal oil droplet size distributions of larger median diameters, whereas chemical dispersion produced bi- or tri-modal lognormal oil droplet size distributions of smaller median diameters over a wider range. The wave tank in flow-through mode simulating wave- and current-driven hydrodynamic conditions revealed that nearly 8 % to 19 % of the test crude oils were dispersed and diluted under regular wave and breaking wave conditions, respectively, in the absence of dispersants. In the presence of dispersants, about 21% to 36% of the crude oils were dispersed and diluted under regular waves, and 42% to 62% under breaking waves. Consistently, physical dispersion under regular waves produced large oil droplets, whereas chemical dispersion under breaking waves created small droplets.

These data on the effectiveness of dispersants as a function of sea state are significant contributions to the development of improved predictive models on dispersant effectiveness and better operational guidelines for dispersant use. Results of our experiential studies using the wave tank system have advanced our mechanistic understanding of dispersant effectiveness under ambient field conditions. The research has shown that use of dispersants in deep water environments under moderately energetic wave conditions is a promising countermeasure technology for driving floating oil into the water column. Chemical dispersant Corexit 9500 is effective in all low, moderate and high energy test conditions, whereas SPC 1000 can also be very useful in moderate to higher energy conditions. Effective dispersion of oil to achieve small droplet formation is dependent on wave energy and the presence of a chemical dispersant. If either of these two factors is missing, dispersion can only take place in very high energy sea states. Use of chemical dispersants drastically reduces the time required for thorough dispersion

of oil into small oil droplets in the water column to take place in comparison to natural dispersion. When the window of opportunity for oil spill response is narrow (i.e. rapid remediation is critical due to proximity to environmentally sensitive areas), a quick and effective response such as what can be achieved using dispersants may be deemed necessary even under high energy conditions because of their ability to through accelerate the process and efficacy of oil dispersion into the water column and to facilitate oil biodegradation.

Keywords: Wave tank, energy dissipation rate, chemical dispersant effectiveness, particle size distribution, regular waves, breaking waves, currents.

Acknowledgments

This research was funded by the NOAA/UNH Coastal Response Research Center (NOAA Grant Number NA04NOS4190063, UNH Agreement Number 06-085). Additional funding resources are from the Panel of Energy Research and Development (PERD), U.S. EPA (contract No. 68-C-00-159) and Fisheries and Oceans Canada (A-Base). Essential technical and logistical support was provided by Matt Arsenault, Don Belliveau, Jay Bugden, Susan Cobanli, Matt Coady, Paul Kepkay, Jennifer Mason, Xiaowei Ma, John Niven, Peter Thamer and William Yeung. The findings, opinions and recommendations expressed in this report are those of the authors and do not necessarily reflect those of the sponsoring agencies or the University of New Hampshire.

Table of Contents

1.0 Introduction.....	1
2.0 Objectives	3
3.0 Methods.....	4
3.1 Wave generation and hydrodynamic characterization.....	4
3.2. Experimental procedures for oil dispersion in the batch mode.....	9
3.3. Experimental procedures for oil dispersion in the flow-through mode	12
3.4. In-Situ Multiple Simultaneous Scattering and Fluorescence Sensor	13
4.0 Results.....	14
4.1. Wave generation and hydrodynamic characterization.....	14
4.2. Chemical Dispersant effectiveness testing in batch system.....	17
4.2.1 Effects of dispersant and wave conditions on oil distribution in the wave tank...	17
4.2.2 Dispersant effectiveness as a function of energy dissipation rate.....	23
4.2.3 Physically and chemically dispersed oil droplet size distributions.....	29
4.2.4 Significant factors determining the average dispersed oil droplet sizes	33
4.3. Chemical dispersant effectiveness testing in the flow-through wave tank.....	38
4.3.1 Effects of dispersant and wave conditions on oil dispersion effectiveness	38
4.3.2 Effects of dispersant and wave conditions on droplet size distribution.....	46
4.4. In-Situ multiple simultaneous scattering and fluorescence sensor	49
5.0 Discussion and Importance to Oil Spill Response/Restoration	51
6.0 Technology Transfer and Communications.....	55
7.0 Achievement and Dissemination	58
8.0 Technical Training.....	61
References.....	62
Appendices.....	A1

List of Figures and Tables

Figure 1: (a) Photograph of wave tank; (b) Wave absorber position; and (c) ADV position.....	8
Figure 2: Schematic representation (all dimensions in cm, not to scale) of the wave tank.....	11
Figure 3: Average energy dissipation rates for regular and breaking waves. Note the effect of the breaker relative to the regular waves deep in the water column.....	16
Figure 4a: Dispersed MESA oil concentration (mg/L) as a function of time and space under regular non-breaking waves with no dispersant.....	18
Figure 4b: Dispersed MESA oil concentration (mg/L) as a function of time and space under regular non-breaking waves with Corexit 9500.....	18
Figure 4c: Dispersed MESA oil concentration (mg/L) as a function of time and space under regular non-breaking waves with SPC 1000.....	19
Figure 5a: Dispersed MESA oil concentration (mg/L) as a function of time and space under spilling breaking waves with no dispersant.....	20
Figure 5b: Dispersed MESA oil concentration (mg/L) as a function of time and space under spilling breaking waves with Corexit 9500.....	20
Figure 5c: Dispersed MESA oil concentration (mg/L) as a function of time and space under spilling breaking waves with SPC 1000.....	21
Figure 6a: Dispersed MESA oil concentration (mg/L) as a function of time and space under plunging breaking waves with no dispersant.....	22
Figure 6b: Dispersed MESA oil concentration (mg/L) as a function of time and space under plunging breaking waves with Corexit 9500.....	22
Figure 6c: Dispersed MESA oil concentration (mg/L) as a function of time and space under plunging breaking waves with SPC 1000.....	23
Table 3: Average water column dispersed oil concentrations (mg/l) as a function of time. Data reported as the average \pm one standard deviation of independent triplicate runs.....	24
Figure 7: DE on MESA crude oil as a function of energy dissipation rate at: (A) 5 min, (B) 30 min, (C) 60 min, and (D) 120 min. Data shown are mean and one standard deviation of independent triplicate runs. Lines are best-fit regression of Equation 5.....	26
Figure 8: DE on ANS crude oil as a function of energy dissipation rate at: (A) 5 min, (B) 30 min, (C) 60 min, and (D) 120 min. Data shown are mean and one standard deviation of independent triplicate runs. Lines are best-fit regression of Equation 5.....	27
Figure 9: Volumetric (left) and cumulative (right) MESA oil droplet size distributions dispersed by water (A&B), Corexit 9500 (C&D), and SPC 1000 (E&F) under regular wave conditions.....	30
Figure 10: Volumetric (left) and cumulative (right) MESA oil droplet size distributions dispersed by water (A&B), Corexit 9500 (C&D), and SPC 1000 (E&F) under spilling breaking wave conditions.....	31
Figure 11: Volumetric (left) and cumulative (right) MESA oil droplet size distributions dispersed by water (A&B), Corexit 9500 (C&D), and SPC 1000 (E&F) under plunging breaking wave conditions.....	32
Figure 12: Dispersed MESA oil droplet size (volume mean diameter) as a function of time under: (A) regular non-breaking, (B) spilling breaking, and (C) plunging breaking wave conditions.....	35

Figure 13: Dispersed ANS oil droplet size (volume mean diameter) as a function of time under: (A) regular non-breaking, (B) spilling breaking, and (C) plunging breaking wave conditions.....	36
Figure 14: Dispersed MESA oil concentration as a function of time in the middle of the tank 10m downstream under: (A) regular wave, and (B) breaking wave conditions	39
Figure 15: Dispersed ANS oil concentration as a function of time in the middle of the tank 10m downstream under: (A) regular wave, and (B) breaking wave conditions.....	40
Figure 16: Equivalent dispersed oil concentrations at the surface of the wave tank at four different horizontal locations for the two tested crude oils: (A) 2m upstream; (B) 2 m; (C) 6 m; and (D) 10 m downstream. Note the different Y-axis scale for (D).....	42
Figure 17: Equivalent dispersed oil concentrations in the middle of the wave tank at four different horizontal locations for the two tested crude oils: (A) 2m upstream; (B) 2 m downstream; (C) 6 m downstream; and (D) 10 m downstream.....	43
Figure 18: Equivalent dispersed oil concentrations at the bottom of the wave tank at four different horizontal locations for the two tested crude oils: (A) 2m upstream; (B) 2 m downstream; (C) 6 m downstream; and (D) 10 m downstream.....	44
Figure 19: Dispersant effectiveness as a function wave conditions on: (A) MESA; (B) ANS. Data shown are average with one standard deviation of three independent replicate runs. .	45
Figure 20: Effect of dispersant type [(A) water; (B) Corexit 9500; and (C) SPC 1000] and wave conditions [regular (open circles) and breaking (solid dots)] on average dispersed MESA oil droplet size.....	48
Figure 21: Effect of dispersant type [(A) water; (B) Corexit 9500; and (C) SPC 1000] and wave conditions [regular (open circles) and breaking (solid dots)] on average dispersed ANS oil droplet size.....	49
Figure 22: Wet Labs Environmental Characterization Optics (ECO) triplet sensor.	50
Table 1: Dispersant effectiveness testing in the batch system.....	10
Table 2: Dispersant Effectiveness Testing in the Flow-through System.....	12
Table 4: Four-way factorial ANOVA of the main factor and multi-factor interaction effects on the dispersant effectiveness. Significant factors are flagged (*).....	28
Table 5: Tukey’s paired comparison of the different effects between treatment levels on DE (%) in the water column. Significant differences are flagged by * based on 95% simultaneous confidence intervals for specified linear combinations.	29
Table 6: Droplet size distribution statistics.....	33
Table 7: Factorial analysis of variance of the effects on the average water column dispersed oil droplet sizes. Statistically significant factors are flagged with *.....	37
Table 8: Tukey’s paired comparison of the different effects between treatment levels on the average dispersed oil droplet size in the water column. Significant differences are flagged by * based on 95% simultaneous confidence intervals for specified linear combinations...	38
Table 9: Student and postdoctoral trainee of this project	61

List of Appendices

Appendix A1: Velocity series for across tank component “v” of low frequency waves generated with a 7 cm stroke at depths of (a) 10.7 cm, (b) 23.3 cm, and (c) 33.3 cm. Also shown by the dashed line is the water level for each series.	1
Appendix A2: Velocity series for across tank component “v” of high frequency waves generated with a 7 cm stroke at depths of (a) 10.7 cm, (b) 23.3 cm, and (c) 33.3 cm. Also shown by the dashed line is the water level for each series.	2
Appendix A3: Velocity series for across tank component “v” of low frequency waves generated with a 12 cm stroke at depths of (a) 13.3 cm, (b) 27.3 cm, and (c) 39.3 cm. Also shown by the dashed line is the water level for each series.	3
Appendix A4: Velocity series for across tank component “v” of high frequency waves generated with a 12 cm stroke at depths of (a) 13.3 cm, (b) 27.3 cm, and (c) 39.3 cm. Also shown by the dashed line is the water level for each series.	4
Appendix A6: Three component velocity spectra for the plunging breaking waves at a depth of 13.3 cm. The dominant frequencies of the system ($= 1/\Delta t$) are displayed. The Nyquist ($f/2$) frequency for the ADV sensor is $(200 \text{ Hz} / 2) = 100 \text{ Hz}$	6
Appendix A7: Series for filtered across tank velocity “v” for (a) LF 7 cm stroke, (b) HF 7 cm stroke, (c) LF 12 cm stroke and (d) HF 12 cm stroke. Also shown (dashed) is the original velocity. Series are centered on their respective zeros.	7
Appendix A8: Series for filtered across tank velocity “v” for the plunging breaker. Also shown (dashed) is the original velocity. Series are centered around their respective zeros.	8
Appendix A9: Energy dissipation rates calculated over the regular wave low frequency (LF) 7 cm stroke data set for depth of (a) 10.7 cm, (b) 23.3 cm and (c) 33.3 cm.	9
Appendix A10: Energy dissipation rates calculated over the regular wave low frequency (LF) 12 cm stroke data set for depths of (a) 13.3 cm, (b) 27.3 cm, and (c) 39.3 cm.	10
Appendix A11: Energy dissipation rates calculated over the regular wave high frequency (HF) 7 cm stroke data set for depth of (a) 10.7 cm, (b) 23.3 cm and (c) 33.3 cm.	11
Appendix A12: Energy dissipation rates calculated over the regular wave high frequency (HF) 12 cm stroke data set for depths of (a) 13.3 cm, (b) 27.3 cm, and (c) 39.3 cm.	12
Appendix A13: Energy dissipation rates calculated over the plunging breaker, 12 cm stroke data set for depth of (a) 6 cm, (b) 21.21 cm and (c) 41.49 cm.	13
Appendix A14: Average temperature-response fluorometer results of ANS crude oil.	14
Appendix A15: Average temperature-response fluorometer results of MESA crude oil.	16
Appendix A16: Average background-subtracted turbidity-response fluorometer results of ANS Crude Oil.	18
Appendix A17: Average background-subtracted turbidity-response fluorometer results of MESA Crude Oil.	20

1.0 Introduction

Natural physical dispersion of oil spills through wave action results in the formation of oil-in-water emulsions of μm -scale oil droplets that are eventually diluted to concentrations below toxic threshold limits (Chapman et al. 2007; Kirby and Law 2008; Lee 2002; Li and Garrett 1998; Shaw 2003; Tkalich and Chan 2002). The importance of wave action for physical and chemical dispersion of oil has been recognized (Delvigne and Sweeney 1988; Li and Garrett 1998; Shaw 2003; Tkalich and Chan 2002). Breaking waves, in particular, play a crucial role in the dispersion of an oil slick by generating velocity shear to break up and transport oil in their turbulent flows (Li and Garrett 1998; Shaw 2003; Tkalich and Chan 2002).

The application of chemical dispersants accelerates dispersion of oil by reducing the oil-water interfacial tension, which facilitates droplet formation and results in reduced droplet collision rates as the oil is diluted in the water column (Chapman et al. 2007; Lessard and Demarco 2000; NRC 2005). In addition, chemical dispersants promote the formation of smaller droplets than those generated solely by physical dispersion, and can also change the surface thermodynamic properties of the oil to increase the stability of these small oil droplets in seawater. With the development of new formulations that are less toxic and more effective for the treatment of viscous oils, the application of chemical dispersants has recently gained popularity as one of the primary oil spill countermeasures for reducing the overall adverse impact of marine oil spills on the environment (NRC 1989; NRC 2005). In addition to operational convenience, the application of dispersants to oil slicks on the sea surface minimizes the harmful effects of floating oil on aquatic wildlife such as birds and marine mammals that frequent the water surface, and potentially mitigates the risk of oil slicks contaminating coastal and shoreline environments (NRC 2005).

Oil dispersion effectiveness depends on hydrodynamic conditions, the chemical properties of both dispersant and oil, and on various environmental factors such as water temperature and salinity (Fingas 2000; NRC 1989; NRC 2005). Oil dispersion effectiveness is determined by several related processes, including initial breakup of the oil slick into small oil droplets, transport and dilution of oil droplets in the water column, and coalescence and resurfacing of oil droplets. The formation of droplets occurs during oil breakup under the influence of mixing energy as the turbulent structure of breaking waves stretch and split the oil by velocity shear. The transport and dilution of oil droplets is then regulated by turbulent diffusion and wave propagation. Coalescence and resurfacing of oil is more likely to occur when the dispersed phase volumetric fraction (concentration) is high. Droplet coalescence kinetics are dependent on collision frequency (proportional to the shear and differential surfacing/settling velocity) and collision efficiency, which is determined by droplet surface thermodynamic properties. The resurfacing of oil is driven by the buoyancy force that is proportional to surface area or the square of droplet size.

Tests of chemical dispersant effectiveness are typically conducted on different scales, ranging from laboratory jar tests to meso-scale wave tank testing and large-scale field trials (NRC 2005). Bench-scale dispersant effectiveness tests (ASTM 2002; EPA 1996; Fingas et al. 1987) in the laboratory have been used for comparison of dispersant product effectiveness (Sorial et al. 2004a; Sorial et al. 2004b; Venosa et al. 2002) and for testing the effects of temperature, salinity

and other environmental factors (Chandrasekar et al. 2005; Chandrasekar et al. 2006; Srinivasan et al. 2007). However, laboratory tests are inherently limited in simulating real field operational performance due to space constraints that are critical for transport and dilution efficiency. In the context of evaluating actual operations at sea, the utility of these tests is limited due primarily to failure to account for the critical dispersion processes in the water column (NRC, 2005). During the physical and chemical dispersion of oil spills, the initial break-up and submergence of a surface oil slick (as well as the secondary break-up of the oil into smaller droplets) depends on the turbulent structures, which also plays an important role in the vertical transport of oil droplets in the water column. To overcome the restrictions inherent in bench-scale tests, larger facilities are required to enable a more comprehensive evaluation of chemical dispersant effectiveness under a more realistic setting. Conversely, sea trials which are expensive and logistically challenging often lead to results that are inconclusive due to limitations in the level of replication and control of experimental variables. In response to an identified need for testing the performance of chemical dispersants under more realistic oceanographic and environmental conditions including wave-induced mixing energies (NRC 2005), a wave tank facility has been constructed at the Bedford Institute of Oceanography (BIO) in Dartmouth, Nova Scotia for reproducible, quantitative evaluation of chemical dispersant effectiveness under a variety of wave conditions.

To account for the important interplay between wave-propagation and wave- induced turbulence, we used the wave tank at BIO to allow for evaluation of chemical dispersant effectiveness under a variety of simulated wave conditions. This wave tank is capable of generating recurrent breaking waves at the same locations by using the frequency sweep technique (Funke and Mansard 1979), wherein a low frequency, fast-moving wave is superimposed onto a high frequency, slow-moving wave, causing the wave to increase in height until it breaks. In characterizing the hydrodynamics of different wave conditions, since the friction associated with velocity shear causes the dissipation of kinetic energy of the fluid, resulting in a temporal and spatial variation of the energy dissipation rate per unit mass of water (ϵ , in $\text{W}\cdot\text{kg}^{-1}$ water), the intensity of microscale turbulence of regular non-breaking and breaking waves was quantified by computing their energy dissipation rate using an autocorrelation function approach (Kaku et al. 2006a; Kresta and Wood 1993). The operational hypothesis is that ϵ plays a major role in the effectiveness of a dispersant, and hence it may serve as an important scalable parameter to characterize chemical dispersant effectiveness under different wave energy conditions in the field.

To understand the intrinsic mechanisms of dispersant effectiveness obtained in a testing system, it is important to measure the dispersed oil droplet size distributions and compare the data with those observed at sea (Lunel 1995). *In-situ* dispersed oil droplet size distributions are controlled by a variety of hydrodynamic and environmental variables. For example, the intensity of the turbulent mixing energy dictates the breakup of large oil droplets into smaller droplets and the depth of submergence of the droplets. The droplet size distributions are also affected by the collision frequency, which has been considered a function of system hydrodynamics, and collision efficiency, which is generally believed to represent the chemistry involved in the coalescence reactions. To date, the droplet-size distributions of physically and chemically dispersed oil have rarely been compared directly under hydrodynamic conditions approaching those existing in the field, and even fewer droplet-size distribution data have been reported in

wave tank testing of dispersant effectiveness (NRC 2005). The latter report emphasized that existing databases must be expanded to determine whether and how factors such as energy dissipation rate, oil type, dispersant characteristics and dispersant use influence the droplet size distribution and formation kinetics. To address this need, the BIO wave tank was used to characterize and compare *in-situ* droplet size distributions of physically and chemically dispersed oil under a variety of non-breaking and breaking wave conditions in the experimental wave tank. The data generated in this study will be useful in optimizing operational guidelines, modeling transport and fate, and potentially evaluating biological effects of chemically dispersed oil.

This wave tank was originally developed to evaluate dispersant effectiveness under different reproducible wave energy conditions with energy dissipation rates similar to those that are encountered in the field. The main goal was to relate quantitatively dispersant effectiveness with energy dissipation rate for varying dispersant formulae, oil types and the weathering status of oil. The wave tank experiments conducted in a batch mode configuration demonstrated the significance of wave conditions to chemical dispersant effectiveness (Li et al. 2008a; Li et al. 2008b; Venosa et al. 2008). However, hydrodynamic characterization of the wave tank operated in the batch mode also revealed the presence of back-flowing underwater currents counter to the direction of the progressive waves generated by the wave maker. This recirculation mechanism is caused by the surface Stoke's drift of the progressive waves (Wickley-Olsen et al. 2008) and is a necessary condition applicable to the conservation of water mass. To counteract the backward underwater current flow and to allow for simulation of natural exposure levels that result from dilution of dispersed oil in an open environment influenced by waves, tides and currents, the wave tank was modified for operation in flow-through mode to simulate the influence of ocean currents. We studied dispersant effectiveness subjected to the combined actions of waves and currents. Such an experimental system allows for dilution caused by the undersea current carrying away the dispersed oil plume.

2.0 Objectives

This research program is a multi-disciplinary collaboration among scientists and engineers from government and academic institutions, whose collective knowledge contributed to produce a highly effective operational response activity and an improved understanding of the mechanism of dispersant action and their potential environmental effects. The objectives of this project are:

- 1) To quantify the natural rates of dispersion for various crude oils over a range of sea states (wave energies)
- 2) To quantify the effectiveness of representative oil dispersant formulations on different types of reference crude oils
- 3) To define the range of wave energy conditions over which dispersant formulations are most effective
- 4) To evaluate emerging methodologies for monitoring the concentration and size of dispersed oil droplets in seawater

Operational guidelines formulated with the results of our research will be used locally, regionally, nationally and internationally to train responders and decision-makers on how, why

and when to apply dispersants to a spill to minimize harm to the environment. The outcome of our research is sound and robust because it is based on scientific facts, and it will stimulate exchanges of ideas among scientists to advance the use of this promising technology as a restoration and response activity. Through the planned outreach of project deliverables to on-scene coordinators and oil spill response organizations, CRRC will be recognized as a source of sound engineering practice in marine spill response. Students and post-docs have been used extensively as part of the laboratory field crew. This provided an excellent learning opportunity for them in their pursuit of higher education and training experience.

3.0 Methods

3.1 Wave generation and hydrodynamic characterization

Important parameters to describing a wave are its length and height, and the water depth over which it propagates (Dean and Dalrymple 1984). The length, L , or wavelength, is the distance from crest to crest (or trough to trough). The height is the vertical distance from trough to crest. The depth is the distance from half the wave height to the bottom of the ocean. Also important are the Still Water Level (SWL) and the Mean Water Level (MWL). The former is the depth of the water in the absence of waves, while the latter is an average water level over time. Shifting motion of the body of water could cause a change in the MWL, which would not be apparent in the SWL. According to Dean, et al, (1984) for the relative depth $h/L > 0.5$, the waves are considered deep water waves. Essentially, the waves do not “feel” the ocean floor. But this limit should be viewed qualitatively, because even for h/L as low as 0.3, one could still treat the wave as a deep-water wave (Melville et al. 2002).

For deep water (i.e., $h/L > 0.5$) the first order theory indicates that the wavelength, L , is related to the wave period, T , by the equation

$$L = \frac{g}{2\pi} T^2 \quad (1)$$

where g is the gravity. The celerity of the wave, or wave speed, is

$$C = \frac{L}{T} = \frac{g}{2\pi} T \quad (2)$$

The above relation is through insertion of Eq. (1) in Eq. (2). Coastal engineering uses this relation as the “dispersion equation” (different from oil dispersion, the breakup of an oil slick into droplets). Take note that a wave with a larger period will travel faster than a wave with a smaller period. Dispersion of oil, i.e. the formation of small droplets from a slick, is not the same as the aforementioned concept.

Using the first order theory for deep water waves, the water profile $n(x,t)$ relative to the MWL is given by:

$$\eta(x, t) = \frac{H}{2} \cos(kx - \sigma t) \quad (3)$$

Where $n(x, t)$ is a function of position x and time t , H is the wave height (from crest to trough), k is the wave number defined as:

$$k = \frac{2\pi}{L} \quad (4)$$

And σ is the angular (or radian) frequency defined as:

$$\sigma = \frac{2\pi}{T} \quad (5)$$

The water velocity under a deep-water progressive wave to a second order approximation (Stoke's Theory) is given by:

$$u(x, z, t) = \frac{Hgk}{2\sigma} \cos(kx - \sigma t) + \frac{3H^2\sigma k}{16} e^{2kz} \cos 2(kx - \sigma t) \quad (6)$$

and

$$w(x, z, t) = \frac{Hgk}{2\sigma} \sin(kx - \sigma t) + \frac{3H^2\sigma k}{16} e^{2kz} \sin 2(kx - \sigma t) \quad (7)$$

Here we see that the water velocity decreases with depth. For a wave to break, the velocity of the water at the crest must be higher than the celerity. Traveling faster than the wave, the water mass at the crest will move faster than the wave and either “spill” or “plunge” ahead of the wave face.

Kinetic energy dissipates through laminar and turbulent shears in the water column. A relation between energy dissipation, ε and the absolute velocity gradient G (s^{-1}) at every location in the fluid (Camp and Stein 1943; Tennekes and Lumley 1999) is:

$$\varepsilon = \nu G^2 \quad (8)$$

Where ν is the kinematic viscosity of water (approximately $10^{-6} m^2/s$ for water at $20^\circ C$). The hydraulic regime in the tank is turbulent due to the relatively large dimensions of the tank. In addition, in fairly broad situations the velocity gradient due to turbulence (i.e., the temporal variation of velocity at one location) is much larger than that due to variation of the velocity over space (Kaku et al. 2002; Rao and Brodkey 1972; Wu and Patterson 1989). For these reasons, we assume in this work that all mixing-related quantities (energy dissipation rate and absolute velocity gradients) are due solely to turbulence.

In turbulent mixing, large eddies carry the kinetic energy obtained from the general motion of the fluid (Batchelor 1970; Hinze 1955). These eddies break into smaller eddies, which in turn break

into smaller eddies down to a scale known as the Kolmogorov scale where molecular viscosity effects become dominant (Kolmogorov 1949). The breaking waves in this study had a Kolmogorov scale,

$$\eta = \left(\frac{\nu^3}{\varepsilon} \right)^{\frac{1}{4}} \quad (9)$$

Kolmogorov scale is of approximately 100 microns near the surface.

Not all turbulent flows manifest churning and foaming. Thus, an apparently laminar flow could be in reality turbulent. A quantitative means to detect the presence of turbulence is through evaluation of the Fourier spectrum of the water velocity, which (the spectrum) represents the kinetic energy content at various scales. In turbulent flow, the spectrum has the following property (Kolmogorov 1949):

$$E \propto k^{-5/3} \quad (10)$$

where the symbol indicates proportionality. Thus, the spectrum has a power law behavior in function of the wave number. For a time series of measurements at a point, a turbulent flow has the following spectrum:

$$E \propto f^{-5/3} \quad (11)$$

where f represents the frequency of velocity fluctuations. Eq. 11 is valid in situations where Taylor's "frozen turbulence" hypothesis is applicable (Hinze 1955, p. 41; Monin and A.M.Yalgom 1971,1975, p.11). The hypothesis stipulates that turbulent eddies are advected without a change in their statistical properties, allowing inference of properties from a time series at a point. The small-scale structure of turbulence is independent of any orientation effects, and is thus locally isotropic. This cascade of energy can be detected through observance of the $-5/3$ slope in a spectrum.

In isotropic turbulence, the dissipation rate per unit mass is simplified to (Tennekes and Lumley 1972)

$$\varepsilon = 15\nu \overline{\left(\frac{\partial u_i}{\partial x_i} \right)^2} \quad (12)$$

where u_i ($i=x, y, z$) is the instantaneous velocity in any "i" direction. Considering the periodic motion of water due to waves, one may write:

$$u_i(s,t) = \left(\overline{U}_i(s) + \tilde{u}_i(s,t) \right) + u_i'(s,t); i = x, y, z \quad (13)$$

Where \overline{U}_i is the time-averaged (mean) velocity that depends solely on location (it generally decreases with depth), \tilde{u}_i is the oscillatory component due to the oscillatory motion of waves (it depends on both location in the tank and time), and u_i' is the component due to turbulence. A moving average of the time series can give the oscillatory component of u_i (essentially a smooth line that would exist even in the absence of turbulence).

There are many methods for evaluating the energy dissipation rate. These are discussed in Kaku et al. (2006b) and references therein. In this work, the autocorrelation function approach is used, and it provides the energy dissipation rate as follows (Kresta and Wood 1993; Wu and Patterson 1989):

$$\varepsilon = A \frac{(u_{rms}')^2}{\tau_{E_i}} \quad (14)$$

where u_{rms}' is the root mean square (RMS) value of the turbulent component of velocity, A is a constant of order unity (one in this work), and τ_{E_i} is the integral time scale obtained by:

$$\tau_{E_i} = \int_0^{\infty} R_{E_i} dt \quad (15)$$

Where R_{E_i} is the temporal autocorrelation function,

$$R_{E_i} = \frac{\overline{u_i'(t)u_i'(t+\tau)}}{(u_i')^2} \quad (16)$$

where τ is the time lag. Note that R_{E_i} is assumed the same in all direction, a direct consequence of the isotropic turbulence assumption. An upper limit of infinity is impractical in Eq. (15), and the point of first zero crossing (i.e., where the autocorrelation function reaches the value of zero) may be used (Wu et al. 1989).

The wave tank is 32 meters long, two meters high, 0.6 meter wide, and equipped with a flap-type wavemaker placed 1.5 m from the tank wall (Figure 1). The Acoustic Doppler Velocimeter (ADV) and wave gauge was placed 13.54 m from the wavemaker. Porous screens were placed opposite the wave maker to minimize reflection by dissipating wave energy upon passing of the waves through them.

Wave generation was obtained as a result of the rotation of an eccentric fly wheel. The flywheel was connected from one end to a motor and from the other to the flap via an actuator shaft. The flywheel was driven through a gear by a five horse-power (3.75 KW) motor. The motor runs at constant speed, thus producing a sinusoidal in time actuator motion of period T . The wavemaker generates waves of periods ranging from 0.2 to 2.5 seconds. Note that the flap-type wavemaker is more suitable to generate deep-water waves than the piston-type (Hughes 1990).

Figure 1a



Figure 1b

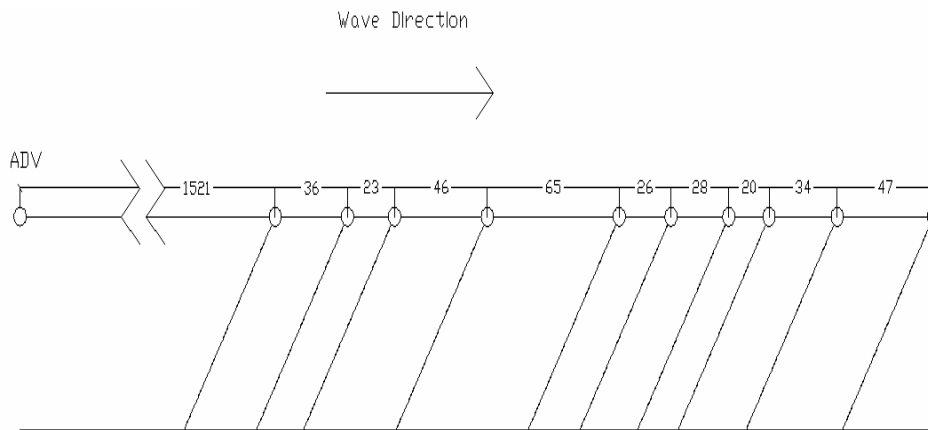
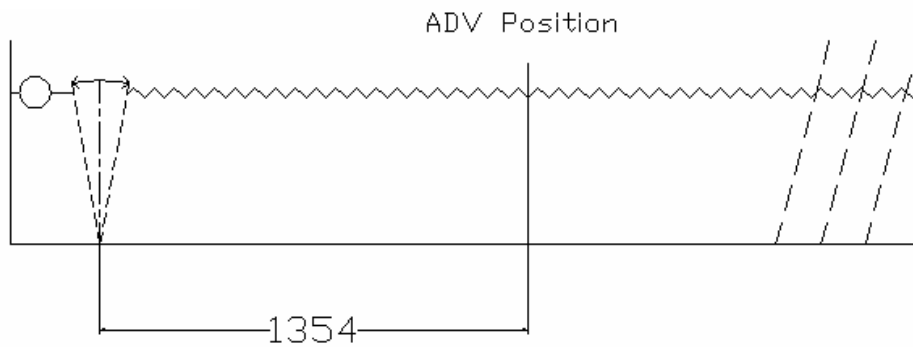


Figure 1c



Dimensions are in centimeters. Not to scale.

Figure 1: (a) Photograph of wave tank; (b) Wave absorber position; and (c) ADV position.

The water level was measured using a wave gauge with an accuracy of 1.0 mm. The wave gauge is based on capacitance measurement, which varies in response to the submerged portion of the rod. The output from the transmitter is voltage. The wave gauge was calibrated by raising and lowering the gauge to levels of 125 cm, 150 cm and 175 cm. At each of these levels a voltage reading was recorded. Hence, a three point calibration curve was obtained. Drift was noted in the reading at latter times. Moisture buildup on locations (out of water) of the sensor likely caused the drift. Complete drying of the sensor would remedy the problem. The readings were logged to Labview data collection software (www.labview.com), and the recorded voltage was converted to water level based on the calibration curve. The data were logged at a frequency of 50 Hz (i.e., one data point every 0.02 seconds).

An ADV (Nortek Inc.) was used to provide three-directional velocity measurements. The probe is comprised of two components, the signal conditioning module and the acoustic sensor. The acoustic sensor of the ADV consists of four rods circling a transmitter. The receivers are oriented such that they will intersect the control volume. This control volume is defined by the shape of the transmit beam (approximated as cylindrical, though actually conical) with ends given by the length of the receive window for the probe. This control volume is approximately 5 cm from the acoustic sensor (thus non-intrusive) with a diameter and length of 1.8 mm and 7 mm, respectively. This gives a control volume of approximately 0.126 cm^3 . The acoustic sensor is mounted to a stem that connects to the signal-conditioning module to be perpendicular to the major axis of the probe. The advantage of this arrangement is to allow velocity in the x-z plane to flow unobstructed. The ADV readings were output at 200 Hz. Thus, the measuring interval was 0.005 seconds. The probe of the ADV was placed centrally in the breaking zone (Figure 1). The ADV comes calibrated from the company.

3.2. Experimental procedures for oil dispersion in the batch mode

The chemical dispersant effectiveness was investigated for two dispersants (Corexit 9500, and SPC1000) plus water (as no-dispersant control) on two crude oils (Medium South American [MESA] and Alaska North Slope [ANS]) under three wave conditions (regular non-breaking wave, spilling breaking wave and plunging breaking wave) in the batch mode. MESA oil was weathered by evaporation (sparging with air for 130 h) to simulate the loss (approximately 14%) of volatile components at sea shortly after a spill. ANS oil was fresh and not weathered to test the dispersant effectiveness assuming an idea oil spill response scenario where dispersant application is available immediately available in the incident. The ANS oil was kindly provided by Dr. Jim Clark (Exxon Mobil Research and Engineering Co.), with Coding UN1267, PGI. The main fractions, namely saturates, aromatics, resins, and asphaltene, of the ANS oil were 32.0, 39.3, 24.4, and 4.3%, respectively, as characterized by using Iatroscan assay.

A three-factor mixed-level factorial experiment was designed to include 18 treatments with triplicate runs for each treatment, resulting in 54 runs for the entire design (Table 1). Treatments were applied in random order to minimize the impacts of confounding factors such as temperature, salinity and wind on the dispersant effectiveness of crude oil.

Table 1: Dispersant effectiveness testing in the batch system

Treatment	Dispersants	Oils	Waves
1	Water	MESA	Regular non-breaking wave
2	Corexit 9500		
3	SPC 1000		
4	Water	ANS	
5	Corexit 9500		
6	SPC 1000		
7	Water	MESA	Spilling Breaker
8	Corexit 9500		
9	SPC 1000		
10	Water	ANS	
11	Corexit 9500		
12	SPC 1000		
13	Water	MESA	Plunger Breaker
14	Corexit 9500		
15	SPC 1000		
16	Water	ANS	
17	Corexit 9500		
18	SPC 1000		

For each experiment, seawater was pumped directly from the Bedford Basin through a double layer sock-filter (Atlantic Purification Ltd, Dartmouth, NS, Canada) with a pore size of 25 and 5 μm for the coarse and fine filters, respectively. The background temperature, salinity and fluorescence intensity and particle size distribution were recorded before the experiment started. For each experiment, 300 ml of crude oil was gently poured onto the surface of the water within a 40cm (inner diameter) tubular ring (constructed of NSF-51 reinforced clear PVC) 10 m from the wave generation paddle. Immediately after oil addition, 12 ml of dispersant (water for the control) was sprayed conically on top of the oil through a pressurized nozzle (60 psi; 0.635mm i.d.) at a dispersant-to-oil ratio (DOR) of 1:25. The ring was then lifted immediately prior to contact with the first wave. The desired wave conditions were operated continually during the 2h experiment. Samples were collected by using a set of 100ml syringes connected with a stainless steel manifold from four horizontal locations (8, 12, 16, and 20 m downstream from the wave maker), three depths (5, 75, and 140 cm from the average water surface), and four time points (5, 30, 60, 120 min). Sampling locations are shown in Figure 2. These samples were subdivided for oil chemical analysis using dichloromethane (DCM) extraction followed by ultraviolet spectrophotometry (UVS) (Venosa et al. 2002) (Venosa et al., 2008) and ultraviolet fluorescence analysis (Kepkay et al. 2002) (Kepkay et al. 2008) of dispersed oil concentration. After each experiment, the oil-containing seawater was completely drained with gas pumps, treated by filtration through an oleophilic oil absorbing material in a filtration column, and disposed of to the basin. The inner surfaces of the wave tank, including walls and floor, wave absorbers and wave generation paddle were thoroughly cleaned by power wash. The LISST was carefully washed with cleaning solution to remove oil, and thoroughly rinsed with tap water. The detection and emission windows were cleaned using a special lens-cleaning reagent.

3.3. Experimental procedures for oil dispersion in the flow-through mode

The chemical dispersant effectiveness was also investigated for the same dispersants and oil types under regular non-breaking wave and plunging breaking wave conditions in the flow-through mode to simulate current-driven dilution effect. The wave parameters for the flow-through system were the same as the batch system, except a current flow at 60 gallons per min (GPM) was introduced to the system to simulate the transport of waves in the open ocean. A three-factor mixed-level factorial experiment was designed to include 12 treatments with triplicate runs for each treatment, resulting in 36 runs for the entire design (Table 2). Treatments were applied in random order to minimize the impacts of confounding factors such as temperature, salinity and wind on the dispersant effectiveness of crude oil.

Table 2: Dispersant Effectiveness Testing in the Flow-through System

Treatment	Dispersants	Oils	Waves
1	Water	MESA	Regular non-breaking wave
2	Corexit 9500		
3	SPC 1000		
4	Water	ANS	
5	Corexit 9500		
6	SPC 1000		
7	Water	MESA	Plunging breaking
8	Corexit 9500		
9	SPC 1000		
10	Water	ANS	
11	Corexit 9500		
12	SPC 1000		

The same protocols were used for each experiment as those in the batch-mode experiments with the addition of measurements for background temperature, salinity, fluorescence intensity and particle size distribution that were recorded from the time the flow-through system was turned on prior to the initiation of the oil experiments; the desired wave conditions were operated continually for 1 hour (versus 2 hours for batch-mode); samples were taken at five time points (2, 5, 15, 30, 60 min), and; ultraviolet fluorescence analysis was not conducted following UVS analysis.

Dispersed oil droplet size distribution was measured using a laser *in-situ* scattering and transmissiometer (LISST-100X, Type C, Sequoia Scientific, Seattle, WA). The data acquisition was conducted at real time operation mode throughout each experiment, with an average of 10 measurements for each sample being measured every 3 seconds. The *in-situ* dispersed oil droplet size distribution was measured at one depth (60 cm from the average water surface) on one horizontal location (16 m downstream from the wave-maker) continuously over the entire 1 h experimental period.

3.4. In-Situ Multiple Simultaneous Scattering and Fluorescence Sensor

Laboratory Calibration Phase: Alaska North Slope (ANS) crude oil was analyzed to determine the overall aromatic content for the laboratory calibration of the In-Situ Multiple Scattering and Fluorescence Sensor. The ANS oil was chosen for its relatively high dispersibility and its high aromatic (fluorescence) content. Oil extracts were analyzed for aromatic and alkylated-aromatic hydrocarbons, using modified EPA SW-846 method 8270 (US EPA), on a Hewlett-Packard 5890 gas chromatograph (GC) and 5971 mass spectrometer (MS) system. Data collected from the characterization analysis were used to build whole oil and individual component databases.

Response and Linearity Testing: A 100-L cylindrical tank was used during the laboratory dispersion testing to test the Response and Linearity of the instrument. The oil and dispersant were mixed using a variable-speed (20-200 rpm) Lightnin® Mixer with a stainless steel mixing impeller. Corexit 9500 was pre-mixed with the oil at a DOR of 1:25 for all experiments. Nominal oil concentrations of 10, 100, 1,000, and 10,000 ppb were tested during this experiment. The dynamic droplet size distribution and raw count data were measured from the light scattering and fluorescence sensors, respectively, for a period of five minutes. The test was performed three times over the nominal oil concentration range.

GC/MS Correlation Testing: The GC/MS correlation test was designed to relate fluorescence counts to the actual oil concentration (mg/L) within the test reactor and was performed concurrently with the concentration and linearity testing. During each test a 1-L sample was removed from the reactor and preserved in a glass sample bottle for analysis.

Turbidity Testing: The turbidity test (ASTM 2130) was performed to evaluate the multi-sensor's ability to accurately measure the concentration of dispersed oil within turbid seawater. This experiment was designed to evaluate the multi-sensor at surrogate turbidity concentrations of 100, 1,000, and 10,000 nephelometric turbidity units (NTU) and nominal oil concentrations of 100, 1,000, and 10,000 µg/L. This experiment can determine a realistic operating range and demonstrate the multi-sensor's capacity to accurately measure oil concentration within a turbid environment. The test was performed three times over the nominal oil concentration and turbidity ranges.

The field testing of the in-situ multiple simultaneous scattering and fluorescence sensor was conducted by deploying the instrument in the wave tank facility at BIO. Experiments were performed to evaluate the multi-sensor at nominal ANS oil concentrations of 10, 100, 1,000, and 10,000 µg/L at a DOR of 1:25. The dynamic droplet size distributions and raw count data were recorded from the light scattering and fluorescence sensors, respectively, for a period of five min. Temperature, salinity, turbidity, and COD were recorded during the individual tests. Triplicate 1-L samples were collected during the testing, preserved through acidification, and returned to the LSU laboratory for GC/MS analysis.

4.0 Results

4.1. Wave generation and hydrodynamic characterization

To generate regular waves in the tank, one needs simply to select the design wave period (or frequency) and set the motor to it for the intended duration. Due to the dissipative role of viscosity, the height of regular waves decreases as they propagate in the tank away from the wavemaker. Thus, to cause the wave height to increase and eventually break, one needs to “inject” momentum into the wave. This was done using the frequency sweep method discussed at length by Funke et al (1979). The method relies on the fact that waves propagate away from the wavemaker proportionally to their periods. Thus, if one generates a train of short-period (high frequency) waves followed by a train of long-period (low frequency) waves, the long-period waves would catch up to the short-period ones and inject momentum into them, especially at the crest of the long waves (Phillips 1977 p. 149).

Four settings of regular waves were investigated. They were for Low Frequency, LF, ($T \approx 2.1$ s and 2.0 s for 7cm and 12 cm strokes, respectively) and High Frequency, HF, ($T \approx 1.18$ s, for both strokes). The wavemaker ran for at least twenty minutes before the sampling began, which was approximately five minutes for the regular waves.

The plunging breaking waves were generated with a 12 cm stroke and periods $T \approx 2.0$ sec and $T \approx 1.18$ sec). Since the propagation speed of a wave in deep water is proportional to its period, the low frequency LF waves “catch up” to the high frequency HF waves resulting in breaking. Twenty minutes elapsed before the readings were made, which was for 30 minutes.

The dominant frequency of the waves was computed using spectral analysis of the time series of water level measurements. This was done for two reasons. First, an uncertainty exists in the set frequency on the dial because the gear box was not performing as accurately as expected. Second, it is possible that the motion of the flap was affected by the generated waves (splash from behind the flap and reflection). This unwanted effect would inadvertently alter the frequency that was set. These periods were then used in the frequency filtration discussed later.

Appendix A (1-4) shows the across-tank velocity, “ v ”, of the regular waves for high and low frequency, and both strokes. Generally, the velocity decreased with depth, although for the deepest depths (1-4c), the velocity appeared very spiky, with magnitudes similar to the mid-depth (1-4b). Wave heights for the 7 cm stroke waves were about 8 cm and 10 cm for low and high frequency, respectively. The wave heights for the 12 cm stroke waves were around 15 cm and 20 cm for low and high frequency, respectively. The breaker occurred at approximately 13.54 m downstream of the wavemaker, essentially at mid-distance in the tank minimizing therefore the effects of standing waves that occur near the wavemaker (Dean and Dalrymple 1984 p. 175), and the wave absorber.

Appendix A (5) shows the time series of the across tank component v for plunging breaking waves. The series shows the kinematics of the wave in a period of 10 sec surrounding the breaker. The breaker occurred at about $t = 2$ sec. The velocity increases immediately after the breaker (5a). The breaker causes an increase in velocity around $t = 7$ sec (5b) and causes no

noticeable increase in velocity at the deepest depth (5c). Wave height at breaking increased to about 25 cm. Breaking is induced when $H/L \geq 0.14$ or 0.16 (Dean and Dalrymple 1984) when considering the breaking height with the actual period of 1 sec in the experiment for the high frequency waves.

Appendix A (6) reports the Fourier spectra for the plunging breaker experiment. In the figure the two peaks correspond to the high and low frequency waves. The energy in “u” and “w” was considerably larger than that for “v”. This is from the higher velocity predominant in the “u” and “w” direction. Spectral peaks in the three components are also at higher frequencies than the noted in the figure. This is from harmonics of the dominant frequencies. The overall lower energy in the “v” component allow the frequency multiples to appear more dominant. The “v” spectrum closely follows the $(-5/3)$ law (Eq. 11) more closely than the other two components. The flattening of the “u” and “w” components of the spectra are unlikely from noise, as noise would manifest itself equally in all components. It is possible that the harmonics dominated the higher frequencies for the “u” and “w” components. This property gives the “v” component as the suitable choice in computing the energy dissipation rate. Noise in the system does appear at frequencies greater than 50 Hz ($\approx \exp [3.9]$)

To calculate the energy dissipation rate, the values of the velocity fluctuations are needed. With Eq. 13 as a guideline, the velocity components consist of the mean flow and the fluctuations. An Infinite Impulse Response (IIR) “notch” filter separated the large scale flow from the small scale (Press et al. 1992). Spectral analysis dictated the removal of the frequencies. For the regular waves, the filter removed at the dominant frequencies and their harmonics. The goal was to leave the inertial sub-range undisturbed.

Appendix A (7) shows the filtered and unfiltered (original) “v” component for each of the type of regular wave used in the experiment. The filter removed the large-scale periodicity of the velocity, suggesting the effectiveness of the routine. The remaining (filtered) velocities are the fluctuations (v').

A combination of the high and low frequency wave filters were applied to the breaking wave (i.e. all filters applied to both high and low frequency waves were applied to the breaking waves). Appendix A (8) shows the affect of the filter on the plunging breaker. From Appendix A (5), we see that the breaker occurred at about $t = 2$ sec. The increase in velocity at around 3.8 sec is in both the filtered and unfiltered data. Turbulence from the breaker caused this local peak in the filtered velocity.

The autocorrelation function, R_E , (Eq. 16) was performed over the time series of the “v” velocity at each depth of the ADV. The Euler correlation time, τ_{Ei} , is the area below R_E from the vertical axis until the first zero crossing. Numerical integration gave time scales of around 0.1 sec for the regular wave experiments near the surface. The time scales for breaking increased to about 1 sec near the surface. Eq. (14) averages the velocity fluctuations over the time scale. This approach provides the average energy dissipation rate over the time scale, but does not provide information of the fine temporal scales of turbulence. For this reason, the following equation was used instead of Eq. (14):

$$\varepsilon_j = A \frac{(\mathbf{v}'_j)^2}{\tau_E} \quad (17)$$

where the index j refers to time. Here, at any time $t = j \Delta t$ (where Δt is equal to 0.02 sec), the ε is computed. The computed value of ε at each depth used its corresponding time scale. Appendix A (9-12) shows the ε calculated over time for the regular waves. These are at the same depths as the previously displayed velocity measurements. Qualitatively, the ε does not vary much over the whole series, with the exception of individual “spikes” every few seconds. The values generally decreased with depth.

Appendix A (13) displays ε for the plunging breaker at three depths. As expected, ε are higher near the surface. Breaking took place every 25 seconds. As such, the near surface plot has ε increase sharply during breaking and/or soon after the event. ε are elevated before the breaking events from the shear in the water when the low frequency waves overtake the high frequency waves. Deep in the column, the breaker does not clearly affect the ε .

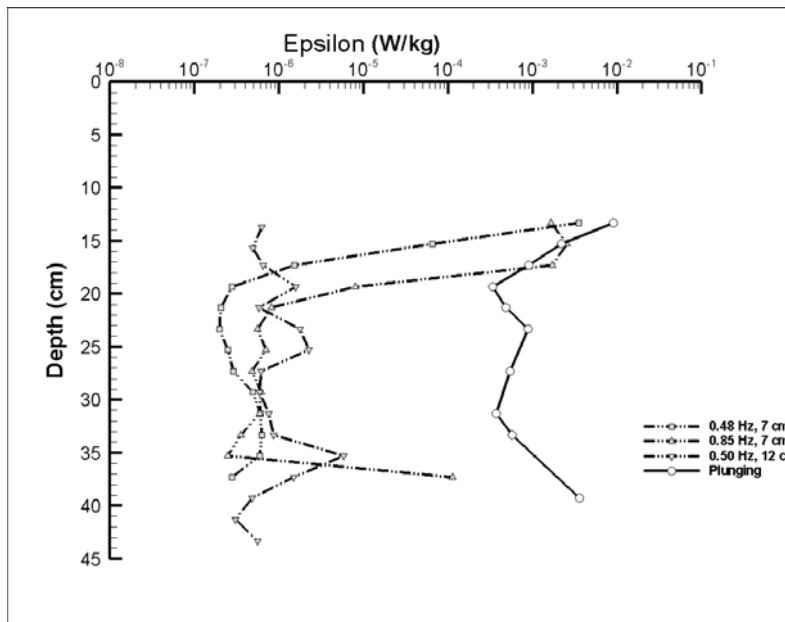


Figure 3: Average energy dissipation rates for regular and breaking waves. Note the effect of the breaker relative to the regular waves deep in the water column.

Figure 3 shows the average energy dissipation rates for the regular and breaking experiments for decreasing depths. The incorrect data from HF 12 cm experiment is not included in the plot. Here we see that the dissipation rates tend to decrease with depth and are much higher near the surface. The increase in dissipation at the deeper depths is likely caused by currents in the tank. The regular waves were averaged over the whole experiment, while the breaking waves had the top three values for each breaking packet averaged.

4.2. Chemical Dispersant effectiveness testing in batch system

4.2.1 Effects of dispersant and wave conditions on oil distribution in the wave tank

To evaluate dispersant effectiveness, the fraction of added oil entrained in the water column of the wave tank must be determined. This can be accomplished either by measuring the amount of oil remaining on the surface after mixing in the presence of chemical dispersants or by measuring the oil concentration in the water column (NRC 2005, refs therein). The indirect method of measuring oil at the surface has been questioned because of incomplete recovery of oil fractions from compartments that cannot be explicitly measured, such as those evaporated into the atmosphere and irreversibly absorbed to the walls (Fingas and Ka'aihue 2004). In contrast, we collected a large number of samples with high resolution in space and time to directly measure the oil dispersed in the water column. The oil concentrations were determined by extraction of oil from the samples using dichloromethane, followed by reading absorbance at three wavelengths using ultraviolet spectrometry (Venosa et al., 2002). Figures 4 to 6 display representative contour plots of the MESA oil concentration in the wave tank. The ANS oil distributions in the wave tank (data not shown) were similar to those of MESA oil.

Figure 4A shows the control condition where only seawater was sprayed onto the oil slick under regular wave conditions. The added oil, which remained on the surface, was rapidly transported to the end of the tank due to the absence of dispersant that would reduce the oil-water interfacial tension and the lack of sufficient mixing energy to break up the slick. The ineffective natural dispersion of oil under regular wave conditions is clearly shown in Figure 4A, with high oil concentration on the surface near the wave absorbers, and the slow movement of dispersed oil upstream. In contrast, dispersion of MESA oil was significantly more effective over time after the slick was sprayed with either Corexit 9500 or SPC 1000, respectively (Figures 4B and 4C). Although the distribution of oil in the tank was similar to the control condition at five minutes, the oil became progressively more dispersed over time as its concentration steadily declined at the furthest downstream surface sampling, and the oil plume dispersed upstream and deeper into the water column. The overall dispersion was more evident after the addition of Corexit 9500 (Figure 4B) than SPC 1000 (Figure 4C).

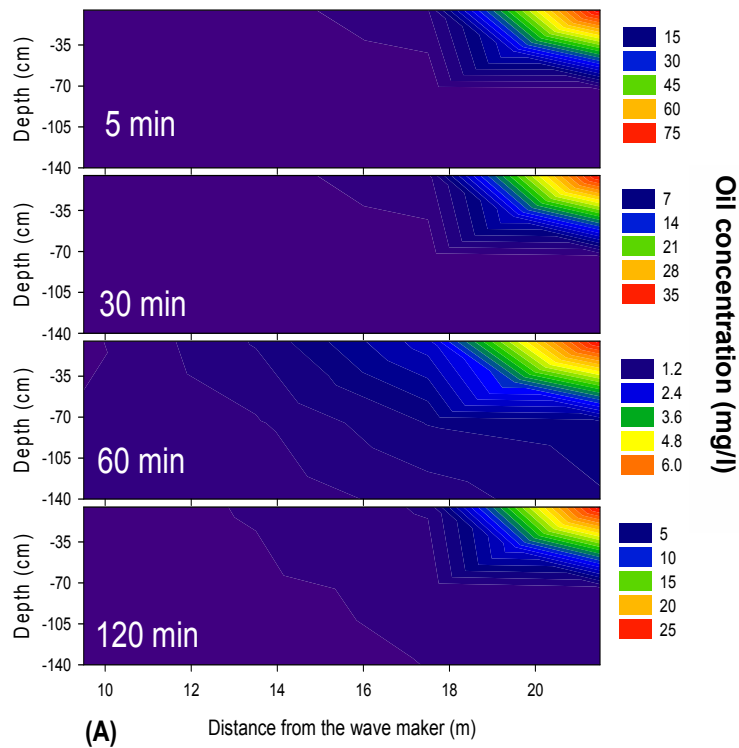


Figure 4a: Dispersed MESA oil concentration (mg/L) as a function of time and space under regular non-breaking waves with no dispersant.

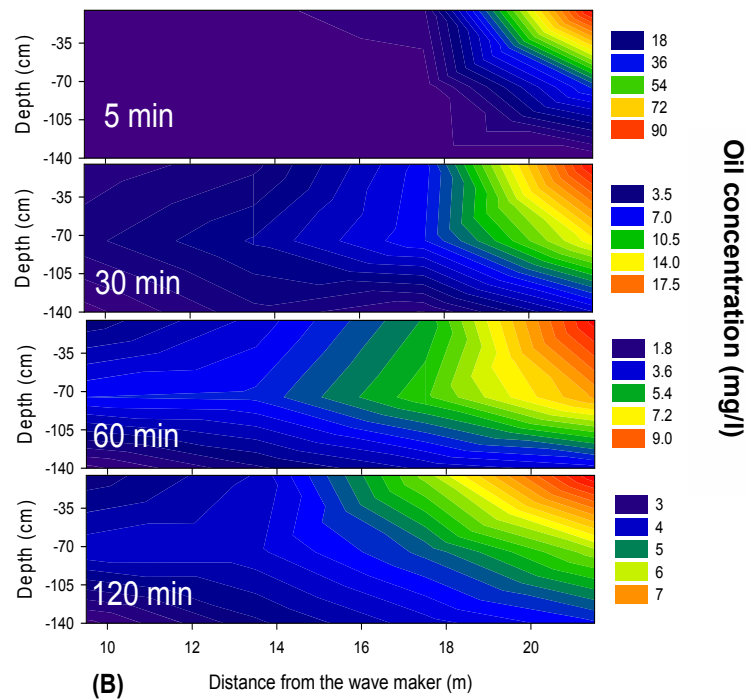


Figure 4b: Dispersed MESA oil concentration (mg/L) as a function of time and space under regular non-breaking waves with Corexit 9500.

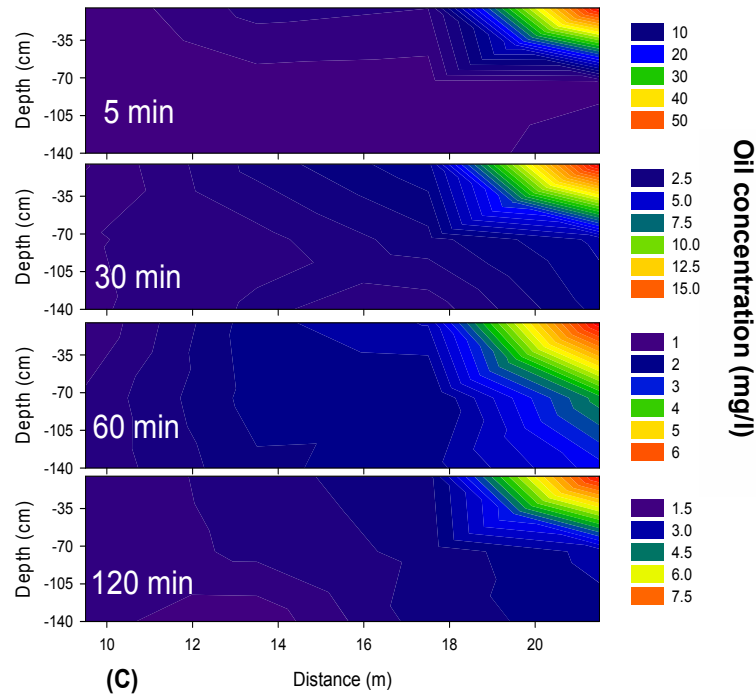


Figure 4c: Dispersed MESA oil concentration (mg/L) as a function of time and space under regular non-breaking waves with SPC 1000.

Under spilling breaking waves (Figure 5, next pages), the spreading of oil at the surface was enhanced under physical dispersion (Figure 5A) and chemical dispersion (Figures 5B and 5C). This was probably attributable to the dissipation of total kinetic energy as microscale turbulent eddies under the breaking waves, dampening the downstream drift velocity of the water and increasing the turbulent diffusion of dispersed oil droplets. Chemical dispersion by Corexit 9500 (Figure 3B) or SPC 1000 (Figure 5C) under spilling breaking waves increased oil dispersion significantly compared to the regular wave conditions (Figure 5A, B, C), as indicated by the movement of oil farther upstream. However, the depth of penetration of the oil plume was limited to the middle and upper half of the tank, similar to dispersion under regular wave conditions.

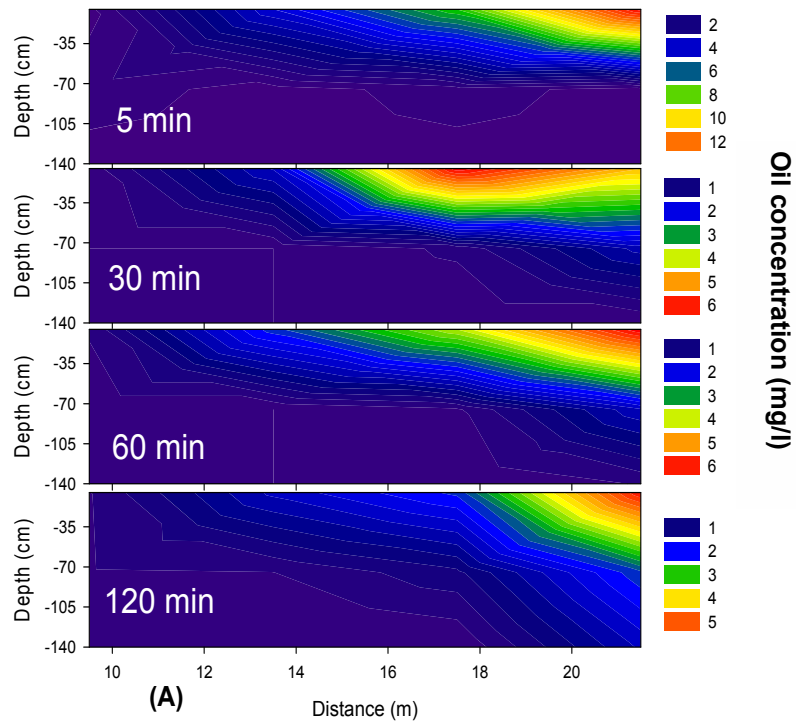


Figure 5a: Dispersed MESA oil concentration (mg/L) as a function of time and space under spilling breaking waves with no dispersant.

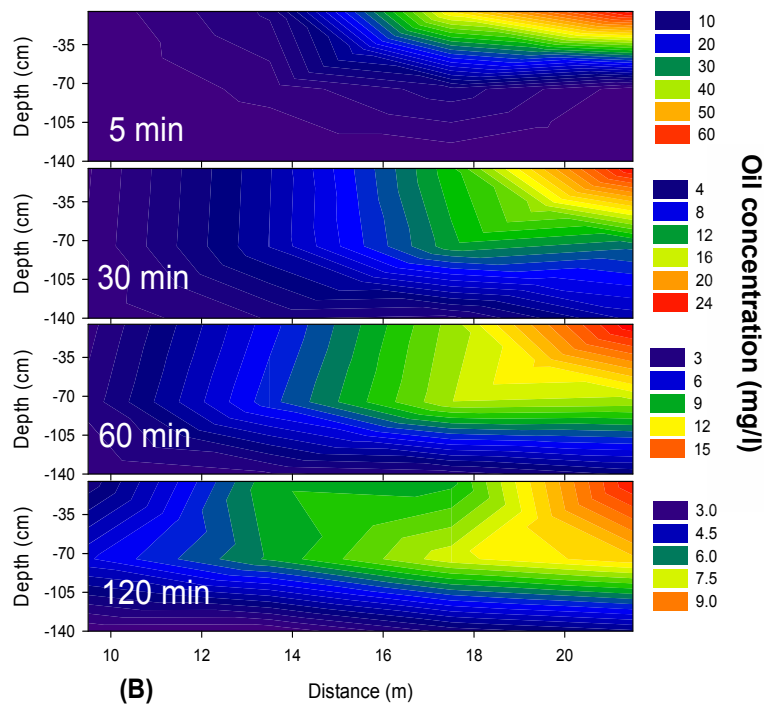


Figure 5b: Dispersed MESA oil concentration (mg/L) as a function of time and space under spilling breaking waves with Corexit 9500.

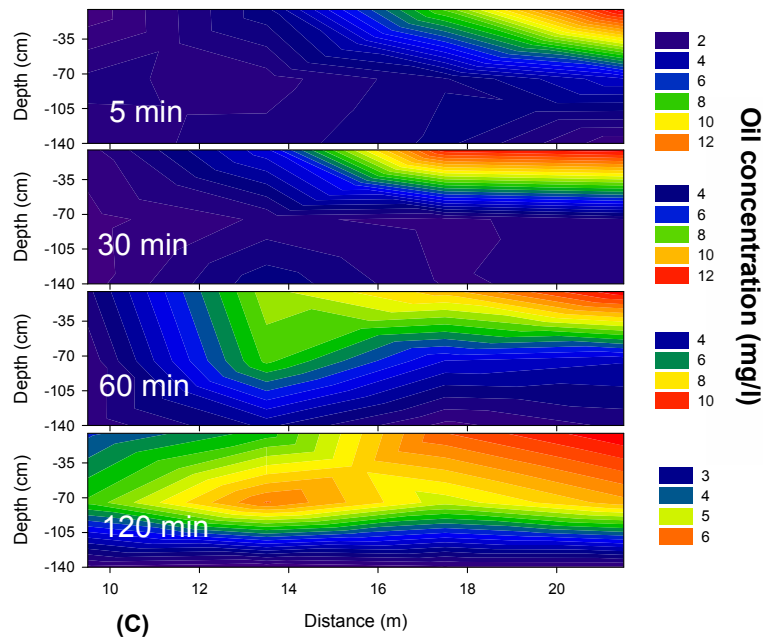


Figure 5c: Dispersed MESA oil concentration (mg/L) as a function of time and space under spilling breaking waves with SPC 1000.

Under plunging breaking waves (Figures 6A, B, C, next pages), spreading of the oil plume was even more pronounced compared to the non-breaking and spilling breaking waves. In the no-dispersant control condition, spreading at the surface was higher as shown by the reduced net drifting of oil at the surface (Figure 6A). In the presence of chemical dispersants, the oil plume appeared virtually homogenized in the wave tank at all depths due to the combined effect of more vigorous turbulent diffusion created by the plunging breaking waves and the presence of chemical dispersants (Figures 6B and 6C).

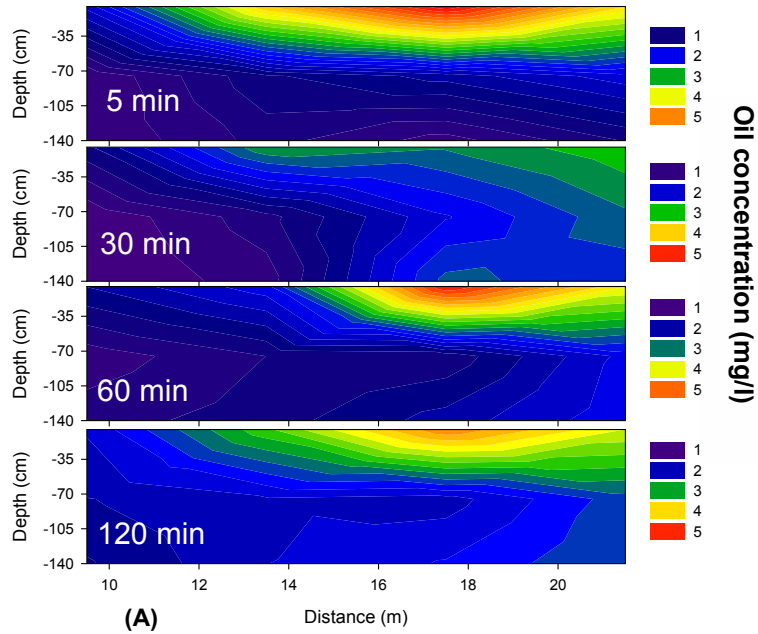


Figure 6a: Dispersed MESA oil concentration (mg/L) as a function of time and space under plunging breaking waves with no dispersant.

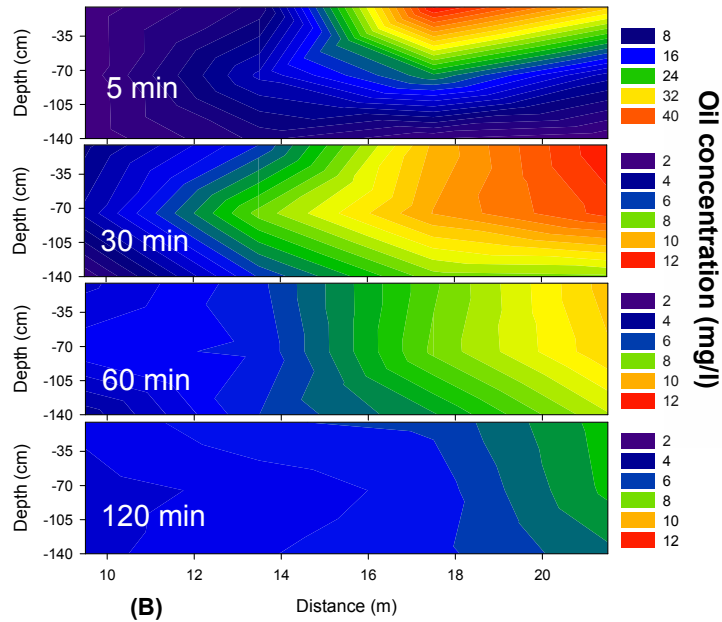


Figure 6b: Dispersed MESA oil concentration (mg/L) as a function of time and space under plunging breaking waves with Corexit 9500.

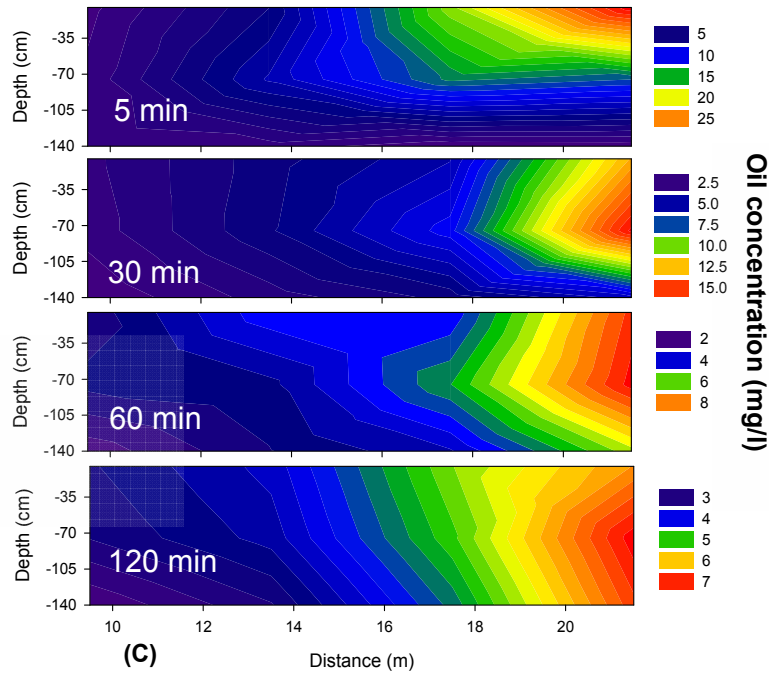


Figure 6c: Dispersed MESA oil concentration (mg/L) as a function of time and space under plunging breaking waves with SPC 1000.

The effect of breaking waves on the oil distribution (in particular the penetration depth of dispersed oil) is related to a number of contributing factors. As waves break, it is estimated that 30% to 50% of the dissipated wave energy entrains oil droplets into the water column (Lamarre and Melville 1991; Tkalich and Chan 2002), and effectively determines the first-order oil entrainment rate (Tkalich and Chan 2002). Breaking waves develop a mixing layer in the upper water column, and the penetration of oil results in a uniform mixing of the droplets, with the mixing layer proportional to the height of breaking waves (Delvigne and Sweeney 1988; Tkalich and Chan 2002). Moreover, breaking waves generate micro-scale turbulence with the smallest eddies having the greatest velocity gradients, leading to deformation, elongation and eventual breakup of larger droplets, forming a large number of small droplets that have lower buoyancy and more rapid diffusion efficiency (Delvigne et al. 1987; Li and Garrett 1998).

4.2.2 Dispersant effectiveness as a function of energy dissipation rate

To compare the effect of wave and dispersant on oil dispersion effectiveness, the average dispersed oil concentration in the bulk water column was calculated from the oil concentrations of the two lower depths and all four horizontal locations of water samples of the independent triplicate experiments for each treatment. Oil dispersion time (5, 30, 60, and 120 min) was treated separately to identify the time effect on the overall dispersion effectiveness for three dispersants on two oils under three different wave conditions. The higher values of the surface oil concentration, especially the one at the furthest downstream location, are the very indication of poor dispersion effectiveness, so it is more reasonable to exclude the surface measurements

from the calculation of the average dispersed oil concentration in the water column. Table 3 shows the calculated bulk water column average oil concentrations.

Table 3: Average water column dispersed oil concentrations (mg/l) as a function of time. Data reported as the average \pm one standard deviation of independent triplicate runs.

Oil	Wave	Dispersant	5 min	30 min	60 min	120 min
MESA	Regular	Water	0.31 \pm 0.02	0.44 \pm 0.26	0.86 \pm 0.65	1.05 \pm 0.73
		Corexit	0.39 \pm 0.28	3.39 \pm 2.74	3.89 \pm 1.85	4.05 \pm 1.40
		SPC	0.69 \pm 0.79	1.36 \pm 1.09	2.00 \pm 1.54	2.09 \pm 1.51
	Spilling	Water	0.31 \pm 0.09	0.39 \pm 0.14	0.42 \pm 0.22	0.71 \pm 0.22
		Corexit	1.46 \pm 1.57	5.04 \pm 1.05	5.19 \pm 1.46	4.79 \pm 1.46
		SPC	2.40 \pm 2.39	2.84 \pm 2.71	3.61 \pm 2.96	3.64 \pm 2.83
	Plunging	Water	0.77 \pm 0.27	1.55 \pm 0.58	1.66 \pm 0.43	2.07 \pm 0.46
		Corexit	4.31 \pm 0.95	7.09 \pm 0.85	6.50 \pm 0.29	5.43 \pm 0.15
		SPC	3.39 \pm 1.85	4.65 \pm 1.62	4.31 \pm 1.29	4.40 \pm 0.70
ANS	Regular	Water	0.67 \pm 0.77	0.81 \pm 0.57	1.19 \pm 0.57	1.37 \pm 0.69
		Corexit	2.26 \pm 2.17	3.32 \pm 2.61	3.68 \pm 1.03	3.93 \pm 0.75
		SPC	1.49 \pm 1.06	2.12 \pm 1.60	2.21 \pm 1.71	2.59 \pm 1.93
	Spilling	Water	0.25 \pm 0.08	0.25 \pm 0.09	0.47 \pm 0.47	0.55 \pm 0.33
		Corexit	4.77 \pm 1.00	8.58 \pm 0.65	8.21 \pm 1.05	6.55 \pm 0.34
		SPC	1.97 \pm 2.14	3.14 \pm 3.64	2.92 \pm 2.86	2.97 \pm 2.21
	Plunging	Water	0.28 \pm 0.15	1.01 \pm 0.61	1.39 \pm 0.65	1.61 \pm 0.36
		Corexit	4.09 \pm 3.65	8.37 \pm 1.61	7.73 \pm 0.75	6.91 \pm 0.50
		SPC	2.91 \pm 1.04	5.89 \pm 3.06	5.69 \pm 1.92	5.75 \pm 1.06

Dispersant effectiveness (DE) was determined by estimating the average dispersed oil concentration in the water column for the two chemical dispersant treatments and the no-dispersant (physically dispersed) control as a function of ϵ . This was performed by calculating the average oil concentrations of the eight samples recovered from the four horizontal locations and two lower depths of the water column in the wave tank. It is reasonable to exclude the surface samples from the calculation of the average dispersed oil concentration in the water column because the high oil concentrations on the surface of the water at the wave absorber end of the tank were largely controlled by surface drift, and would skew the calculations of DE. Intuitively, the extremely high oil concentration of the samples recovered from the surface in front of the wave absorbers under regular waves in the absence of dispersants is a clear indication of poor oil dispersion efficiency.

Figures 7 and 8 present the estimated DE of the three dispersant types (including water as the control) on the two crude oils as a function of ϵ . Different degrees of physical dispersion of the MESA and ANS crude were measured at each energy dissipation rate. The physical DE of MESA crude ranged from 4% to 9% at 5 min (Figure 5A), and then steadily increased with time, approaching 12% to 24% after 2 h (Figure 5D). Similarly, the physical DE of ANS crude was between 3.5% and 9% at 5 min (Figure 6A) and increased to between 10% and 19% at 2 h (Fig. 6D). Delvigne and Sweeney (1988) have reported that the physical dispersion of oil in a grid column generated droplets that were mostly larger than 50 μm in turbulence at energy dissipation rates of up to 3.5 $\text{W}\cdot\text{kg}^{-1}$, but they observed only a very small fraction of oil dispersed by breaking waves under a surface slick in their flume experiments. Lunel (1993, 1995) found that the dispersion of Forties crude oil with and without dispersant applied at sea generated a similar number of large oil droplets ($> 70 \mu\text{m}$), but dispersion of the oil with dispersant produced a much greater number of small droplets ($< 70 \mu\text{m}$). However, since none of these authors have reported physical DE explicitly, it is impossible to compare their results with our current work, beyond the consistency that physical dispersion of oil was expected. It was even more difficult to obtain physical DE of oil when bench-scale testing apparatus was used, due to coalescence and re-surfacing of oil from the relatively large water to oil ratio and wall effect of the confined space, (Chandrasekar et al. 2005; Chandrasekar et al. 2006).

Chemical dispersants were effective under all three wave conditions (Figures 7 and 8), with oil dispersion most effective under plunging breaking wave conditions and least effective under regular non-breaking wave conditions. The dispersant Corexit 9500 appeared twice as effective as SPC 1000 for the dispersion of MESA crude at the two lower energy dissipation rates, but the DE of the two dispersants was closer after oil was dispersed for 2 h at high energy dissipation rates. A similar trend was observed for the dispersion of ANS crude. At all three energy dissipation rates, though, the DE of Corexit 9500 was consistently higher than that of SPC 1000, and both were significantly higher than the control. The DE of the control was significantly increased as a function of time at high energy dissipation rates. The SPC 1000 was less effective at the two lower energy dissipation rates. In contrast, the Corexit 9500 appeared equally effective at the two higher energy dissipation rates but less effective at the low energy dissipation rate.

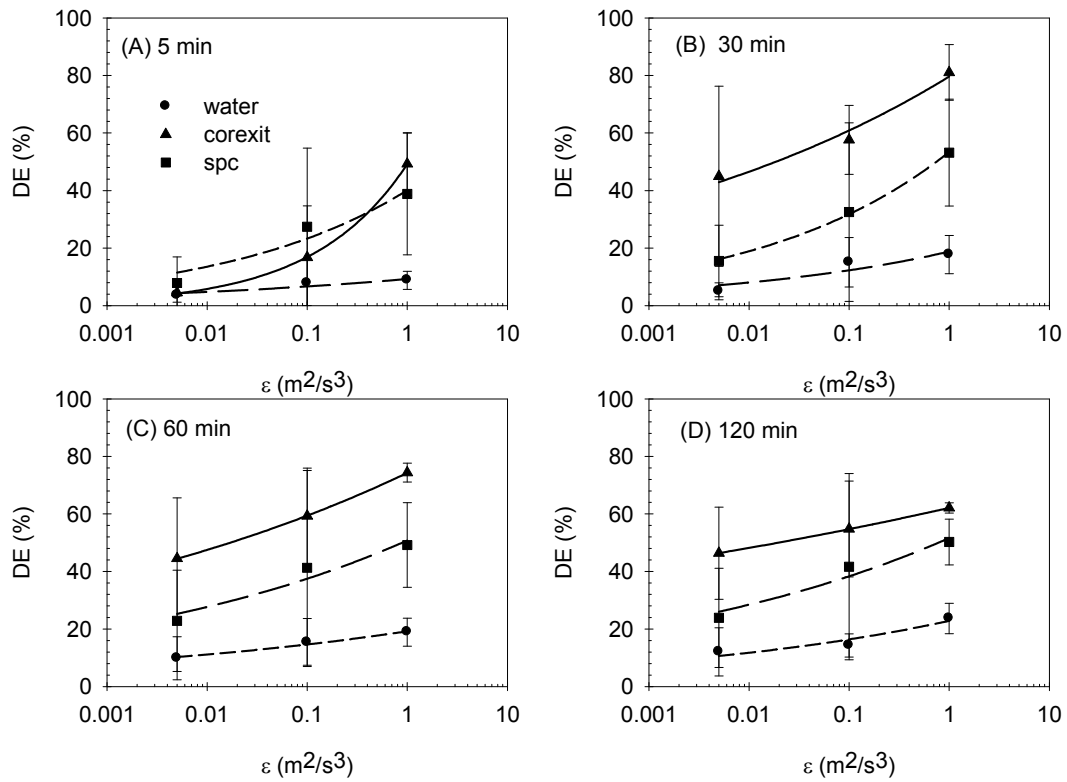


Figure 7: DE on MESA crude oil as a function of energy dissipation rate at: (A) 5 min, (B) 30 min, (C) 60 min, and (D) 120 min. Data shown are mean and one standard deviation of independent triplicate runs. Lines are best-fit regression of Equation 5.

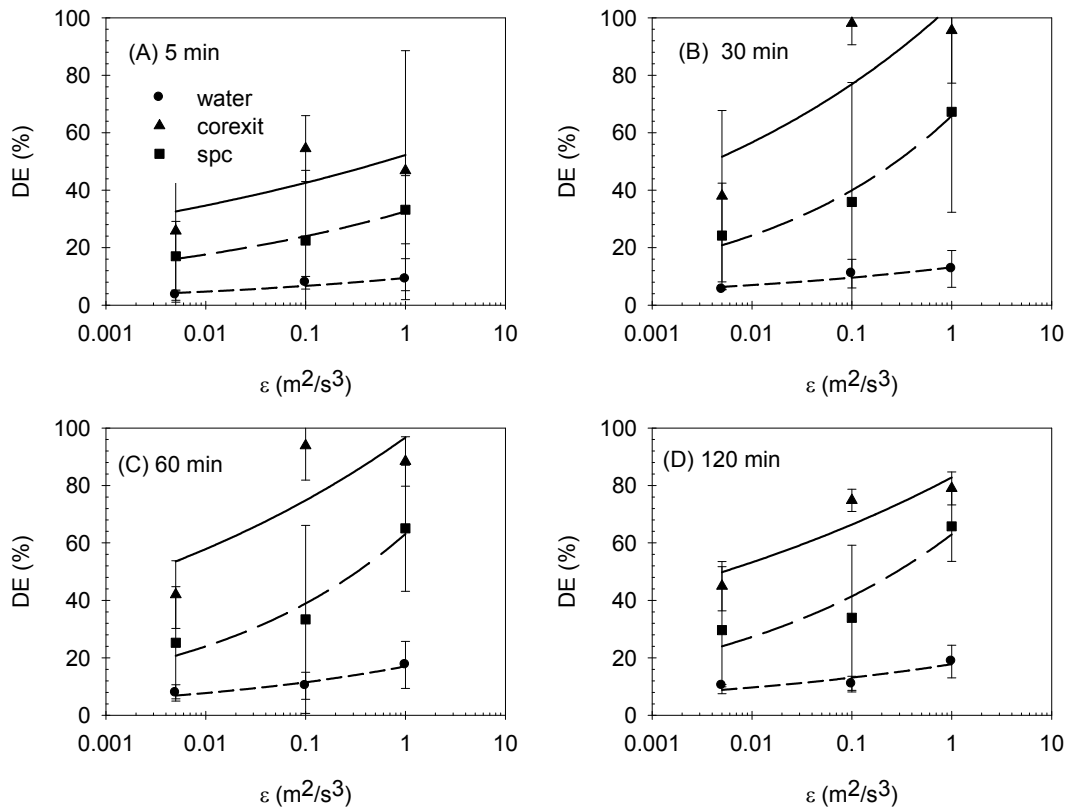


Figure 8: DE on ANS crude oil as a function of energy dissipation rate at: (A) 5 min, (B) 30 min, (C) 60 min, and (D) 120 min. Data shown are mean and one standard deviation of independent triplicate runs. Lines are best-fit regression of Equation 5.

To delineate the effect of each treatment factor on the oil dispersion, a four-way factorial analysis of variance (ANOVA) was conducted to determine the effects of main factors and multifactor interactions on the DE. The main factors tested included dispersant type (three levels), wave condition (three levels), oil type (two levels), and oil dispersion time (four levels). The oil dispersion time (5, 30, 60, and 120 min) was analyzed separately to identify the time required to achieve the maximum overall DE for the three dispersant conditions on the two oils under the three imposed wave conditions. The results of the ANOVA are summarized in Table 4. The ANOVA revealed that there was one significant three-factor interaction (dispersant by oil by wave, $p = 0.017$) and three significant two-factor interactions (dispersant by oil, $p = 0.016$; dispersant by wave, $p = 0.00001$; and dispersant by time, $p = 0.00385$). Interactions of these factors indicate that they had opposite effects on the DE. There was no two-way time-by-wave interaction. All four main factors showed very strong significant effects on the DE (oil, $P = 0.0074$; wave, dispersant type, and dispersion time, $P < 0.0000001$).

Table 4: Four-way factorial ANOVA of the main factor and multi-factor interaction effects on the dispersant effectiveness. Significant factors are flagged (*).

	Degree of freedom	Sum of square	Mean square	F value	Pr (F)
Dispersant (Disp)	2	627.8180	313.9090	140.2928	0.0000000 *
Wave	2	163.0560	81.5280	36.4366	0.0000000 *
Time	3	100.6297	33.5432	14.9912	0.0000000 *
Oil	1	16.5033	16.5033	7.3757	0.0074208 *
Disp/Oil	2	19.0702	9.5351	4.2614	0.0159212 *
Disp/Wave	4	69.9299	17.4825	7.8133	0.0000100 *
Oil/Wave	2	1.9648	0.9824	0.4391	0.6455039
Disp/Time	6	45.2753	7.5459	3.3724	0.0038509 *
Oil/Time	3	0.4255	0.1418	0.0634	0.9790765
Wave/Time	6	7.1573	1.1929	0.5331	0.7824024
Disp/Oil/Wave	4	28.0072	7.0018	3.1293	0.0167294 *
Disp/Oil/Time	6	1.9656	0.3276	0.1464	0.9895068
Disp/Wave/Time	12	6.7733	0.5644	0.2523	0.9948054
Oil/Wave/Time	6	8.4322	1.4054	0.6281	0.7075827
Disp/Wave/Oil/Time	12	5.4511	0.4543	0.2030	0.9981657
Residuals	144	322.2041	2.2375		

The Tukey’s paired comparison method was used to compare the effects of different levels of the main factors that have been identified to significantly affect the DE; the results are listed in Table 5. The two tested dispersants both have significantly higher DE than the water control (increasing DE by an average margin of 48% and 26%, respectively, for Corexit 9500 and SPC 1000); Corexit 9500 was more effective than SPC 1000 by a 22% higher DE. As for the effect of the wave condition, spilling breaking waves significantly increased DE by 12% compared to the regular non-breaking waves; plunging breaking waves significantly increased the DE by an additional 13% compared to the spilling breaking waves. With regard to dispersion time, the extent of oil dispersion increased significantly from 5 min to 30 min, and leveled off thereafter.

Table 5: Tukey’s paired comparison of the different effects between treatment levels on DE (%) in the water column. Significant differences are flagged by * based on 95% simultaneous confidence intervals for specified linear combinations.

Treatment	Level	Estimates	Standard error	Lower limit	Upper limit
Dispersant	Corexit - SPC	21.6 *	2.98	14.6	28.7
	Corexit - Water	47.7 *	2.98	40.6	54.7
	SPC - Water	26.1 *	2.98	19.0	33.0
Wave	Plunging - Regular	24.3 *	2.98	17.3	31.4
	Plunging - Spilling	12.3 *	2.98	5.5	19.5
	Spilling - Regular	11.8 *	2.98	4.7	18.9
Time	30 min – 5 min	17.8 *	3.29	9.3	26.4
	60 min – 5 min	18.5 *	3.29	10.0	27.1
	120 min – 5 min	17.6 *	3.29	9.1	26.2
	60 min – 30 min	0.73	3.29	-7.8	9.3
	120 min – 30 min	-0.19	3.29	-8.7	8.4

4.2.3 Physically and chemically dispersed oil droplet size distributions

Figures 9 to 11 display representative dispersed MESA crude oil droplet size distributions measured near the surface of the wave tank for physical and chemical dispersion of oil under three different wave conditions. Table 6 summarizes the droplet size distribution statistics. Similar droplet size distributions were obtained in the middle and near the bottom of the wave tank (data not shown). The dispersed oil droplet size distribution data were also recorded for ANS crude from all three depths under different experimental conditions (data not shown). These data were similar to those for MESA. Physical dispersion (i.e., dispersion in absence of a chemical dispersant) of MESA oil created mono-modal lognormal droplet size distributions under regular wave conditions throughout the entire experiment (Fig. 9A, B). Bi- or tri-modal lognormal distributions were generated initially (first 10 min), which were further dispersed to mono-modal distributions, under spilling and plunging breakers (Fig. 10A,B; 11A,B). In the presence of chemical dispersants, however, multi-modal lognormal size distributions were produced under all three wave conditions throughout the entire duration of the dispersion experiment (Fig. 9C, E - 11C, E). A large number of oil droplets with droplet size less than 10 μm were created in the presence of chemical dispersants, especially by dispersant Corexit 9500. Application of dispersants expanded the range of size distributions as indicated by larger geometric standard deviations (GSD) associated with chemical dispersants (Table 6). Chemical dispersants also caused much higher dispersed phase volume concentrations (areas under the droplet size distributions) than physical dispersion (Figures 9-11). However, the droplet size distribution patterns of the chemically dispersed oil droplets were essentially the same after 30 min under all three wave conditions, as indicated by the percentage cumulative droplet size distributions (Fig. 9D,F; 10D,F; 11D,F).

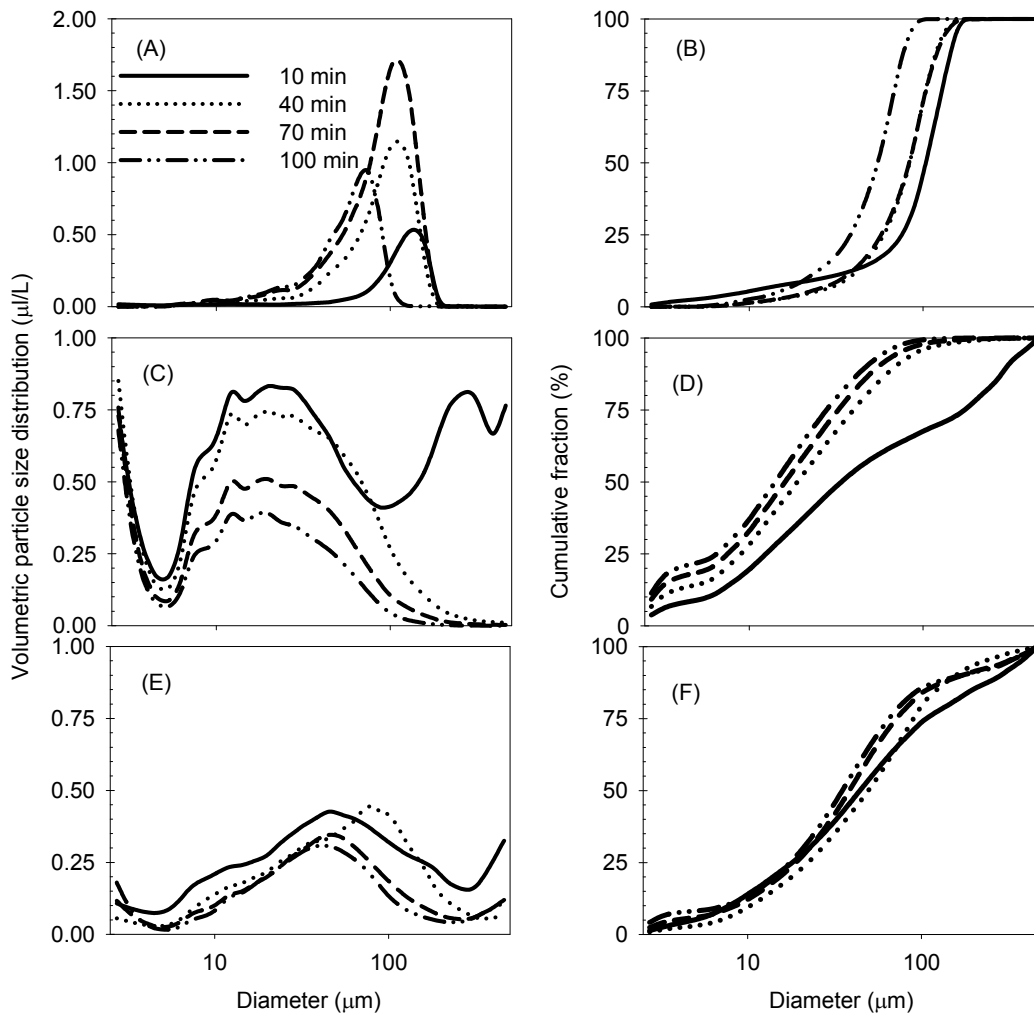


Figure 9: Volumetric (left) and cumulative (right) MESA oil droplet size distributions dispersed by water (A&B), Corexit 9500 (C&D), and SPC 1000 (E&F) under regular wave conditions.

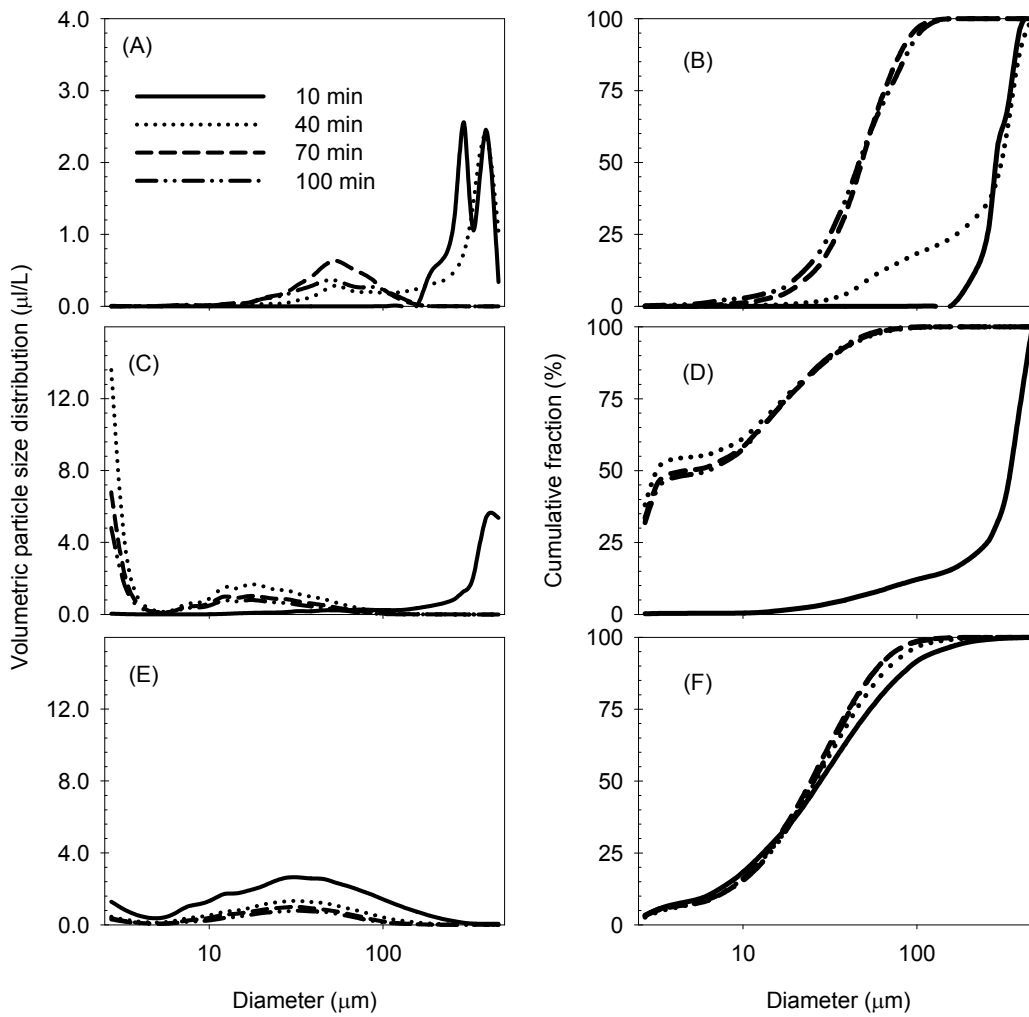


Figure 10: Volumetric (left) and cumulative (right) MESA oil droplet size distributions dispersed by water (A&B), Corexit 9500 (C&D), and SPC 1000 (E&F) under spilling breaking wave conditions.

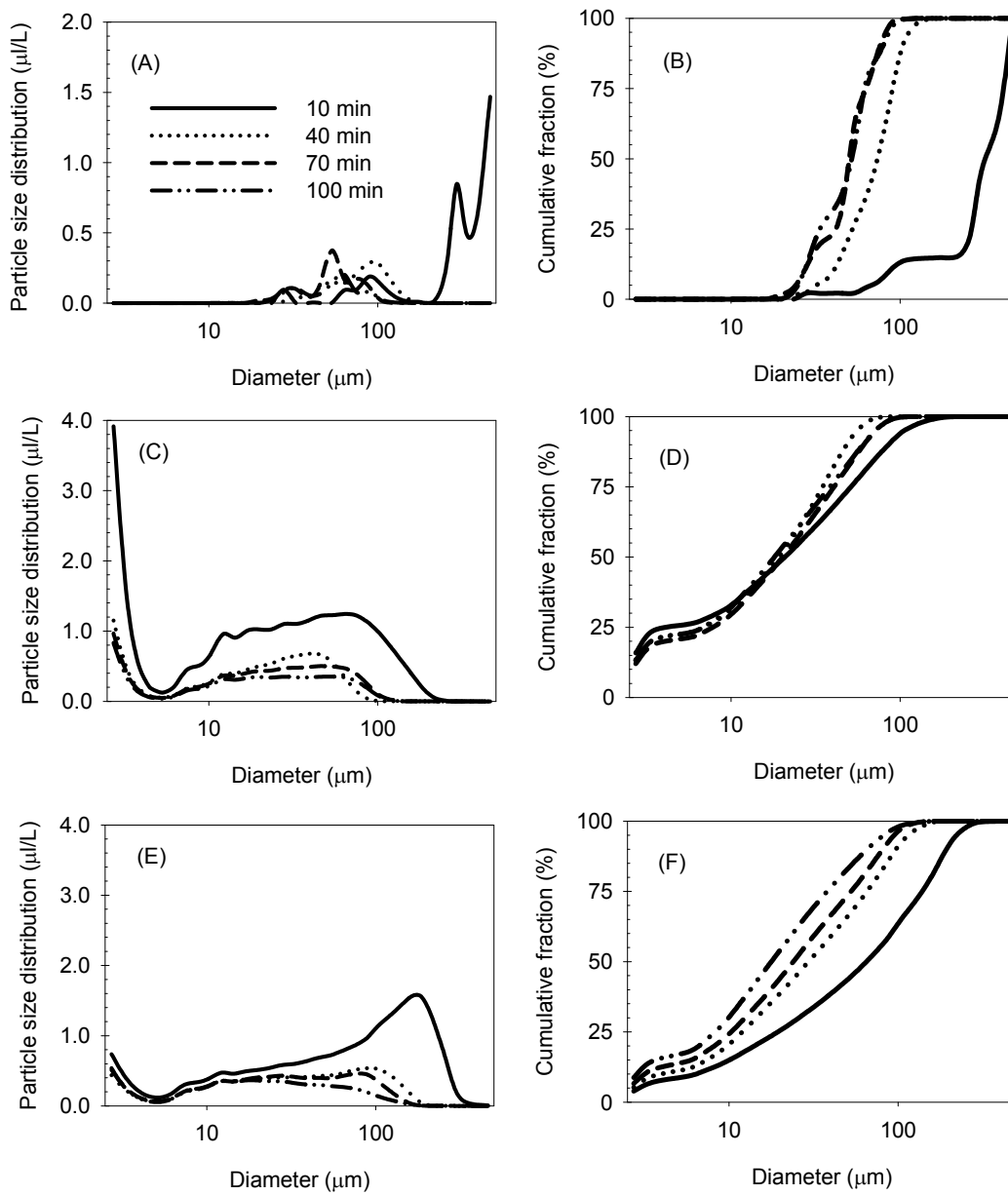


Figure 11: Volumetric (left) and cumulative (right) MESA oil droplet size distributions dispersed by water (A&B), Corexit 9500 (C&D), and SPC 1000 (E&F) under plunging breaking wave conditions.

Table 6: Droplet size distribution statistics

Wave	Dispersant	Time (min)	d16 ^a	d50 ^a	d84 ^a	GSD ^b	Modes	% < 70 μm
Regular	Water	10	53	104	143	1.64	1	22%
		40	46	80	116	1.59	1	34%
		70	45	80	114	1.59	1	35%
		100	28	55	74	1.63	1	75%
	Corexit	10	8	33	250	> 3.16	4	62%
		40	6	19	55	3.03	2	90%
		70	3.5	16	45	3.59	2	94%
		100	3	14	38	3.56	2	96%
	SPC	10	11	45	186	4.11	3	65%
		40	15	50	120	2.83	3	65%
		70	13	39	100	2.77	3	72%
		100	12	35	90	2.74	3	77%
Spilling	Water	10	230	280	360	1.25	2	0%
		40	85	310	380	2.11	2	13%
		70	29	50	75	1.61	1	78%
		100	25	48	80	1.79	1	75%
	Corexit	10	160	350	430	1.64	1	95%
		40	2.5	3	25	3.16	2	99%
		70	2.5	5	25	3.16	2	99%
		100	2.5	7	25	3.16	2	99%
	SPC	10	9	28	74	2.87	2	82%
		40	10	27	58	2.41	2	90%
		70	10	25	50	2.24	2	93%
		100	10.5	24	50	2.18	2	93%
Plunging	Water	10	225	330	430	1.38	4	5%
		40	45	70	96	1.46	2	45%
		70	31	50	70	1.50	2	82%
		100	29	48	68	1.53	2	92%
	Corexit	10	2.8	22	70	5.00	2	88%
		40	3	19	43	3.79	2	100%
		70	3	20	52	4.16	2	98%
		100	3	18	53	4.20	2	98%
	SPC	10	11	64	170	3.93	2	50%
		40	8	30	80	3.16	2	77%
		70	7	24	70	3.16	2	84%
		100	4	18	52	3.61	2	92%

^a d_{16%}, d_{50%}, d_{84%} represent the 16%, 50%, or 84% of total mass of the droplets that are smaller than this diameter (μm); d_{50%} is the mass median diameter.

^b GSD stands for geometric standard deviation.

4.2.4 Significant factors determining the average dispersed oil droplet sizes

The full spectrum of particle size distribution at each sampling time was converted to volume mean diameter (VMD) to compare the influence of different treatment conditions, including wave conditions, dispersant type and oil type, on the average droplet size. The VMD from physical dispersion (absence of dispersants) under all wave conditions started with wide

fluctuations but generally decreased over time. The time-series VMD were in good agreement at all three depths under regular waves and plunging breaking waves, but were smaller at the bottom than in the middle and near the surface under spilling breaking wave conditions, probably caused by less penetration depth of the spilling breaking waves. The VMD from the chemical dispersants were larger near the bottom than near the surface and in the middle of the wave tank under regular waves, but had wider fluctuations in the middle of the wave tank than near the surface and the bottom of the wave tank under spilling and plunging breaking waves conditions.

Figures 12 and 13 illustrate the average dispersed oil droplet VMD at the surface of the wave tank as a function of time at the end of each measurement period for MESA and ANS crude, respectively. Similar trends of the time-series average VMD under different dispersant and wave conditions were observed at the other two depths (in the middle and near the bottom) of the wave tank (data not shown). After 10 min, physically dispersed oil droplets were large ($VMD > 160 \mu\text{m}$) under all three wave conditions (Fig. 12, 13). In contrast, chemical dispersants (both Corexit 9500 and SPC 1000) created the largest oil droplets ($VMD_{\text{MESA}} > 140 \mu\text{m}$, $VMD_{\text{ANS}} > 200 \mu\text{m}$) under regular non-breaking waves and the smallest droplets ($VMD_{\text{MESA}} < 80 \mu\text{m}$, $VMD_{\text{ANS}} < 120 \mu\text{m}$) under plunging breaking waves, with the average VMD more dependent on dispersant and oil type under spilling breaking wave conditions. As oil dispersion progressed, the average VMD declined at a rate dependent on dispersant type and wave conditions. Physical dispersion of both crude oils appears to have required the longest time (100 min) to reach the ultimate stable VMD under regular non-breaking wave conditions and the shortest time (40 min) under plunging breaking wave conditions. Chemical dispersants obviously facilitated better dispersion at lower energy dissipation rates under regular non-breaking and spilling breaking wave conditions. Corexit 9500 reduced the average VMD for both MESA and ANS under all three wave conditions at all four time points (Fig. 12A-C). SPC1000, however, decreased the average VMD markedly under spilling and plunging breaking waves for MESA, but reduced the average VMD even more dramatically under regular wave and spilling breaking waves for ANS. The effect of dispersant was clearly illustrated by the ultimate VMD for each combination of dispersant, wave, and oil: physically dispersed MESA and ANS oil droplets had $VMD > 100 \mu\text{m}$ under all three wave conditions; SPC 1000 dispersed MESA to $150 \mu\text{m}$ under regular non-breaking waves and less than $70 \mu\text{m}$ under spilling and plunging breaking wave conditions, but it dispersed ANS crude to around $100 \mu\text{m}$ under all three wave conditions. Corexit 9500, however, dispersed both MESA and ANS to small sizes ($< 70 \mu\text{m}$) under all three wave conditions.

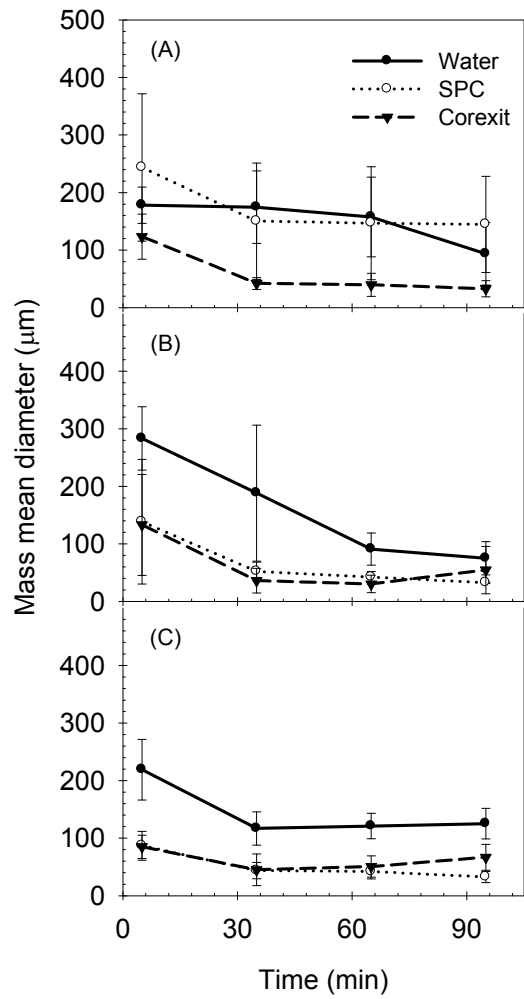


Figure 12: Dispersed MESA oil droplet size (volume mean diameter) as a function of time under: (A) regular non-breaking, (B) spilling breaking, and (C) plunging breaking wave conditions.

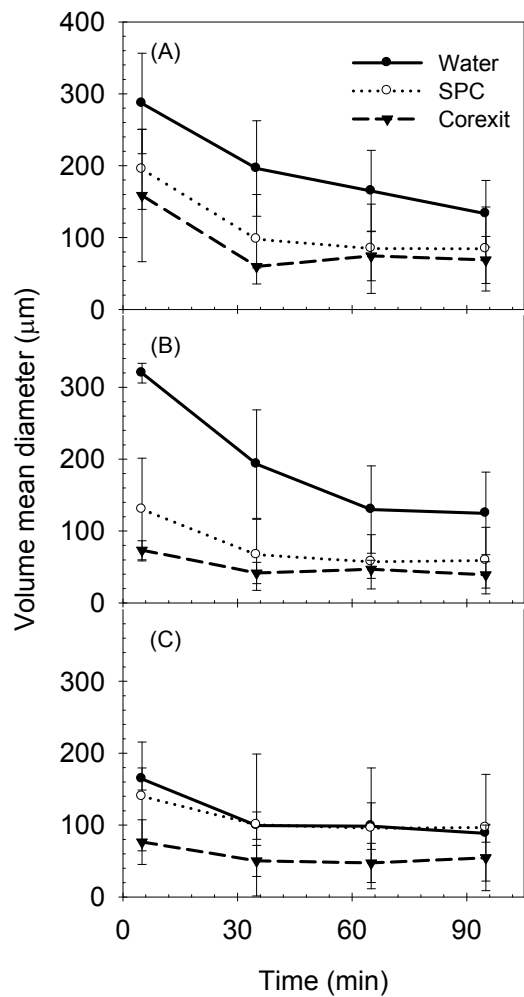


Figure 13: Dispersed ANS oil droplet size (volume mean diameter) as a function of time under: (A) regular non-breaking, (B) spilling breaking, and (C) plunging breaking wave conditions.

A five-way analysis of variance (ANOVA) was performed to test the factorial effects on the average VMD by: (1) wave condition, (2) dispersant type, (3) oil type, (4) dispersion time, and (5) measuring depth. Among these factors, testing of dispersion time allows for the identification of a minimum duration that is required for dispersion of oil into relatively stable average droplet sizes. The effect of water depth was tested to evaluate the spatial variation in the dispersed droplet sizes. The ANOVA results are presented in Table 7. As expected, the high-order interactions (all four- and five-factor and all but one three-factor interactions) are insignificant ($p > 0.25$). There was one significant three-factor interaction (dispersant*oil*wave, $p = 0.000$) and four significant two-factor interactions (depth*time, $p = 0.041$; oil*wave, $p = 0.027$; dispersant*wave, $p = 0.000$; and dispersant*oil, $p = 0.000$), indicating that average dispersed oil droplet size was affected non-uniformly by changes in the interacting variable. Besides the significant multi-factor interactions, three of the five main factors (wave type, dispersant type, and dispersion time, $p < 0.0000001$) were identified to have strong, statistically significant effects on the average dispersed oil droplet sizes. Two other tested main factors did not affect

average droplet sizes significantly: oil ($p = 0.917$) and sampling depth ($p = 0.865$). The significant effects of various factors were further compared at each treatment level with the Tukey's paired comparison test. The results are summarized in Table 8. The two dispersants significantly reduced the dispersed oil droplet size, with the average VMD being reduced by 91.5 μm by Corexit 9500 and 36.6 μm by SPC 1000. The plunging wave conditions significantly reduced the average dispersed droplet size by 35.7 μm . The average dispersed oil droplet sizes declined significantly by 42 μm between the first and second dispersion period. The differences in the average dispersed oil droplet sizes after 30 min were statistically insignificant ($p > 0.05$).

Table 7: Factorial analysis of variance of the effects on the average water column dispersed oil droplet sizes. Statistically significant factors are flagged with *.

	Df	Sum of Sq	Mean Sq	F Value	Pr(F)
Dispersant	2	915,915	45,7957.5	118.6329	0.0000 *
Oil	1	42	42.0	0.0109	0.9169
Wave	2	185,989	92,994.7	24.0901	0.0000 *
Depth	2	1,124	561.8	0.1455	0.8650
Time	3	338,033	112,677.7	29.1889	0.0000 *
Dispersant:Oil	2	75,480	37,740.2	9.7765	0.0001 *
Dispersant:Wave	4	84,215	21,053.8	5.4539	0.0003 *
Oil:Wave	2	28,265	14,132.4	3.6610	0.0265 *
Dispersant:Depth	4	12,944	3,235.9	0.8383	0.5014
Oil:Depth	2	5,011	2,505.5	0.6491	0.5231
Wave:Depth	4	18,572	4,643.0	1.2028	0.3089
Dispersant:Time	6	47,433	7,905.6	2.0479	0.0582
Oil:Time	3	1,777	592.5	0.1535	0.9274
Wave:Time	6	47,863	7,977.1	2.0665	0.0560
Depth:Time	6	51,246	8,541.0	2.2125	0.0409 *
Dispersant:Oil:Wave	4	306,795	76,698.9	19.8687	0.0000 *
Dispersant:Oil:Depth	4	20,321	5,080.3	1.3160	0.2631
Dispersant:Wave:Depth	8	25,722	3,215.3	0.8329	0.5739
Oil:Wave:Depth	4	10,791	2,697.8	0.6989	0.5931
Dispersant:Oil:Time	6	10,436	1,739.3	0.4506	0.8446
Dispersant:Wave:Time	12	29,459	2,455.0	0.6359	0.8117
Oil:Wave:Time	6	1,642	273.7	0.0709	0.9986
Dispersant:Depth:Time	12	15,634	1,302.8	0.3375	0.9820
Oil:Depth:Time	6	3,360	559.9	0.1450	0.9900
Wave:Depth:Time	12	9,548	795.7	0.2061	0.9982
Dispersant:Oil:Wave:Depth	8	11,042	1,380.3	0.3576	0.9422
Dispersant:Oil:Wave:Time	12	19,691	1,640.9	0.4251	0.9535
Dispersant:Oil:Depth:Time	12	6,975	581.3	0.1506	0.9996
Dispersant:Wave:Depth:Time	24	45,060	1,877.5	0.4864	0.9820
Oil:Wave:Depth:Time	12	17,553	1,462.8	0.3789	0.9707
Dispersant:Oil:Wave:Depth:Time	24	20,595	858.1	0.2223	1.0000
Residuals	432	1,667,645	3,860.3		

Table 8: Tukey’s paired comparison of the different effects between treatment levels on the average dispersed oil droplet size in the water column. Significant differences are flagged by * based on 95% simultaneous confidence intervals for specified linear combinations.

Factor	Level mean (µm)	Difference estimates	Standard error	Lower limit	Upper limit
Dispersant	Water 152.9	Corexit-SPC = -54.9 *	5.98	-69.0	-40.9
	Corexit 61.4	Corexit-Water = -91.5 *	5.98	-106.0	-77.4
	SPC 116.3	SPC – Water = -36.6 *	5.98	-50.6	-22.5
Wave	Regular 121.9	Plunger-Regular = -35.7 *	5.98	-49.7	-21.6
	Spiller 122.4	Plunger-Spiller = -36.2 *	5.98	-50.3	-22.2
	Plunger 86.2	Spiller – Regular = 0.566	5.98	-14.6	13.5
Time ^a	P1 148.5	P2 – P1 = -41.9 *	6.9	-59.7	-24.1
	P2 106.6	P3 – P1 = -53.5 *	6.9	-71.3	-35.7
	P3 94.9	P4 – P1 = -57.7 *	6.9	-75.5	-39.9
	P4 90.8	P3 – P2 = -11.7	6.9	-29.5	6.2
		P4 – P2 = -15.8	6.9	-33.6	2.0
		P4 – P3 = -4.13	6.9	-21.9	13.7
Depth	Surface 112.0	Middle-Surface = -3.00	5.98	-17.1	11.1
	Middle 109.0	Bottom-Surface = -2.53	5.98	-16.6	11.5
	Bottom 109.5	Bottom-Middle = 0.47	5.98	-13.6	14.5
Oil	MESA 109.9	ANS-MESA = 0.51	4.88	-9.1	10.1
	ANS 110.4				

^a Time factor is expressed as P1, P2, P3, or P4 to denote the first, second, third and fourth half-an-hour of measurement period. Within the same time period, the measurements in the middle and the bottom of the tank are 10 and 20 min later than those at the surface, respectively.

4.3. Chemical dispersant effectiveness testing in the flow-through wave tank

4.3.1 Effects of dispersant and wave conditions on oil dispersion effectiveness

The effectiveness of dispersants under different wave conditions with currents was evaluated by monitoring spatial and temporal oil distribution in the flow-through wave tank. Figures 14 and 15 show the representative dispersed MESA and ANS oil concentrations, respectively, as a function of time in the middle depth (75 cm below the surface) at a location 10 m downstream from the initial slick. The dispersed oil concentration at mid-depth increased rapidly (within 5-10 min) and then decreased steadily due to the dilution effect of the current. The effects of wave

conditions and dispersants are also clearly evident: dispersants increased oil concentrations several-fold under both regular and breaking wave conditions, with the breaking waves creating much higher oil concentrations than regular non-breaking waves. Similar oil distribution profiles were observed and recorded for the other sampling locations and depths within the test facility, with variability in oil concentrations and the time for the peak oil concentrations to occur (data not shown). To compare the effects of dispersant type and wave conditions on oil dispersion in this dynamic environment, the time-series oil concentrations at each sampling position (horizontal location and depth) were converted to an equivalent oil concentration that had the same flux of oil as the time-dependent oil concentrations over the experimental period (one hour).

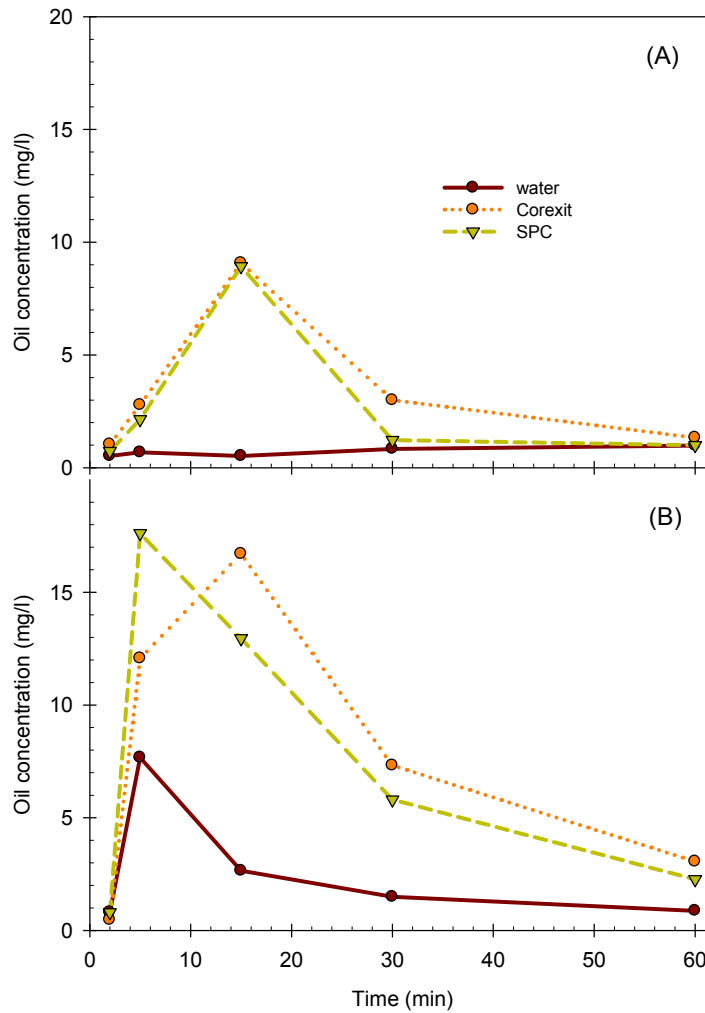


Figure 14: Dispersed MESA oil concentration as a function of time in the middle of the tank 10m downstream under: (A) regular wave, and (B) breaking wave conditions

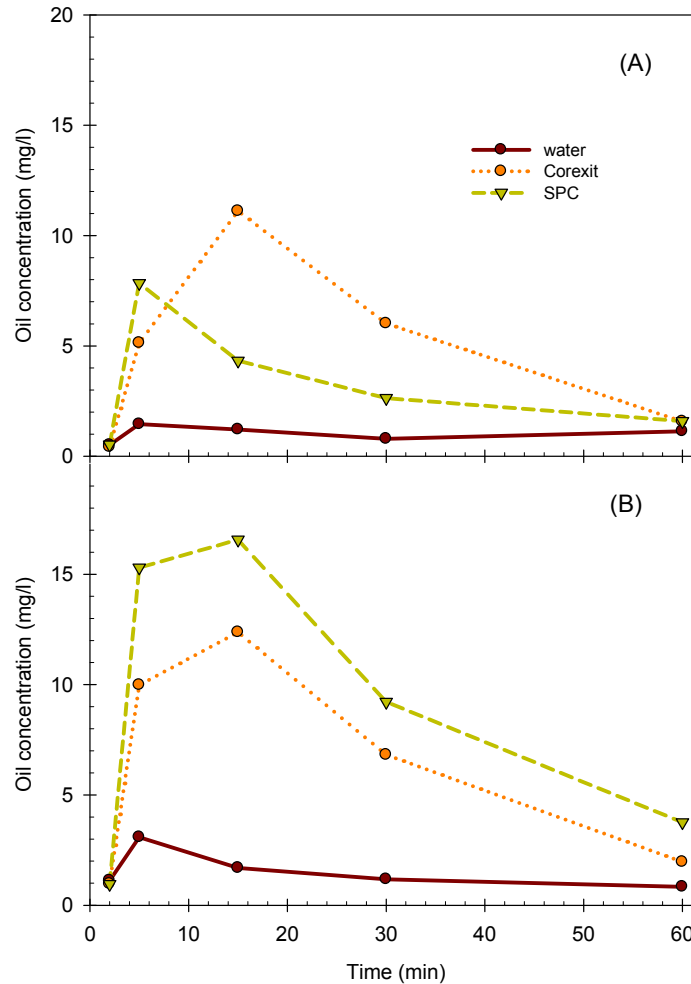


Figure 15: Dispersed ANS oil concentration as a function of time in the middle of the tank 10m downstream under: (A) regular wave, and (B) breaking wave conditions.

Figures 16 to 18 summarize the equivalent oil concentration at different horizontal locations and depths. The upstream (2m from the oil addition) location had consistently low oil (MESA or ANS) concentrations (about 1 mg/l) at all three depths for all dispersant types and wave conditions (Figures 16-18, A), where the effects of wave conditions and dispersants were insignificant for the dispersed oil concentrations ($p > 0.05$). Low oil concentrations (about 1 to 2 mg/l) were also observed at the bottom of the wave tank at three downstream locations (Figure 18, B-D), and the effects of wave conditions and dispersant type on oil concentrations at these spots were also insignificant ($p > 0.05$). The insignificant effects of dispersant type and wave conditions were likely due to the strong current flow, which counteracted turbulent diffusion of oil, resulting in lower water column oil concentrations at all depths upstream and the bottom of the downstream locations.

Dramatic effects of dispersants on oil distribution are evident from oil concentrations at the

surface and in the middle of the wave tank at the downstream locations (Figures 16C-16D and 17C-17D). Dispersants significantly ($p < 0.05$) increased oil concentration in the middle of the wave tank (Figure 17C-17D), indicating that dispersants enhanced penetration of oil into the water column. Dispersants also increased ($p = 0.05$) the surface oil concentration at 6m downstream location (Figure 16C), indicating that dispersants stimulated horizontal spreading of oil. These effects are observed under both regular non-breaking and breaking wave conditions, but the extent appeared stronger under breaking waves. This is consistent with the batch system wave tank experimental results, showing that Corexit 9500 was effective in low, moderate and higher energy conditions, whereas SPC 1000 worked better in moderate and higher energy conditions (Venosa et al. 2008). Although the effectiveness of the two dispersants was significantly different in the batch system, the difference was insignificant ($p > 0.05$) in the flow-through system (Figures 16 to 18). This may be due to the fast dilution of dispersed oil in the flow-through system to prevent re-coalescence of the dispersed oil droplets, particularly for the water-soluble dispersant SPC 1000.

The effect of wave conditions on oil distribution is clearly demonstrated by the measured oil concentrations at the surface of the 10 m downstream location (Figure 16D). The measured oil concentrations under regular waves were substantially higher than under plunging breaking wave conditions, indicating that breaking waves are more effective in transferring oil from the surface deeper into the water column. The effect of breaking waves is related to a series of contributing factors. During the breaking of waves, it has been estimated that 30% to 50% of the dissipated wave energy entrains the oil droplets in the water column (Lamarre and Melville 1991; Tkalich and Chan 2002). This energy determines the first-order oil entrainment rate (Tkalich and Chan 2002). Breaking waves develop a mixing layer in the upper part of the water column, and the penetration of oil results in a uniform mixing of the droplets, with the mixing layer proportional to the height of breaking waves (Delvigne and Sweeney 1988; Tkalich and Chan 2002). Moreover, breaking waves generate micro-scale turbulence with the smallest eddies that have the greatest velocity gradients, resulting in deformation, elongation and eventually breakup of larger droplets (Delvigne et al. 1987; Li and Garrett 1998).

When the oil slick was dispersed into small droplets and conveyed into the water column, the plume was consequently carried away from the mixing zone through current movement and dilution in the water column. In the field, the dispersed oil droplets are eventually removed via accelerated biodegradation and other routes of natural attenuation. The rapid dilution of oil from the central mixing zone is desired for minimizing exposure of pelagic species, for their biological effects from exposure to petroleum hydrocarbon compounds are proportional to the intensity and the duration of exposure time. The effects of dispersants and wave conditions on the dynamic dispersion effectiveness (DDE) of the dispersed oil within the experimental duration can be evaluated by computing the fraction of dispersed oil flowing out of the wave tank with the effluent current plume and the residual dispersed oil in the water column of the water tank at the end of each experiment. In this regard, the flow-through wave tank can be viewed as a vessel in which mixing by the surface regular non-breaking waves or irregular breaking waves is coexistent with the plug flow of the uniform currents. Mixing by waves caused the deviation of the flow pattern from an ideal plug flow of currents.

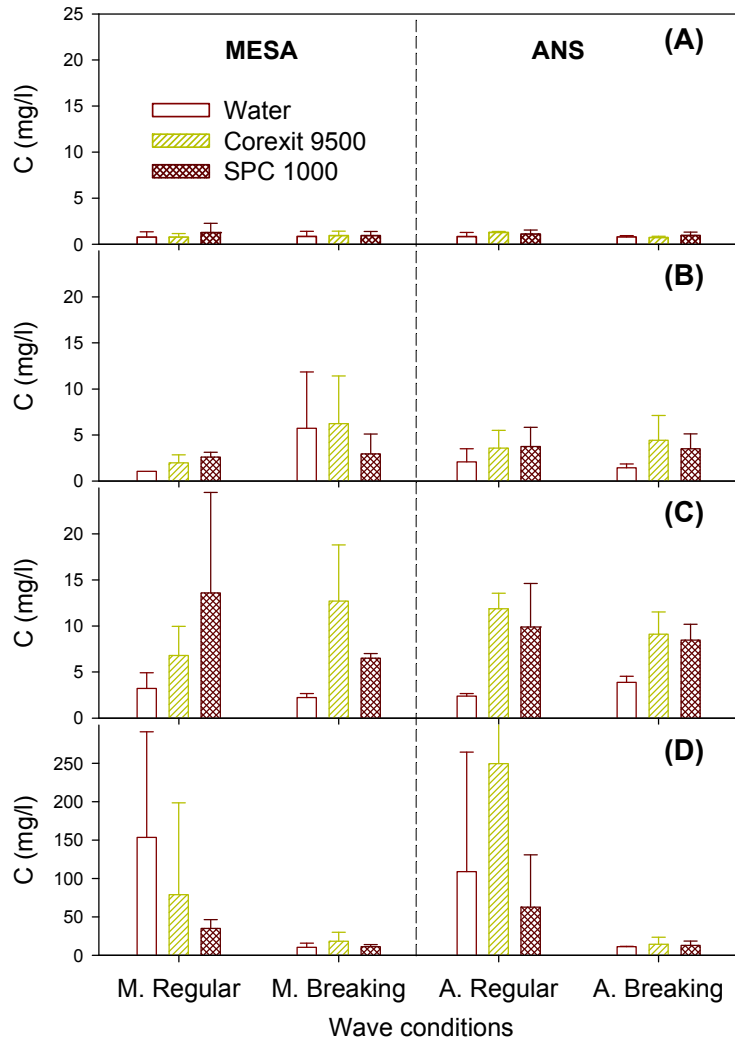


Figure 16: Equivalent dispersed oil concentrations at the surface of the wave tank at four different horizontal locations for the two tested crude oils: (A) 2m upstream; (B) 2 m; (C) 6 m; and (D) 10 m downstream. Note the different Y-axis scale for (D).

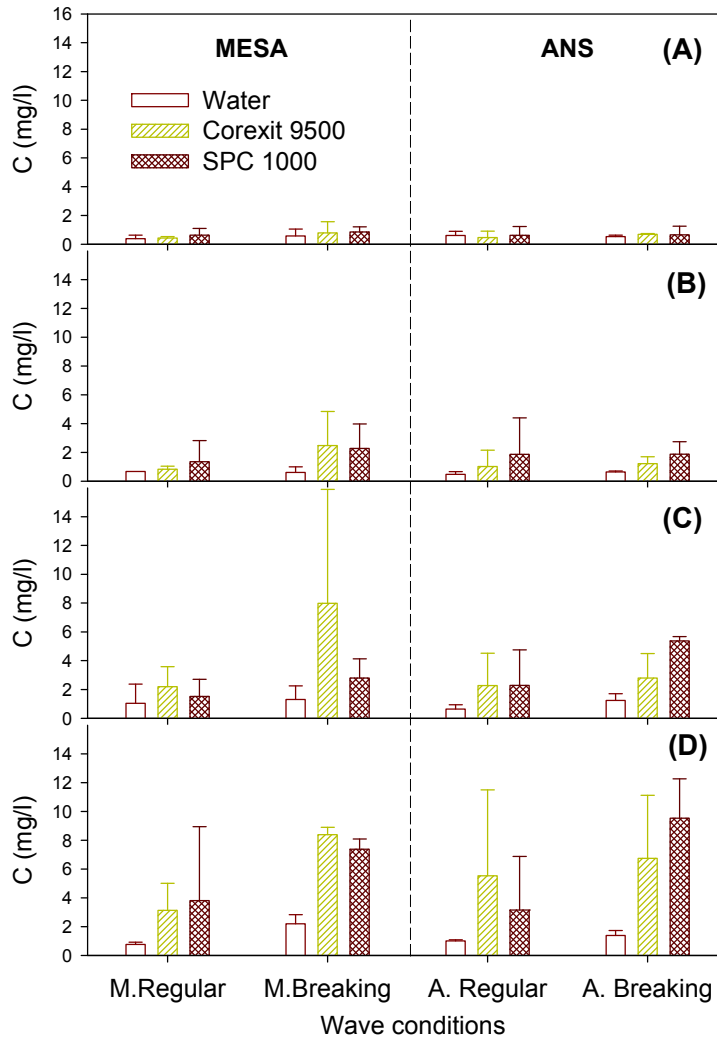


Figure 17: Equivalent dispersed oil concentrations in the middle of the wave tank at four different horizontal locations for the two tested crude oils: (A) 2m upstream; (B) 2 m downstream; (C) 6 m downstream; and (D) 10 m downstream.

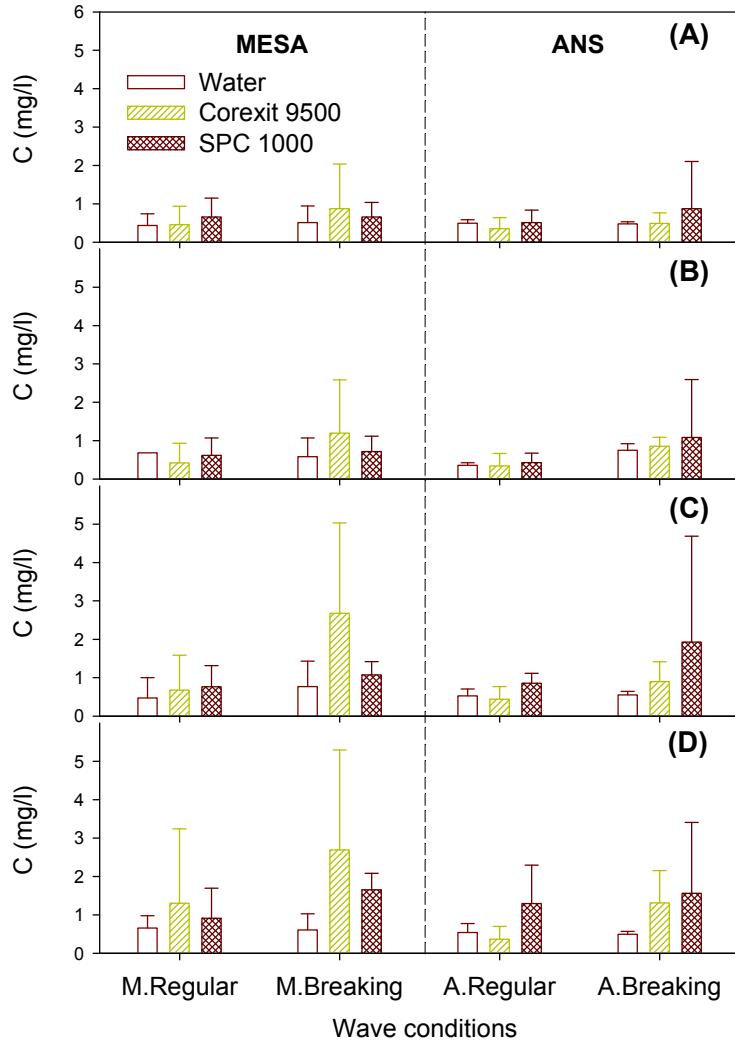


Figure 18: Equivalent dispersed oil concentrations at the bottom of the wave tank at four different horizontal locations for the two tested crude oils: (A) 2m upstream; (B) 2 m downstream; (C) 6 m downstream; and (D) 10 m downstream.

Figure 19 presents the estimated DDE of the MESA and ANS oils as a result of physical and chemical dispersion under the two wave conditions. For physical dispersion of MESA (Fig. 19A) under regular wave conditions, the DDE in the water column was 8% under regular waves but increased to 19% under breaking waves. The application of Corexit 9500 or SPC 1000 increased the DDE to 22% and 30% respectively under regular wave conditions. The combination of chemical dispersants and breaking wave conditions increased DDE to more than 56% and 46%, respectively, with Corexit 9500 and SPC 1000. Statistical ANOVA indicated both chemical dispersants ($p = 0.02$) and breaking waves ($p = 0.01$) significantly increased the DDE of MESA dispersion, but there was no significant difference between Corexit 9500 and SPC 1000 ($p = 0.96$). Similarly, dispersants ($p = 0.02$) significantly increased the DDE of ANS in the water

column (Fig. 19B) but no significant difference was found between Corexit 9500 and SPC 1000 ($p = 0.76$). Physical dispersion of ANS under regular wave and breaking wave conditions resulted in DDE in the water column to be 10% and 12%, respectively. Chemical dispersion by Corexit 9500 significantly increased DDE to 36% under regular wave conditions, and to 42% under breaking wave conditions. Dispersion by SPC 1000 increased the DDE to 25% under regular wave conditions and to 62% under plunging breaking wave conditions. Although breaking wave conditions were always associated with higher DDE of ANS, ANOVA indicated that the wave effect was insignificant ($p = 0.13$), due primarily to the relatively large error bars of triplicate runs but could also be attributed to the higher dispersibility of fresh ANS versus weathered MESA crude oil. The inhibition of dispersant effectiveness by increased weathering status of crude oil was reported in many studies (Chandrasekar et al. 2005; Moles et al. 2002; Nordvik 1995; White et al. 2002).

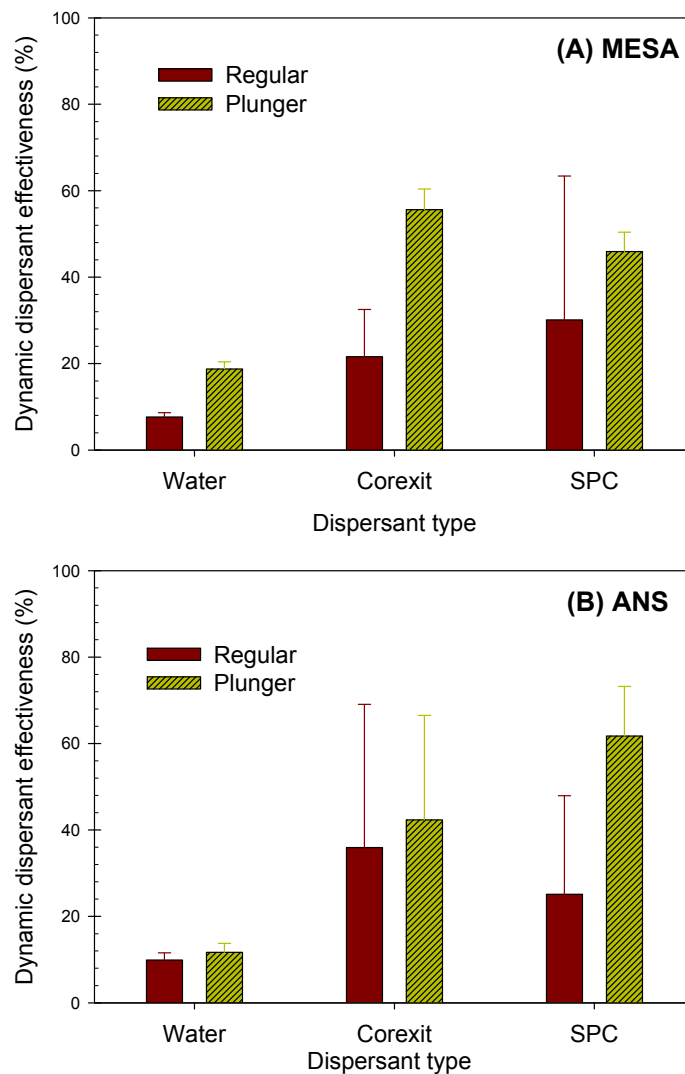


Figure 19: Dispersant effectiveness as a function wave conditions on: (A) MESA; (B) ANS. Data shown are average with one standard deviation of three independent replicate runs.

4.3.2 Effects of dispersant and wave conditions on droplet size distribution

Dispersant effectiveness is ultimately determined by the dispersed oil droplet size distribution (Darling et al. 1990; Lewis et al. 1985). Small droplets with sizes of tens of microns have small rise speeds and tend to remain suspended in the water column and become widely dispersed in the water column by turbulent diffusion and can be potentially removed more rapidly by biodegradation (Li and Garrett 1998). Conversely, large oil drops with radii of hundreds of microns tend to re-coalesce and resurface unless very strong mixing energy exists to overcome their buoyancy. Therefore, smaller droplets are much more favorable from the prospective of oil spill mitigation. Laboratory and field measurements suggest that for an effective dispersion of oil in which the dispersed oil droplets remain suspended in the water column, average droplet sizes have to be less than 50 to 70 μm (Lunel 1993; Lunel 1995).

In this work, the dispersed oil droplet size distribution was measured by a laser particle counter (LISST-100X) that was suspended in the water column at the end of the flow through wave tank. The dispersed oil droplet size distribution was recorded continuously as a function of time in real-time mode. The recorded size distribution at each snapshot was in the mono-modal logarithmic normal distribution for the physically dispersed oil and multi-modal log-normal distribution for the chemically dispersed oil (data not shown). These oil distribution patterns are consistent with the dispersed particle size distributions that were observed in the batch system wave tank experiments on chemical dispersant effectiveness testing (Li et al. 2008b). To compare the effects of wave conditions and dispersant type on the average dispersed oil droplet size distribution in the water column, we calculated the volumetric mean diameter (VMD) of the dispersed oil.

Figures 20 and 21 summarize the effect of dispersant type and wave energy on the average dispersed oil droplet VMD for MESA and ANS, respectively. The droplets started at the same VMD level regardless of dispersant and wave conditions. In the absence of chemical dispersant (Fig. 20A, 21A), the oil droplet sizes remained large and highly variable (VMD \sim 150-400 μm) under the regular wave condition, but were rapidly reduced in size and variability (VMD \sim 150-200 μm) under breaking wave conditions. In the presence of chemical dispersant Corexit 9500 (Fig. 20B, 21B), the dispersed oil droplet sizes remained large but considerably reduced in variability (VMD \sim 300 μm) under regular wave conditions; these sizes were dramatically reduced (VMD \sim 50 μm) under breaking wave conditions within 10 min, and maintained at this small size for the rest of the experiment. SPC 1000 rapidly dispersed oil droplets (VMD of approximately 75-100- μm) under both regular and breaking wave conditions (Fig. 20C, 21C). The sizes persisted or slightly increased afterwards under regular wave conditions, probably due to re-coalescence and resurfacing after the depletion of water soluble SPC 1000 surfactants by current flow over time. Depletion of surfactants with prolonged mixing of oil in water emulsion stabilized by surfactants was reported in mixing tank system (Sanchez et al. 2001). However, the VMD continually decreased to about 50 μm under breaking wave conditions due to the high energy dissipation rate and turbulent diffusion.

The average size of the physically and chemically dispersed oil agree well with the results of our previous batch experimental studies (Li et al. 2008a; Li et al. 2008b) and those of the literature (Byford et al. 1984; Darling et al. 1990; Lunel 1995). The introduction of current in the flow-

through wave tank, however, did not further reduce oil droplet size from what had been observed in the batch system (Li et al. 2008b). This can be attributed to the similarity of micro-scale turbulence, particularly energy dissipation rates measured during the hydrodynamic characterization of the batch system (Wickley-Olsen et al. 2008) and the flow-through system (unpublished data). The flow pattern, however, was clearly different when the wave tank was changed from the batch to the flow-through mode. In particular, the backflow near the bottom of the wave tank in the batch system was overcome by the forward current in the flow-through system, which purged the smaller dispersed oil droplets that were suspended in the water column out of the wave tank. This reduced the inter-drop collision frequency that would cause re-coalescence and resurfacing of the smaller dispersed oil droplets, while retaining the larger oil droplets floating at the surface to maintain high drop-eddy collision frequency for the breakage of droplets into small particles (Tsouris and Tavlarides 1994). Under breaking waves, however, although the larger droplets surfaced, they were continually broken into smaller droplets because of the high energy dissipation rate, and therefore these droplets were eventually purged downstream.

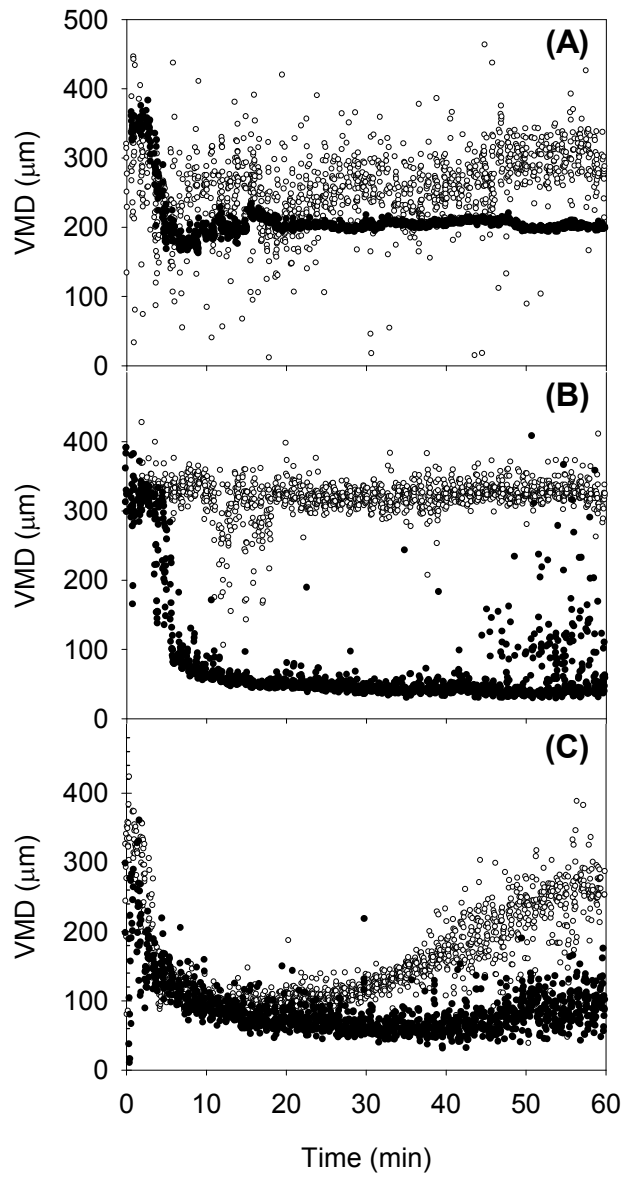


Figure 20: Effect of dispersant type [(A) water; (B) Corexit 9500; and (C) SPC 1000] and wave conditions [regular (open circles) and breaking (solid dots)] on average dispersed MESA oil droplet size.

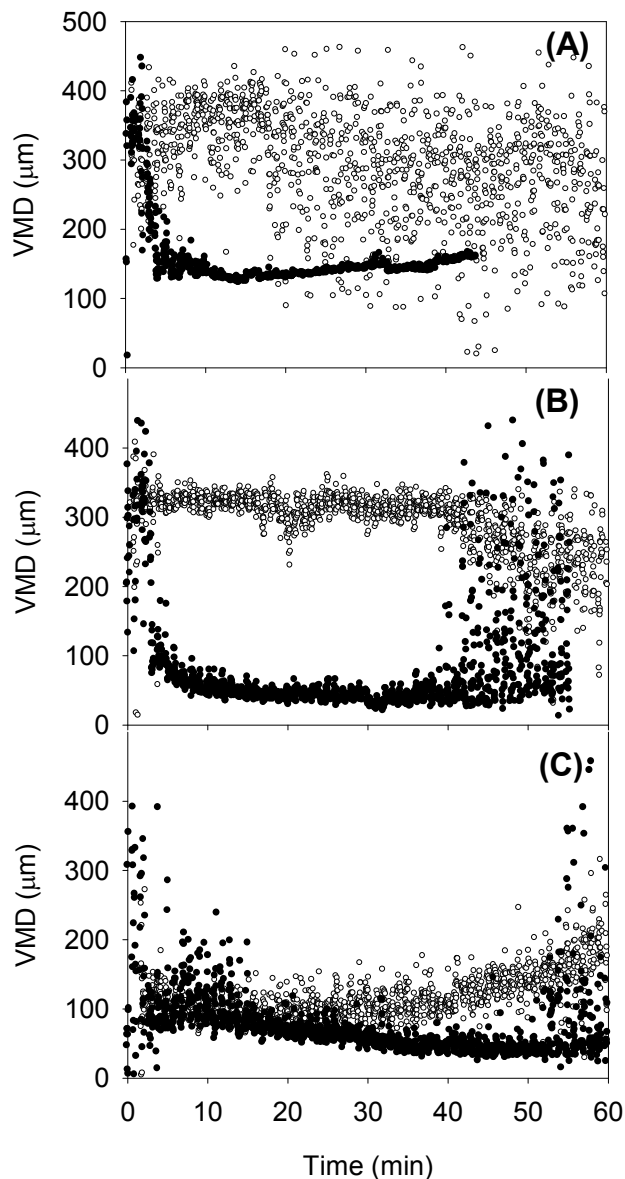


Figure 21: Effect of dispersant type [(A) water; (B) Corexit 9500; and (C) SPC 1000] and wave conditions [regular (open circles) and breaking (solid dots)] on average dispersed ANS oil droplet size.

4.4. In-Situ multiple simultaneous scattering and fluorescence sensor

To overcome the disadvantages of current Special Monitoring of Applied Response Technologies (SMART) such as single wavelength, pump and detection system requirements, large power source requirements, analog readout, limited depth (4m) and outdated software, a novel Wet Labs Environmental Characterization Optics (ECO) triplet sensor (Figure 22) was developed. This device has a suite of advantages, including:

- Small footprint battery
- Performs free space measurement and requires no pump, small footprint, internal battery
- Accommodates a variety of deployment options
- Two (2) fluorescence sensors & one (1) scattering light sensor
- Can operate at depths to 600m
- PC-compatible software package



Figure 22: Wet Labs Environmental Characterization Optics (ECO) triplet sensor.

Fluorescence is a property of some materials in which light is absorbed at specific wavelengths and subsequently emitted at a longer wavelength. The excitation wavelength is the characteristic wavelength that results in an emission of light. WET Labs has pioneered the use of Light Emitting Diodes (LEDs) in fluorimeters. Fluorescence Wavelength: Chlorophyll EX/EM 470/695 nm; CDOM EX/EM 370/460 nm. The volume scattering function (VSF) describes the directional dependence of this scattering. The VSF of particles depends on their size, shape, and internal index of refraction distribution. It has been determined that the backscattering coefficient is proportional to the light scattering at 117 degrees. Estimate of total turbidity Scattering Wavelength: 660 nm.

Weathered Alaskan North Slope crude oil was dispersed at various concentrations and monitored using the Wet Labs Environmental Characterization Optics (ECO) Triplet Sensor. Observation of potential interferences and instrument operational ranges were investigated in a modified standard jar test (40L). Oil was dispersed using a variable-speed (20-200 rpm) Lightnin® Mixer with a stainless steel mixing impeller. Wet Labs ECO 3 Triplet mounted directly in the reactor, at Scattering Wavelength: 660 nm; Fluorescence Wavelength: Chlorophyll EX/EM 470/695 nm, CDOM EX/EM 370/460 nm. Corexit® 9500 was pre-mixed with the oil and applied at 20:1 ratio (v/v) using synthetic seawater (Instant Ocean) at 32ppt at 20°C and the TPH oil concentrations of 3000, 5000, 12000, 22000, 48000, and 70000 ppb by adding specific amounts of stock solution to the reactor. The mixer was operated at 50-75 rpm (to reduce air bubbles). A

sampling frequency of one reading per second was selected. The system was allowed to equilibrate for five minutes, and the raw count data from ECO 3 Triplet were collected using Windows Hyper-terminal software at each concentration at three separate events.

The results indicated that CDOM fluorescence was linear over the entire TPH concentration range (3,000-70,000 ug/L, $R^2=0.9896$). Chlorophyll fluorescence linearity covered a narrow TPH concentration range (3,000-20,000 ug/L, $R^2=0.9686$). Backscattering (660 nm) was linear over the entire TPH concentration range (3,000-70,000 ug/L, $R^2=0.9654$). CDOM fluorescence and backscattering (660 nm) proved to be most effective over broad concentration range. Results also showed good correlation between fluorescence and GC-MS (TPH) values, indicating that the unit is a useful tool for measuring chemically dispersed oil in nearshore marine environments. The in-situ fluorometer is capable of accurate detection of oil plumes in natural environments, and its ease of use (i.e. solid state, no field calibration) and simplified and fast deployment is a benefit to spill response community.

5.0 Discussion and Importance to Oil Spill Response/Restoration

The data presented here have demonstrated the significant effects of dispersant type, wave type and dispersion time on chemical dispersant effectiveness. Testing chemical dispersant effectiveness in wave tanks must have a careful control of hydrodynamic conditions, oil type and dispersion time to ensure the results are comparable. These quantitative data also suggest that interpretation of laboratory and wave tank chemical dispersant effectiveness testing data in the field must consider field operational conditions and environmental factors. This study demonstrated the quantitative relationship between chemical dispersant effectiveness and energy dissipation rate when the effects of two dispersants on two crude oils were evaluated under three different wave conditions in an experimental wave tank. The mixing energies of these wave conditions were close to those encountered in the field when oil spills are treated with chemical dispersants. The data reported here support the importance of breaking wave conditions in facilitating chemical dispersant effectiveness (Delvigne and Sweeney 1988; Li et al. 2008a; Nilson et al. 1985; Shaw 2003; Tkalic and Chan 2002). The oil-based dispersant, Corexit 9500, was more effective than the water-soluble dispersant, SPC 1000, in dispersing the two crude oils under all three wave types and energy levels. More studies are needed to evaluate dilution effects on the performance of these dispersants. These results together with the oil droplet size distribution data (Li et al. 2008b) will be used in developing better operational guidelines (document in preparation by Lee and Merlin for IMO) for dispersant use and improved predictive models of dispersant effectiveness for the field.

In-situ dispersed oil droplet size distribution is governed by a number of factors, including mixing energy, dispersant application and dispersant type, oil type and weathering status, and seawater temperature and salinity. Among these factors, breaking waves have been documented to play a crucial role in dispersion of oil slicks by generating velocity shear to break up and transport oil in turbulent flow (Li and Garrett 1998; Shaw 2003; Tkalic and Chan 2002). The effects of mixing energy on dispersed oil droplet size distributions and consequently dispersant effectiveness have been reported in laboratory tests (Byford et al. 1984; Chandrasekar et al. 2005; Lewis et al. 1985; Ma et al. 2008; Sorial et al. 2004a) and in field trials under low and high

energy regimes caused by various wind effects (Lunel 1993; Lunel 1995). In this study, the effect of wave-generated mixing energy on the dispersed oil droplet size distribution was examined under three wave conditions with different energy dissipation rates. The average energy dissipation rates were estimated to be approximately 0.005, 0.1, and 1 $\text{W}\cdot\text{kg}^{-1}$ near the surface at the mixing zone for regular non-breaking waves, spilling breaking waves and plunging breaking waves, respectively. The energy dissipation rates declined exponentially to approximately 0.001 $\text{W}\cdot\text{kg}^{-1}$ for the two breaking wave conditions at a depth of 30 cm and decreased linearly under regular non-breaking wave conditions (Wickley-Olsen et al. 2008). The energy dissipation rate of plunging breaking waves was similar to those measured for breaking waves in the field (Delvigne and Sweeney 1988; Drennan et al. 1996; Terray et al. 1996). Regular non-breaking wave energy was also similar to that reported on the sea surface by Delvigne and Sweeney (1988), and the energy level of spilling breakers was in between. These wave conditions were identified to have significant effects on the droplet size distributions and average droplet size. As a result, dispersant effectiveness for different oil and chemical dispersant combinations was found to be directly correlated to the energy dissipation rate of the three different wave conditions. Even in the absence of dispersants, physical dispersion under plunging breaking wave conditions over an extended period of time generated a large amount of oil droplets suspended in the water column, leading to physical dispersion efficacy of MESA and ANS crude to be approximately 20%. Correspondingly, the observed median droplet size was about 48 μm and more than 90% oil droplets were < 70 μm , a size which Lunel (1995) suggested would remain permanently dispersed in the water column at sea.

The data presented here demonstrated that the application of chemical dispersants substantially altered the dispersed oil droplet size distributions in the wave tank by creating wider range multi-modal size distributions including a large number of small droplets < 10 μm in diameter and significantly reduced the average VMD. Dispersants tested in our system also significantly stimulated the initial oil break up kinetic rate and extent. The influence of chemical dispersants in increasing the number of small droplets in the water column was reported in laboratory tests (Byford et al. 1984; Jasper et al. 1978; Lewis et al. 1985) and field trials (Lunel 1993; Lunel 1995). Jasper et al. (1978) observed that the VMD of dispersed oil was reduced by 30-40% by the presence of a chemical dispersant. Lunel (1995) reported that dispersants increased the number of small droplets (<50 μm) by 5- to 30-fold in a sea trial, but the number of larger droplets (>50 μm) between the dispersant-treated and untreated oil were the same.

A significant difference in the average dispersed droplet sizes was identified between the two tested chemical dispersants, Corexit 9500, an oil-based chemical dispersant, and SPC 1000, a water-based dispersant. The apparent superiority of the oil-based dispersant is probably due to its stronger affiliation with oil in the course of oil dispersion, whereas the water-based dispersant tends to be washed away from the surface of oil droplets over a longer period of time, resulting in re-coalescence and resurfacing of the dispersed oil droplets in less vigorously mixed areas. The rearrangement of surfactant-stabilized oil-in-water emulsions has been reported and was explained as a result of the development of a surfactant depletion-flocculation process (Sanchez et al. 2001).

The significant factors affecting average VMD are in good agreement with those having significant effects on DE that has been evaluated by measurement of the dispersed oil

concentration in the water column. For instance, the effects of Corexit 9500 and SPC 1000 on reducing the average VMD from 153 to 61 (or by 92) and 116 (or by 37) μm , respectively, were correspondingly correlated with their significant effects on increasing the DE by 48% and 26%, respectively. The significant effect of the plunging breaking wave conditions on reducing the average VMD from 122 to 86 (or by 36) μm matched the significant effect of increasing the DE by 25%. In addition, dispersion time was found to significantly decrease the average VMD from 148 to 106 (or by 42) μm and increase the DE by 18% during the first 30 min of dispersion. Such good correlation can be explained by the enhanced DE by dispersants and breaking waves through increasing the fraction of droplets that are more “permanently” dispersed (e.g., $< 70 \mu\text{m}$) in the water column. While reduction of oil-water interfacial tension by chemical dispersants allows for turbulent shears to form droplets on the order of 10 μm , the plunging breaking waves are associated with elevated energy dissipation rates and a lower Kolmogorov scale that reduces the droplet sizes.

Not surprisingly, oil dispersion time is a significant factor in dispersion of crude oils in the wave tank. Initial breakup kinetic rates suggested that the presence of dispersants clearly accelerated the breakup process (Table 4). As a result, chemical dispersion broke up oil into relatively stable droplet size distributions within a short period (~ 30 min), whereas physical dispersion took much longer to reach the ultimate droplet size distributions (Figures 9-13, Tables 6-8). The length of time required to disperse oil into relatively stable droplet size distributions, either in the presence or absence chemical dispersants, is dependent on the system hydrodynamics, especially the intensity and frequency of occurrence of breaking waves. A previous wave tank study conducted with less frequently occurring plunging breaking waves with lower wave energies (Li et al. 2008a) showed that active breakup of oil into smaller droplets continued beyond one hour.

Understanding *in-situ* dispersed oil droplet size distribution has significant implications in optimizing DE testing protocols in systems ranging from small-scale laboratory testing apparatuses to large-scale field trials. Clearly, due to the limitation of the scales, it would be unrealistic to extrapolate the observed droplet size distribution from a bench-scale testing apparatus to the field. To maintain the amount of oil and dispersant that can be precisely measured during standardized laboratory operations, the oil-to-water ratio would have to be much higher than what would be expected in the field, leading to higher oil loading and arbitrarily increased likelihood of re-coalescence and resurfacing of physically and/or chemically dispersed oil droplets (Fingas 2005; Fingas et al. 2002). Wave tank testing of chemical dispersant effectiveness significantly improved development of a testing protocol in regard to more realistic wave-generated mixing energy, which is scalable to the field given careful hydrodynamic characterization. In addition, the oil-to-water ratio is similar to that encountered in the field, resulting in a dispersed phase loading lower than the threshold concentration by which significant re-coalescence of small oil droplets may occur.

From an oil spill response operational point of view, formation of small oil droplets is favorable for mitigation of oil spills on water. The generation of a large number of small dispersed oil droplets is a clear indication of highly effective oil dispersion (Lunel 1993; Lunel 1995). Oil droplets with radii of tens of μm tend to gain sufficient energy to overcome the buoyancy and therefore penetrate deeper into the water column, spread more rapidly (Basheva et al. 1999), and are subject to accelerated biodegradation due to the increased oil-water interfacial area where

most of the microbial oil degradation occurs (Macnaughton et al. 2003; Swannell and Daniel 1999). However, chemical dispersion of oil into smaller droplets may also be more effective at increasing exposure of pelagic and benthic species to chronically toxic concentrations of polycyclic aromatic hydrocarbon compounds (Couillard et al. 2005; Ramachandran et al. 2004). Further research is warranted to evaluate the environmental and ecological risks of using chemical dispersants as an oil spill response at sea, particularly chronic and sublethal impacts of dispersants and chemically dispersed oil on sensitive species.

The effectiveness of two chemical dispersants in dispersing crude oil into the water column as a function of low and high energy waves within an experimental wave tank operated under dynamic flow-through conditions was also evaluated in this study. The data presented demonstrated that the presence of a chemical dispersant under moderately high wave energy conditions significantly increased oil concentration in the water column, reduced dispersed oil droplet size distribution, and accelerated dilution rate of the dispersed oil facilitated by current activity. While breaking wave conditions contribute to the breakup of oil into small droplets due to high energy dissipation rates and enhanced droplet-eddy collision frequency, dispersants may increase the oil breakage efficiency under both regular and breaking wave conditions. We observed initial breakup of the oil slick into small droplets, penetration of the droplets into the water column, and the consequent dilution effect of the current flow during the quantification of dynamic dispersant effectiveness in the water column of the flow-through wave tank. Therefore, the concept of dynamic dispersant effectiveness (DDE) reported here reflects both dispersion of oil into water column and transport and dilution of the dispersed oil droplets through the water column. The DDE reported here might be different from the dispersant effectiveness (DE) obtained in bench-scale jar tests where only the contact efficiency between oil and dispersants is measured in small enclosed surroundings and unlimited collision frequency between oil droplets and eddies may occur, or batch wave tank tests where recirculation of the flow and dispersed oil droplets less rigorous mixing zone may induce re-coalescence and resurfacing of the dispersed oil droplets. Indeed, evaluating the dispersant effectiveness under dynamic flow-through conditions provides a more realistic setting that may be encountered in the field. The established experimental protocol under flow-through conditions in this study will prove useful for evaluating dispersant effectiveness of different chemical dispersant formulations for different oil types under specified wave energy conditions. The obtained data of dispersant effectiveness and particle size distribution as a function of energy dissipation rate provide useful information for developing better operational guidelines for dispersant use and improved predictive models on dispersant effectiveness in the field. The flow-through wave tank system can also be used to conduct environmentally relevant exposure studies on the toxicity of dispersed oil on sensitive marine species.

In summary, the data presented herein clearly demonstrate the importance of the presence of a chemical dispersant in driving surface oil into the water column. The following conclusions of this research will have practical importance to the oil spill response community:

- Dispersant use in deep water environments under moderately energetic wave conditions is a promising countermeasure technology for driving floating oil into the water column and away from water fowl exposure.
- Natural dispersion of oil from the surface into the water column occurs much more readily at high energy dissipation rates compared to low energy dissipation rates. Regular, non-

breaking waves primarily move the oil downstream and the oil remains on the surface of the water.

- Chemical dispersant Corexit 9500 has been shown to be effective in all low, moderate and high energy conditions, whereas SPC 1000 can also be very useful in moderate to high energy conditions. The physical and chemical characteristics of the two dispersants (including surfactant and solvent) may explain the differences between these two dispersants (Corexit 9500 is oil-soluble, whereas SPC 1000 is water-soluble). More basic research is needed to gain a better understanding of the differences in performance.
- Efficacy of oil dispersion in forming small droplets is dependent on wave energy and the presence of a chemical dispersant. If either of those two factors is missing, dispersion can only take place in very high energy sea states.
- Even under high energy breaking wave conditions, use of chemical dispersants drastically reduces the length of time required for thorough dispersion of oil into small oil droplets in the water column, in comparison to natural dispersion by the action of breaking waves alone.
- When the window of opportunity for oil spill response operation is narrow, such as in the event of fast approaching oil patches and/or plumes that pose an imminent threat to shorelines and other sensitive ecosystems, rapid response with chemical dispersants may be deemed necessary even under high energy conditions because of the way in which they accelerate the dispersion of oil into the water column and therefore facilitate faster removal of oil via biodegradation.

6.0 Technology Transfer and Communications

Numerous scientific presentations were made at workshops and conferences attended by members of the oils spill response industry, scientists, academics and environmental regulators. In addition to future in-house applications, the data from this research is being transferred to other research groups involved in the development of predictive numerical models on oil dispersant efficacy. The overall goal of the project is improvement of operational guidelines. In this regard, one of the project PIs (Dr. Kenneth Lee) has agreed to co-chair an international workshop with Francois Merlin (Cedre, France) under the auspices of the International Maritime Organization (IMO) to revise its Operational Guideline for Oil Dispersant Use that is used by the oil spill response community on a global scale.

Furthermore, now that we have validated the application of the wave tank system for studies on oil dispersants, we have created demand for its use in future studies. This includes its use in studies by industry to evaluate the effectiveness of oil dispersants on specific waxy-crude oils found on the Grand Banks of Newfoundland, studies to understand the processes controlling oil-mineral aggregate (OMA) formation funded by MMS, and studies on the toxicity of chemical oil dispersants and oil on various age classes of fish including herring, salmon and cod funded by PWSRCAC and PERD.

This project has supported the development of instrumentation by Drs. P. Kepkay and M.S. Miles for in situ quantification and characterization of oil dispersed in seawater using fluorescence signatures. In particular, Dr. Kepkay's work on the development of UVFS probes has attracted considerable interest from the USCG's SMART Protocol development team.

Our wave tank studies have attracted local (newspapers, etc.), national (DFO website) and international media attention (recent episode of Planet Earth – Discovery Channel).

Presentations include:

Boufadel, M.C., Wickley-Olsen, E., King, T., Li, Z., Lee, K., and Venosa, A.D., 2008. Theoretical Foundation for predicting dispersion effectiveness due to waves. In: *International Oil Spill Conference*. May 4-8, 2008 Savannah, GA.

Boufadel, M.C.*, Li, Z., Lee, K., and Venosa, A.D. 2006. Hydrodynamic characterization of a wave tank facility for the evaluation of oil dispersant effectiveness. Presented at: the 13th Annual International Petroleum Environmental Conference. October 17-20, San Antonio, TX.

Chen, Z., Zhan, C.S., Lee, K., Li, Z., and Boufadel, M.C. 2006. Modeling of oil droplet kinetics under breaking waves. Presented at: the 3rd NATO/CCMS Workshop on Oil Spill Response. October 11-13, Dartmouth, NS.

Kepkay, P., Yeung, C.W., Bugden, J.B.C., Li, Z., and Lee, K. 2008. Ultraviolet Fluorescence Spectroscopy (UVFS): A New Means of Determining the Effect of Chemical Dispersants on Oil Spills. In: *International Oil Spill Conference*. May 4-8, 2008, Savannah, GA.

Lee, K., Li, Z., Kepkay, P., Boufadel, M.C., and Venosa, A.D. 2008. Effects of chemical dispersants on oil-mineral-aggregation in a wave tank. In: *International Oil Spill Conference*. May 4-8, 2008. Savannah, GA.

Lee, K., Li, Z., King, T., Boufadel, M., and Venosa, A.D. (Accepted). Evaluating chemical dispersant efficacy in a flow-through wave tank under regular and breaking wave conditions. Accepted for presentation in the *Interspill'09 Conference and Exhibition*, May 12-14, 2009 Marseille, France

Lee, K., Li, Z., Kepkay, P., Boufadel, M.C., and Venosa, A.D. 2007. Effects of chemical dispersants on oil-mineral aggregation in a wave tank. Presented at the 30th AMOP Technical Seminar (June 5-7, 2007, Edmonton, AB, Canada), Environment Canada, Ottawa, ON, Canada

Lee, K., Boufadel, M.C., and Venosa, A.D. Li, Z., 2006. Wave tank studies for evaluation of dispersant effectiveness and toxicity. Presented at: the 3rd NATO/CCMS Workshop on Oil Spill Response. October 11-13, Dartmouth, NS.

Lee, K.*, Li, Z., Kepkay, P., Boufadel, M.C., and Venosa, A.D. 2006. Formation and transport of oil-mineral aggregates in a wave tank. Presented at: the 13th Annual International Petroleum Environmental Conference. October 17-20, San Antonio, TX.

Li, Z., Lee, K., Kepkay, P., Boufadel, M.C., and Venosa, A.D., 2007. Chemical dispersant effectiveness: oil concentration and droplet size distribution in a wave tank under regular non-breaking and breaking wave conditions. Presented at the 30th AMOP Technical Seminar (June 5-7, 2007, Edmonton, AB, Canada), Environment Canada, Ottawa, ON, Canada

Li, Z., Lee, K., King, T., Boufadel, M.C., and Venosa, A.D., 2007. Wave tank studies on chemical dispersant effectiveness as a function of wave: Implication in spatial and temporal toxicity response. Presented at the 34th Annual Aquatic Toxicity Workshop, September 30 – October 3, 2007 Halifax, NS, Canada).

Li, Z., Lee, K., Kepkay, P., King, T., Boufadel, M.C., and Venosa, A.D. 2006. The application of in-situ laser particle size analysis to monitor the efficacy of chemical oil dispersants. Presented at: the *3rd NATO/CCMS Workshop on Oil Spill Response*. October 11-13, Dartmouth, NS.

Li, Z.*, Lee, K., Kepkay, P., Boufadel, M.C., and Venosa, A.D. 2006. Wave tank studies on dispersant effectiveness as a function of droplet size distribution. Presented at: the *13th Annual International Petroleum Environmental Conference*. October 17-20, San Antonio, TX.

Li, Z., Lee, K., Kepkay, P., Boufadel, M.C., and Venosa, A.D. 2008. Chemical dispersant effectiveness: droplet size distribution as a function of energy dissipation rate. In: *International Oil Spill Conference*. May 4-8, 2008 Savannah, GA.

Miles, S.S., 2006. Real-time Quantitative Measurement of Dispersed and Non-Dispersed Oils Using an In-Situ Multiple Simultaneous Scattering and Fluorescence Sensor. Presented at: the *3rd NATO/CCMS Workshop on Oil Spill Response*. October 11-13, Dartmouth, NS.

Venosa, A.D., Li, Z., Lee, K., Kepkay, P., and Boufadel, M.C., 2006. Wave tank studies on dispersant effectiveness as a function of energy dissipation rate. Presented at: the *3rd NATO/CCMS Workshop on Oil Spill Response*. October 11-13, Dartmouth, NS.

Venosa, A.D., Li, Z., Lee, K., Kepkay, P., and Boufadel, M.C., 2006. Wave tank studies on dispersant effectiveness as a function of energy dissipation rate. Presented at: the *13th Annual International Petroleum Environmental Conference*. October 17-20, San Antonio, TX.

Venosa, A.D., Lee, K., Boufadel, M.C., and Li, Z., 2008. Dispersant effectiveness as a function of energy dissipation rate in a wave tank. In: *International Oil Spill Conference*. May 4-8, 2008 Savannah, GA.

Wickley-Olsen, E., Boufadel, M.C., King, T., Li, Z., Lee, K., and Venosa, A.D., 2008. Regular and breaking waves in wave tank for dispersion effectiveness testing. In: *International Oil Spill Conference*. May 4-8, 2008 Savannah, GA.

Wickley-Olsen, E., Boufadel, M.C., King, T., Li, Z., Lee, K., and Venosa, A.D., 2007. Regular and breaking waves in wave tank for dispersion effectiveness testing. Presented at the 30th AMOP Technical Seminar (June 5-7, 2007, Edmonton, AB, Canada), Environment Canada, Ottawa, ON, Canada

7.0 Achievement and Dissemination

A number of primary publications have directly resulted from this research program:

Botrus, D., M.C. Boufadel, E. Wickley-Olsen, J.W. Weaver, R. Weggel, K. Lee and A.D. Venosa (2008) Wave tank to simulate the movement of oil under breaking waves. Proceedings of the 31st Arctic and Marine Oil Spill Program (AMOP) Technical Seminar on Environmental Contamination and Response. Edmonton Alberta, Canada, June 2-5, 2008. pp. 53-68.

Boufadel, M.C., E. Wickley-Olsen, T. King, T., Z. Li, K. Lee and A.D. Venosa (2008) Theoretical foundation for predicting dispersion effectiveness due to waves. Proceedings of the 2008 International Oil Spill Conference, Savannah, Georgia, USA, May 4-8, 2008. pp. 509-514.

Bugden, J. B. C., C. W. Yeung, P. E. Kepkay, and K. Lee. 2008. Application of Ultraviolet Fluorometry and Excitation-Emission Matrix Spectroscopy (EEMS) to Fingerprint Oil and Chemically Dispersed Oil in Seawater. *Marine Pollution Bulletin*, 56, 677-685

Cole, M. G., King, T. L., and Lee, K. (2007). "Analytical technique for extracting hydrocarbons from water using sample container as extraction vessel in combination with a roller apparatus. *Can. Tech. Rep. Fish. Aquat. Sci.* 2733: vi + 12p."

Kepkay, P.E., C.W. Yeung, J.B.C. Bugden, Z. Li and K. Lee (2008), Ultraviolet Fluorescence Spectroscopy (UVFS): A new means of determining the effect of chemical dispersants on oil spills. Proceedings of the 2008 International Oil Spill Conference, Savannah, Georgia, USA, May 4-8, 2008. pp. 639-644.

Lee, K., Z. Li, P. Kepkay, M.C. Boufadel and A.D. Venosa (2008) Effects of chemical dispersants on oil-mineral-aggregation in a wave tank. Proceedings of the 2008 International Oil Spill Conference, Savannah, Georgia, USA, May 4-8, 2008. pp. 633-638

Lee, K., Z. Li, P. Kepkay, M.C. Boufadel and A.D. Venosa (2008) Wave tank studies on formation and transport of OMA from the chemically dispersed oil. In: *Oil Spill Response: A Global Perspective*, Davidson, W.F., K. Lee and A. Cogswell, A. (eds), NATO Science for Peace and Security Series – C: Environmental Security, Springer Publishing Company. pp. 159-177.

Li, Z., Kepkay, P., Lee, K., King, T., Boufadel, M. C., and Venosa, A. D., (2007), Effects of chemical dispersants and mineral fines on oil dispersion in a wave tank under breaking waves. *Marine Pollution Bulletin*, 54(7): 983-993.

Li, Z., P. Kepkay, M.C. Boufadel, A.D. Venosa and K. Lee (2008). Oil droplet size distribution as a function of energy dissipation rate in an experimental wavetank. Proceedings of the 2008 International Oil Spill Conference, Savannah, Georgia, USA, May 4-8, 2008. pp. 621-626.

Li, Z., Lee, K., Kepkay, P., Boufadel, M.C., and Venosa, A.D. 2008. Chemical dispersant effectiveness: droplet size distribution as a function of energy dissipation rate. In: *International Oil Spill Conference*. May 4-8, 2008 Savannah, GA.

Li, Z., K. Lee, P. Kepkay, T. King, W. Yeung, M.C. Boufadel and A.D. Venosa (2008) Wave tank studies on chemical dispersant effectiveness: Dispersed oil droplet size distribution. In: Oil Spill Response: A Global Perspective, Davidson, W.F., K. Lee and A. Cogswell, A. (eds), NATO Science for Peace and Security Series – C: Environmental Security, Springer Publishing Company. pp. 143-157.

Li, Z., Lee, K., King, T., Boufadel, M.C., and Venosa, A.D. 2008. Assessment of chemical dispersant effectiveness in a wave tank under regular non-breaking and breaking wave conditions. *Marine Pollution Bulletin*, 56, 903-912

Li, Z., Lee, K., King, T., Boufadel, M. C., and Venosa, A. D. (2009). "Evaluating crude oil chemical dispersion efficacy in a flow-through wave tank under regular non-breaking wave and breaking wave conditions." *Marine Pollution Bulletin*, 58, 735-744

Li, Z., Lee, K., King, T., Boufadel, M.C., Venosa, A.D. (In press). "Evaluating oil spill chemical dispersant efficacy in an experimental wave tank: 2, Significant factors determining *in-situ* droplet size distributions." *Environmental Engineering Science*

Li, Z., Lee, K., King, T., Kepkay, P.E., Boufadel, M.C., Venosa, A.D. (In press). "Evaluating oil spill chemical dispersant efficacy in an experimental wave tank: 1, Dispersant effectiveness as a function of energy dissipation rate." *Environmental Engineering Science*

Ma, X., A. Cogswell, K. Lee, Z. Li (2008) Particle size analysis of dispersed oil and oil-mineral aggregates with an automated epi-fluorescence microscopy system. *Environmental Technology*, 29, 737-748.

Venosa, A.D., K. Lee, M.C. Boufadel and Z. Li (2008) Dispersant effectiveness as a function of energy dissipation rate in a wave tank. Proceedings of the 2008 International Oil Spill Conference, Savannah, Georgia, USA, May 4-8, 2008. pp. 777-784.

Wickley-Olsen, E., Boufadel, M.C., King, T., Li, Z., Lee, K., and Venosa, A.D., (2007), Regular and breaking waves in wave tank for dispersion effectiveness testing. Proceedings of: the 30th Arctic and Marine Oilspill Programs (AMOP) Technical Seminar, Edmonton, AB, Canada, 161-187

Wickley-Olsen, E., M.C. Boufadel, T. King, Z. Li, K. Lee and A.D. Venosa (2008), Regular and breaking waves in wave tank for dispersion effectiveness testing. Proceedings of the 2008 International Oil Spill Conference, Savannah, Georgia, USA, May 4-8, 2008. pp. 479-508.

The following publications received indirect benefits (e.g. application of methods/expertise developed) from funding associated with this program:

Chen, Z., C.S. Zhan, K. Lee, Z. Li and M.C. Boufadel (2008). Modeling of oil droplet kinetics under breaking waves. In: Oil Spill Response: A Global Perspective, Davidson, W.F., K. Lee

and A. Cogswell, A. (eds), NATO Science for Peace and Security Series – C: Environmental Security., Springer Publishing Company. pp. 221-236

Davidson, W.F., K. Lee and A. Cogswell, A. (2008), Oil Spill Response: A Global Perspective. NATO Science for Peace and Security Series – C: Environmental Security., Springer Publishing Company. 365 pp.

Hodson, P. V., Khan, C. W., Saravanabhavan, G., Clarke, L., Brown, R. S., Hollebhone, B., Wang, Z., Short, J., Lee, K., and King, T. (2007) Alkyl PAH in crude oil cause chronic toxicity to early life stages of fish. Proceedings of the 30th Arctic and Marine Oilspill Program (AMOP) Technical Seminar, Edmonton, AL, June 4-7, 2007, Environment Canada, pp. 291-299.

Ramachandran, S.D., M.J. Swezey, P.V. Hodson, M. Boudreau, S. Courtenay, T. King, J.A. Dixon and K. Lee (2006) Influence of salinity and fish species on PAH uptake from dispersed MESA crude oil. Marine Pollution Bulletin 52:1182-1189

8.0 Technical Training

This project has provided support and training opportunities to students ranging from high school to graduate students in Canada, the United States of America, and Europe:

Table 9: Student and postdoctoral trainee of this project

Name	Affiliation	Grade Level
Dan Belliveau	Dalhousie University	Undergraduate student
Jennifer Beer	Nova Scotia Community College	Undergraduate student
Venessa Page	Dalhousie University	Undergraduate student
John Niven	Dartmouth High School	High school student
Wolfe Mollin	FRANCE	Undergraduate student
Eric Whitley-Olsen	Temple University	Graduate student
Buffy Ashton	Louisiana State University	Graduate student
William Yeung	DFO/NRC/ McGill University	Doctoral student
Matt Asenault	Dalhousie University	Undergraduate student
Peter Flamming	Dalhousie University /Nova Scotia Community College	Undergraduate student
Jamie Joudrey	Dalhousie University	Undergraduate student
Amanda Hill	Nova Scotia Community College	Undergraduate student

References

- ASTM. (2002). *American Society for Testing and Materials. F2059-00 standard test method for laboratory oil spill dispersant effectiveness using the swirling flask. ASTM 11.04, West Conshohocken, PA. 1536-1539.*
- Basheva, E. S., Gurkov, T. D., Ivanov, I. B., Bantchev, G. B., Campbell, B., and Borwankar, R. P. (1999). "Size dependence of the stability of emulsion drops pressed against a large interface." *Langmuir*, 15(20), 6764-6769.
- Batchelor, G. K. (1970). *The theory of homogeneous turbulence*, Cambridge University Press.
- Byford, D. C., Laskey, P. R., and Lewis, A. "Effect of low temperature and varying energy input on the droplet size distribution of oils treated with dispersants." *The 7th Annual Arctic and Marine Oilspill Program (AMOP) Technical Seminar*, Ottawa, ON, Canada, 208-228
- Camp, T. R., and Stein, P. C. (1943). "Velocity gradients and internal work in fluid motion." *J. of the Boston Society of Civil Engineers*, 30(4), 219-237.
- Chandrasekar, S., Sorial, G. A., and Weaver, J. W. (2005). "Dispersant effectiveness on three oils under various simulated environmental conditions." *Environmental Engineering Science*, 22(3), 324-336.
- Chandrasekar, S., Sorial, G. A., and Weaver, J. W. (2006). "Dispersant effectiveness on oil spills - impact of salinity." *ICES Journal of Marine Science*, 63(8), 1418-1430.
- Chapman, H., Purnell, K., Law, R. J., and Kirby, M. F. (2007). "The use of chemical dispersants to combat oil spills at sea: A review of practice and research needs in Europe." *Marine Pollution Bulletin*, 54(7), 827-838.
- Couillard, C. M., Lee, K., Legare, B., and King, T. L. (2005). "Effect of dispersant on the composition of the water-accommodated fraction of crude oil and its toxicity to larval marine fish." *Environmental Toxicology and Chemistry*, 24(6), 1496-1504.
- Darling, P. S., Mackay, D., Mackay, N., and Brandvik, P. J. (1990). "Droplet size distributions in chemical dispersion of oil spills: toward a mathematical model." *Oil and Chemical Pollution*, 7(3), 173-198.
- Dean, R. G., and Dalrymple, R. A. (1984). *Water wave mechanics for engineers and scientists*. , Prentice-Hall, Inc., Englewood Cliffs, NJ.
- Delvigne, G. A. L., and Sweeney, C. E. (1988). "Natural dispersion of oil." *Oil and Chemical Pollution*, 4(4), 281-310.

Delvigne, G. A. L., Van del Stel, J. A., and Sweeney, C. E. (1987). "Measurements of vertical turbulent dispersion and diffusion of oil droplets and oil particles." *MMS 87-III*, US Department of the Interior, Minerals Management Service, Anchorage, Alaska.

Drennan, W. M., Donelan, M. A., Terray, E. A., and Katsaros, K. B. (1996). "Oceanic turbulence dissipation measurements in SWADE." *Journal of Physical Oceanography*, 26(5), 808-815.

EPA. (1996). "US Environmental Protection Agency (1996). Swirling flask dispersant effectiveness test. Title 40 code of federal regulations, part 300, Appendix C, Narragansett, R.I., 245-250."

Fingas, M. (2005). "Stability and resurfacing of dispersed oil. Prepared for Prince William Sound Regional Citizens' Advisory Council (PWSRCAC). Environmental Technology Center, Environment Canada."

Fingas, M., and Ka'aihue, L. "Dispersant tank testing - A review of procedures and considerations." *Environment Canada Arctic and Marine Oil Spill Program Technical Seminar (AMOP) Proceedings*, 1003-1016.

Fingas, M. F. (2000). "Use of surfactants for environmental applications." *Surfactants: Fundamentals and Applications to the Petroleum Industry*, L. L. Schramm, ed., Cambridge University Press, 461-539.

Fingas, M. F., Hughes, K. A., and Schweitzer, M. A. "Dispersant testing at the environmental emergencies technology division." *the 10th Arctic and Marine Oil Spill Program (AMOP) Technical Seminar*, Edmonton, Alberta, 343-356.

Fingas, M. F., Sigouin, L., Wang, Z., and Thouin, G. "Resurfacing of oil with time in the swirling flask." *The 25th Arctic and Marine Oil Spill Program (AMOP) Technical Seminar*, 773-783.

Funke, E. R., and Mansard, E. P. (1979). "SPLSH A program for the synthesis of episodic waves. Ottawa, Canada, Hydraulics laboratory technical report LTR-HY-65, National Research Council, Ottawa, Canada."

Hinze, J. O. (1955). "Fundamentals of the hydrodynamic mechanism of splitting in dispersion processes." *Journal of AICHE* 1, 289-295.

Hughes, S. A. (1990). *Physical models and laboratory techniques in coastal engineering*, World Scientific, New Jersey.

Jasper, W. L., Kim, T. L., and Wilson, M. P. (1978). "Droplet size distributions in a treated oil-water system." *Chemical Dispersants for the Control of Oil Spills*, ASTM STP 659, L. T. J. McCarthy, G. P. Lindblom, and H. F. Walter, eds., American Society for Testing and Materials, Philadelphia, PA, 203-216.

- Kaku, V. J., Boufadel, M. C., and Venosa, A. D. "Evaluation of mixing energy in the swirling and baffled flasks." *Third International Conference on Oil & Hydrocarbon Spills, Modelling, Analysis & Control*, Rhodes, Greece, 211-218.
- Kaku, V. J., Boufadel, M. C., Venosa, A. D., and Weaver, J. (2006a). "Flow dynamics in eccentrically rotating flasks used for dispersant effectiveness testing." *Environmental Fluid Mechanics*, 6(4), 385-406.
- Kaku, V. J., Boufadel, M. C., Venosa, A. D., and Weaver, J. W. (2006b). "Flow dynamics in eccentrically rotating flasks used for dispersant effectiveness testing." *Environmental Fluid Mechanics*, in press.
- Kepkay, P. E., Bugden, J. B. C., Lee, K., and Stoffyn-Egli, P. (2002). "Application of ultraviolet fluorescence spectroscopy to monitor oil-mineral aggregate formation." *Spill Science & Technology Bulletin*, 8(1), 101-108.
- Kirby, M. F., and Law, R. J. (2008). "Oil spill treatment products approval: The UK approach and potential application to the Gulf region." *Marine Pollution Bulletin*, 56(7), 1243-1247.
- Kolmogorov, A. N. (1949). "The local structure of turbulence in an incompressible fluid for very large Reynolds numbers." *Dokl. Akad. Nauk S.S.S.R.*, 30, 301-305.
- Kresta, S. M., and Wood, P. E. (1993). "The flow field produced by a pitched blade turbine: Characterization of the turbulence and estimation of the dissipation." *Chemical Engineering Science*, 48(10), 1761-1774.
- Lamarre, E., and Melville, W. K. (1991). "Air entrainment and dissipation in breaking waves." *Nature*, 351, 469-472.
- Lee, K. (2002). "Oil-particle interactions in aquatic environments: Influence on the transport, fate, effect and remediation of oil spills." *Spill Science & Technology Bulletin*, 8(1), 3-8.
- Lessard, R. R., and Demarco, G. (2000). "The significance of oil spill dispersants." *Spill Science & Technology Bulletin*, 6(1), 59-68.
- Lewis, A., Byford, D. C., and Laskey, P. R. "The significance of dispersed oil droplet size in determining dispersant effectiveness under various conditions." *International Oil Spill Conference*, 1985.
- Li, M., and Garrett, C. (1998). "The relationship between oil droplet size and upper ocean turbulence." *Marine Pollution Bulletin*, 36, 961-970.
- Li, Z., Lee, K., King, T., Boufadel, M. C., and Venosa, A. D. (2008a). "Assessment of chemical dispersant effectiveness in a wave tank under regular non-breaking and breaking wave conditions." *Marine Pollution Bulletin*, 56(5), 903-912.

- Li, Z., Lee, K., King, T., Boufadel, M. C., and Venosa, A. D. "Oil droplet size distribution as a function of energy dissipation rate in an experimental wave tank " *2008 International Oil Spill Conference*, Savannah, GA.
- Lunel, T. (1993). "Dispersion: Oil droplet size measurement at sea. In: Proceedings of the Sixteenth Arctic and Marine Oil Spill Program (AMOP) Technical Seminar, Calgary, Alberta, Canada. Environment Canada, Ottawa, Ontario, Canada. Pp. 1023-1056 ".
- Lunel, T. (1995). "Understanding the mechanism of dispersion through oil droplet size measurements at sea." *The Use of Chemicals in Oil Spill Response*, ASTM STP 1252, P. Lane, ed., American Society for Testing and Materials, Philadelphia, PA, 240-270.
- Ma, X., Cogswell, A., Li, Z., and Lee, K. (2008). "Particle size analysis of dispersed oil and oil-mineral aggregates with an automated ultraviolet epi-fluorescence microscopy system." *Environmental Technology*, 29(7), 739 - 748.
- Macnaughton, S. J., Swannell, R., Daniel, F., and Bristow, L. (2003). "Biodegradation of dispersed forties crude and alaskan North Slope oils in microcosms under simulated marine conditions." *Spill Science and Technology Bulletin*, 8(2), 179-186.
- Melville, W. K., Veron, F., and White, C. J. (2002). "The velocity field under breaking waves: coherent structures and turbulence." *Journal of Fluid Mechanics*, 454, 203-233.
- Moles, A., Holland, L., and Short, J. (2002). "Effectiveness in the laboratory of Corexit 9527 and 9500 in dispersing fresh, weathered, and emulsion of Alaska North Slope Crude Oil under subarctic conditions." *Spill Science and Technology Bulletin*, 7(5-6), 241-247.
- Monin, A. S., and A.M.Yalgom. (1971,1975). *Statistical Fluid Mechanics, Part I and II*, The MIT Press.
- Nilson, J., Naess, A., and Volent, Z. (1985). "Measurements of oil concentrations in the water column under breaking waves. Norwegian Hydrotechnical Laboratory, Report STF 60 A 85079, Trondheim, Norway."
- Nordvik, A. B. (1995). "The Technology Windows-of-Opportunity for Marine Oil-Spill Response as Related to Oil Weathering and Operations." *Spill Science & Technology Bulletin*, 2(1), 17-46.
- NRC. (1989). "*National Research Council: Using oil spill dispersant on the sea.*" National Academy Press, Washington D.C.
- NRC. (2005). *National Research Council: Understanding Oil Spill Dispersants: Efficacy and Effects*, National Academies Press, Washington, D.C.
- Phillips, O. M. (1977). *The Dynamics of the Upper Ocean*, Cambridge University Press.

Press, W. H., Teukolsky, S. A., Vetterling, W. T., and Flannery, B. P. (1992). *Numerical Recipes in Fortran 77*, Cambridge, Cambridge.

Ramachandran, S. D., Hodson, P. V., Khan, C. W., and Lee, K. (2004). "Oil dispersant increases PAH uptake by fish exposed to crude oil." *Ecotoxicology and Environmental Safety*, 59(3), 300-308.

Rao, M. A., and Brodkey, R. S. (1972). "Continuous Flow Stirred Tank Turbulence Parameters in a Stirred Mixer." *Chemical Engineering Science*, 27, 137-56.

Sanchez, M. C., Berjano, M., Guerrero, A., and Gallegos, C. (2001). "Emulsification rheokinetics of nonionic surfactant-stabilized oil-in-water emulsions." *Langmuir*, 17(18), 5410-5416.

Shaw, J. M. (2003). "A Microscopic View of Oil Slick Break-up and Emulsion Formation in Breaking Waves." *Spill Science & Technology Bulletin*, 8(5-6), 491-501.

Sorial, G. A., Venosa, A. D., Koran, K. M., Holder, E., and King, D. W. (2004a). "Oil spill dispersant effectiveness protocol. I: Impact of operational variables." *Journal of Environmental Engineering-ASCE*, 130(10), 1073-1084.

Sorial, G. A., Venosa, A. D., Koran, K. M., Holder, E., and King, D. W. (2004b). "Oil spill dispersant effectiveness protocol. II: Performance of revised protocol." *Journal of Environmental Engineering-ASCE*, 130(10), 1085-1093.

Srinivasan, R., Lu, Q., Sorial, G. A., Venosa, A. D., and Mullin, J. (2007). "Dispersant effectiveness of heavy fuel oils using baffled flask test." *Environmental Engineering Science*, 24(9), 1307-1320.

Swannell, R. P. J., and Daniel, F. (1999). "Effect of dispersants on oil biodegradation under simulated marine conditions." *International Oil Spill Conference*, 11.

Tennekes, H., and Lumley, J. L. (1972). *A First Course in Turbulence*, MIT Press, Cambridge, MA,.

Tennekes, H., and Lumley, J. L. (1999). *A First Course in Turbulence.*, MIT Press, Cambridge.

Terray, E. A., Donelan, M. A., Agrawal, Y. C., Drennan, W. M., Kahma, K. K., Williams, A. J., Hwang, P. A., and Kitaigorodskii, S. A. (1996). "Estimates of kinetic energy dissipation under breaking waves." *Journal of Physical Oceanography*, 26(5), 792-807.

Tkalich, P., and Chan, E. S. (2002). "Vertical mixing of oil droplets by breaking waves." *Marine Pollution Bulletin*, 44(11), 1219-1229.

Tsouris, C., and Tavlarides, L. L. (1994). "Breakage and coalescence models for drops in turbulent dispersions." *AIChE Journal*, 40(3), 395-406.

Venosa, A. D., King, D. W., and Sorial, G. A. (2002). "The baffled flask test for dispersant effectiveness: A round robin evaluation of reproducibility and repeatability." *Spill Science & Technology Bulletin*, 7(5-6), 299-308.

Venosa, A. D., Lee, K., Boufadel, M. C., Li, Z., King, T., and Wickley-Olsen, E. "Dispersant effectiveness as a function of energy dissipation rate in an experimental wave tank " *2008 International Oil Spill Conference*, Savannah, GA.

White, D. M., Ask, I., and Behr-Andres, C. (2002). "Laboratory study on dispersant effectiveness in Alaskan seawater." *Journal of Cold Regions Engineering*, 16(1), 17-27.

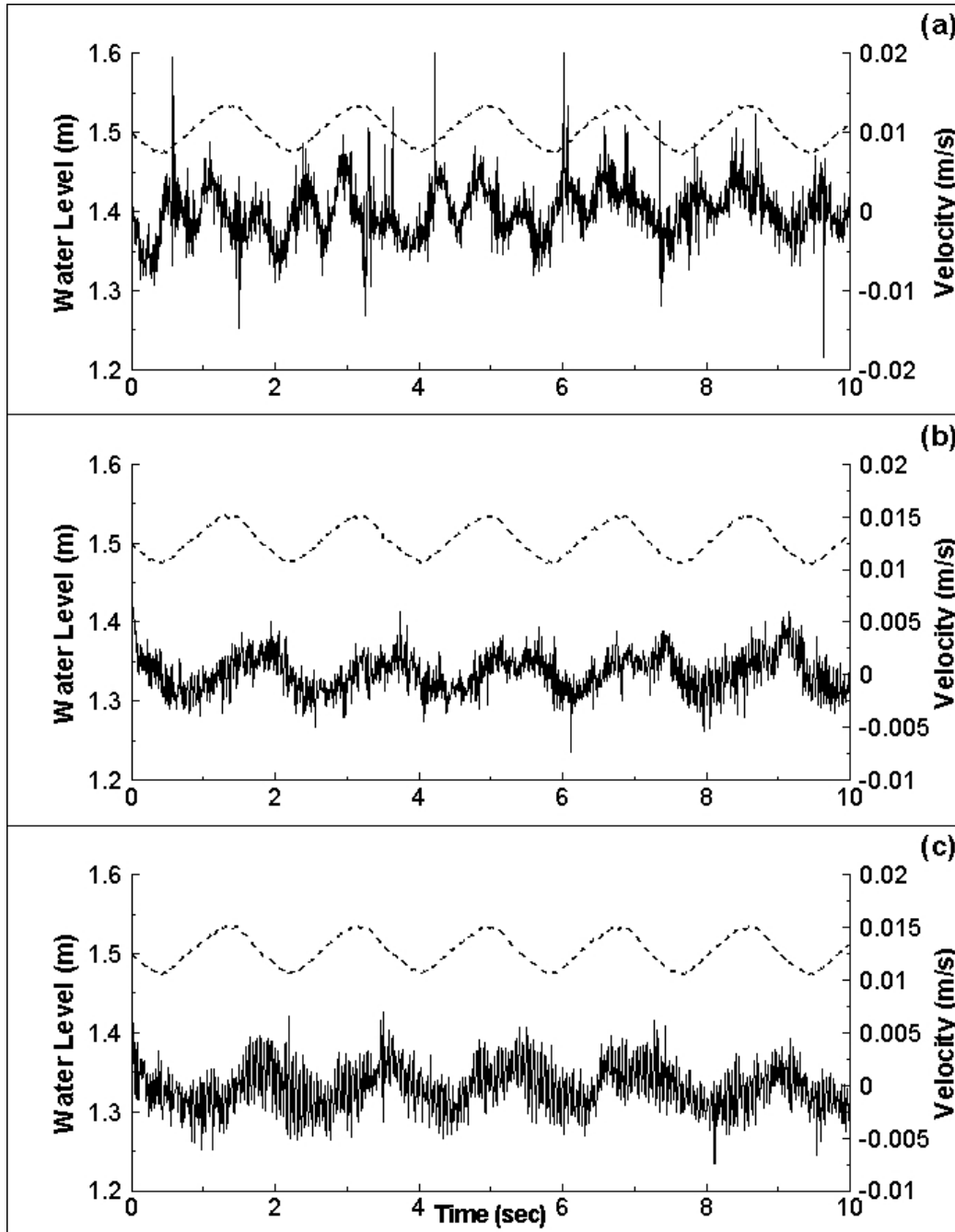
Wickley-Olsen, E., Boufadel, M. C., King, T., Li, Z., Lee, K., and Venosa, A. D. "Regular and Breaking Waves in Wave Tank for Dispersion Effectiveness Testing." *2008 International Oil Spill Conference* Savannah, GA.

Wu, H., and Patterson, G. K. (1989). "Laser-Doppler measurements of turbulent-flow parameters in a stirred mixer." *Chemical Engineering Science*, 44(10), 2207-2221.

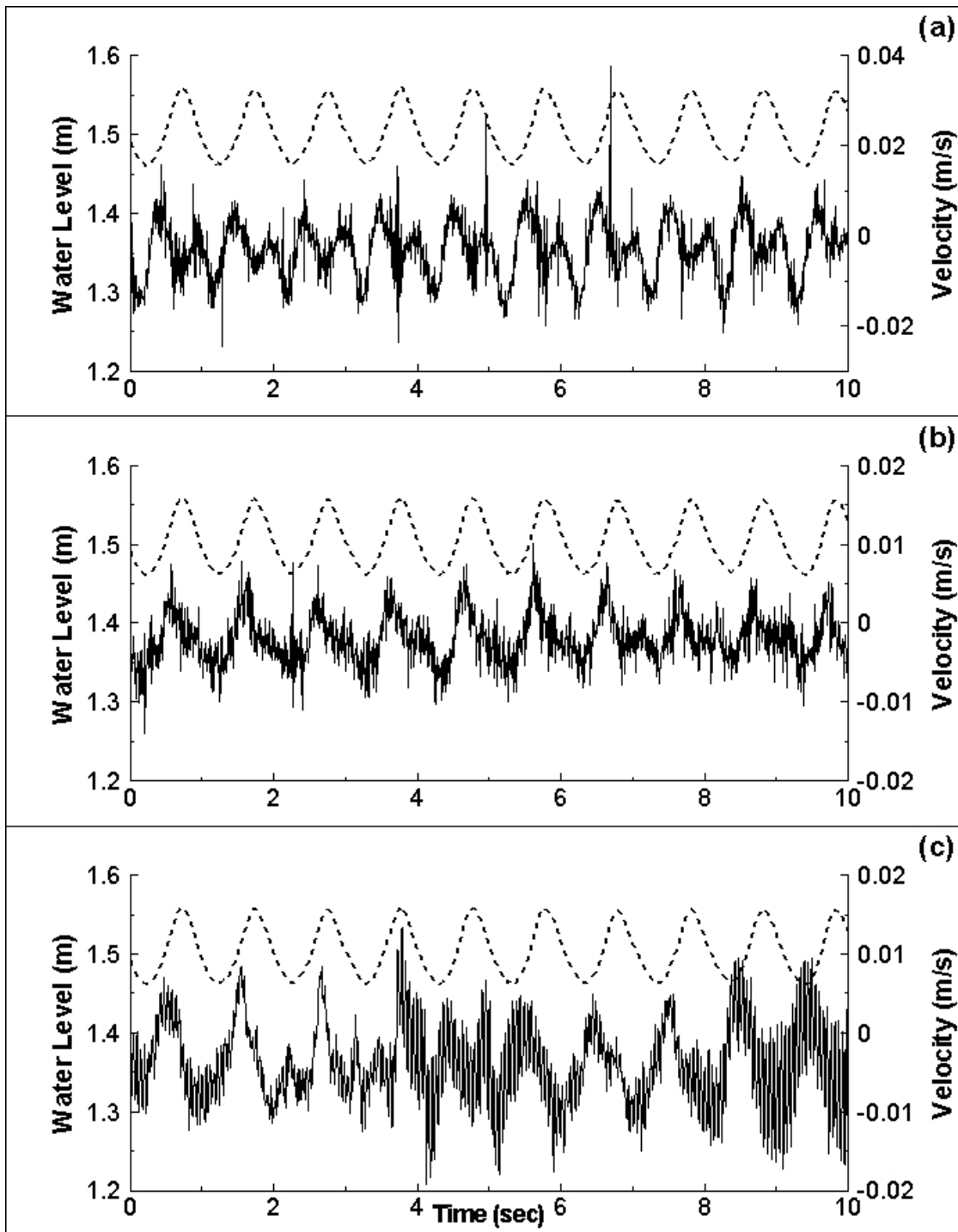
Wu, H., Patterson, G. K., and Doorn, M. v. (1989). "Distribution of Turbulence Energy Dissipation Rates in a Rushton Turbine Stirred Mixer." *Experiments in Fluids*, 8, 153-60.

Appendices

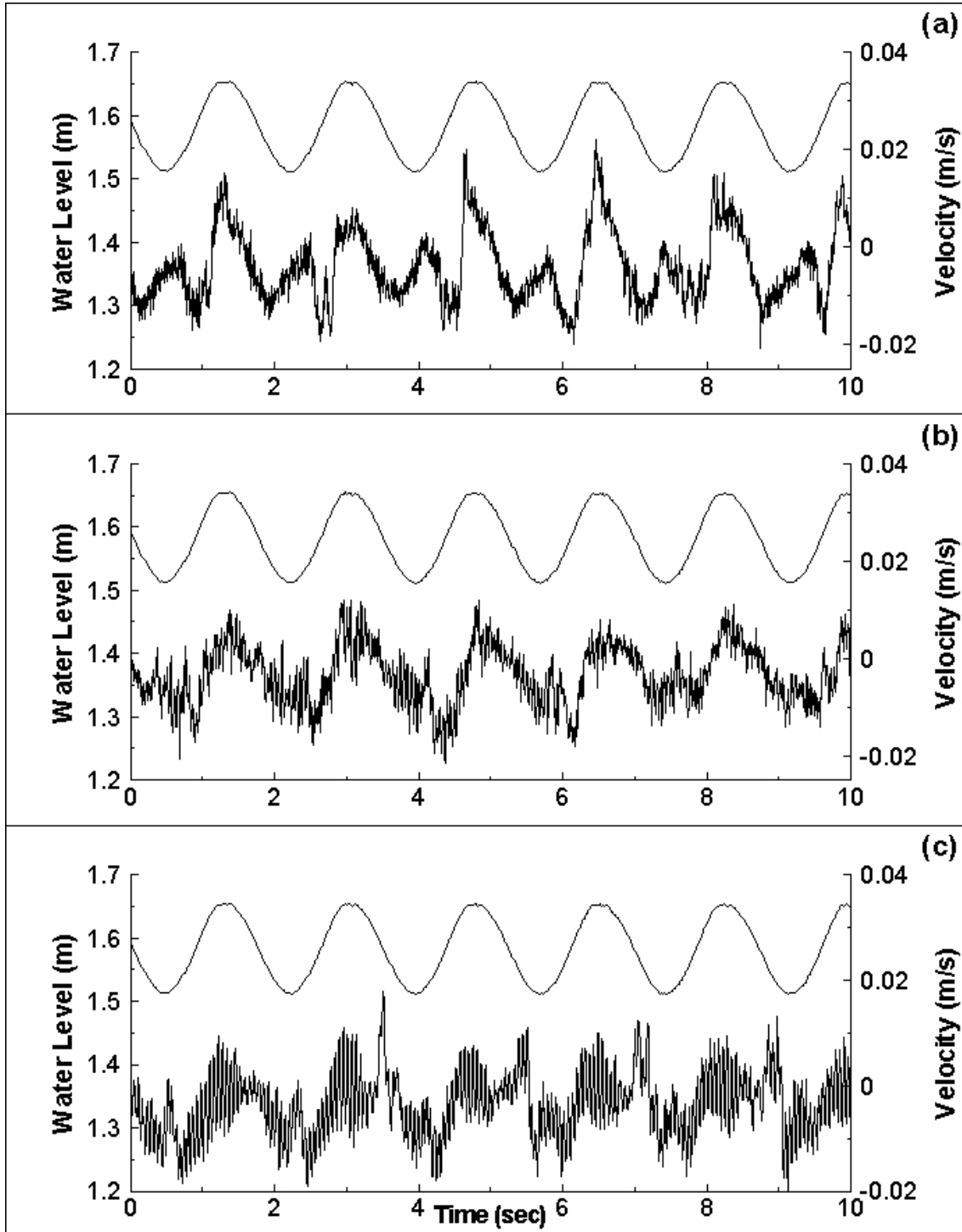
Appendix A1: Velocity series for across tank component “v” of low frequency waves generated with a 7 cm stroke at depths of (a) 10.7 cm, (b) 23.3 cm, and (c) 33.3 cm. Also shown by the dashed line is the water level for each series.



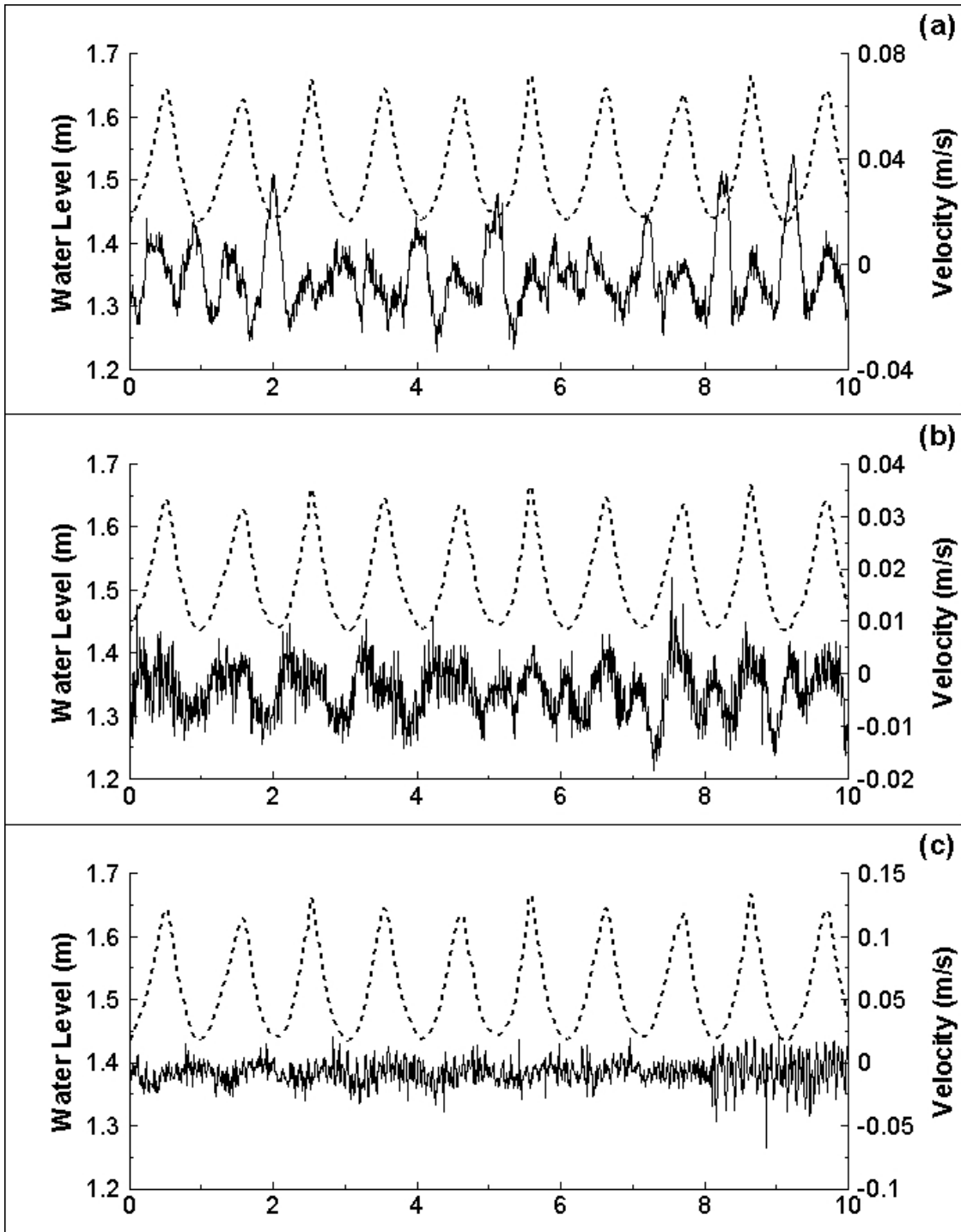
Appendix A2: Velocity series for across tank component “v” of high frequency waves generated with a 7 cm stroke at depths of (a) 10.7 cm, (b) 23.3 cm, and (c) 33.3 cm. Also shown by the dashed line is the water level for each series.



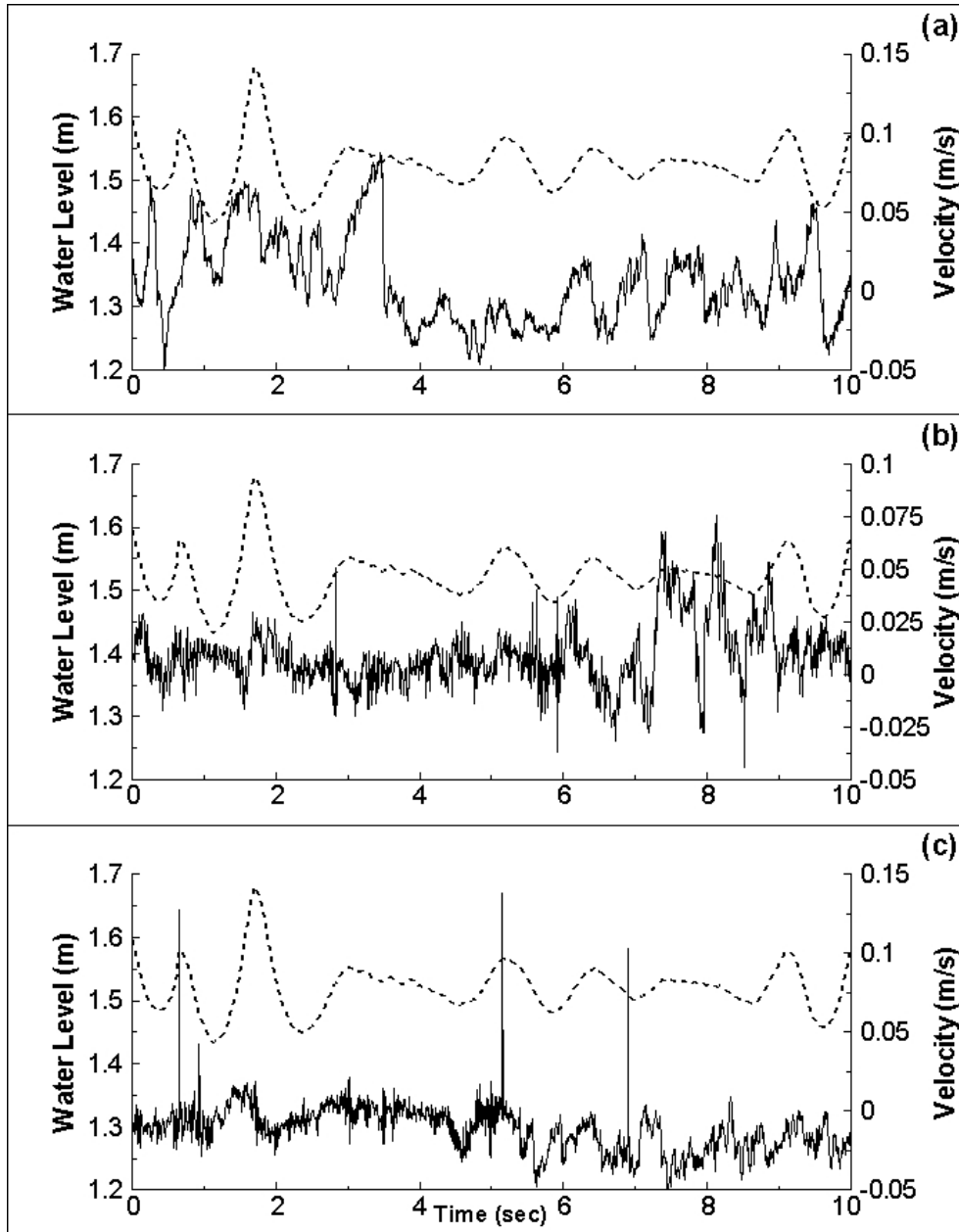
Appendix A3: Velocity series for across tank component “v” of low frequency waves generated with a 12 cm stroke at depths of (a) 13.3 cm, (b) 27.3 cm, and (c) 39.3 cm. Also shown by the dashed line is the water level for each series.



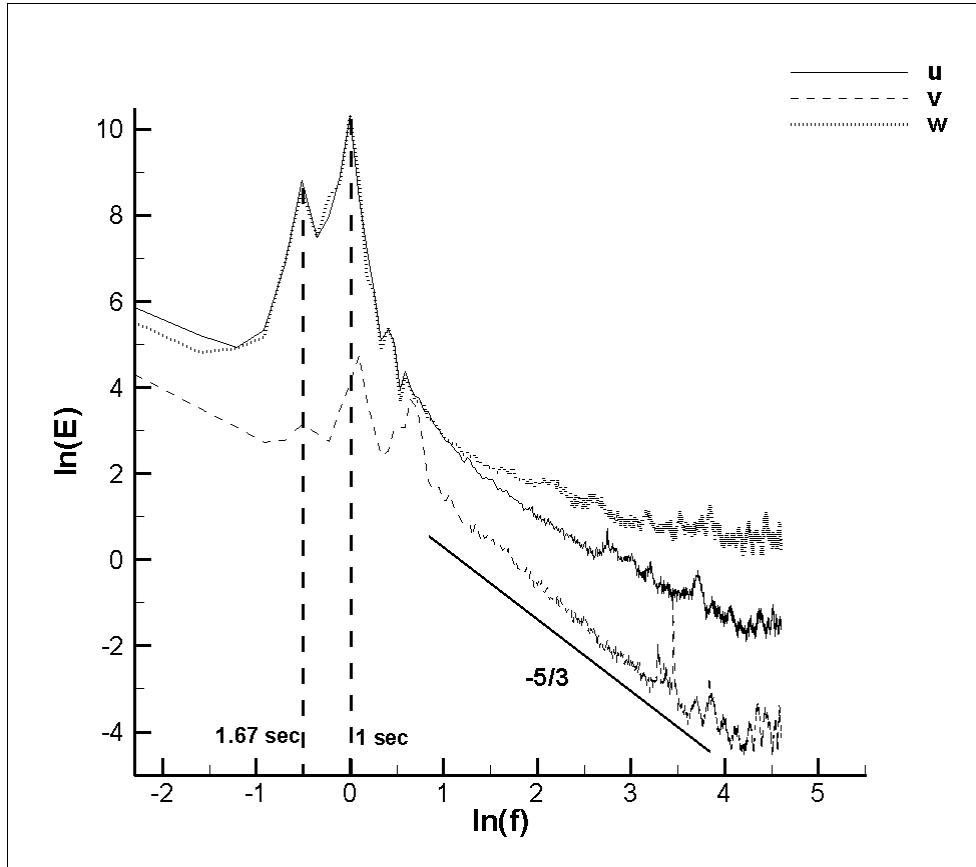
Appendix A4: Velocity series for across tank component “v” of high frequency waves generated with a 12 cm stroke at depths of (a) 13.3 cm, (b) 27.3 cm, and (c) 39.3 cm. Also shown by the dashed line is the water level for each series.



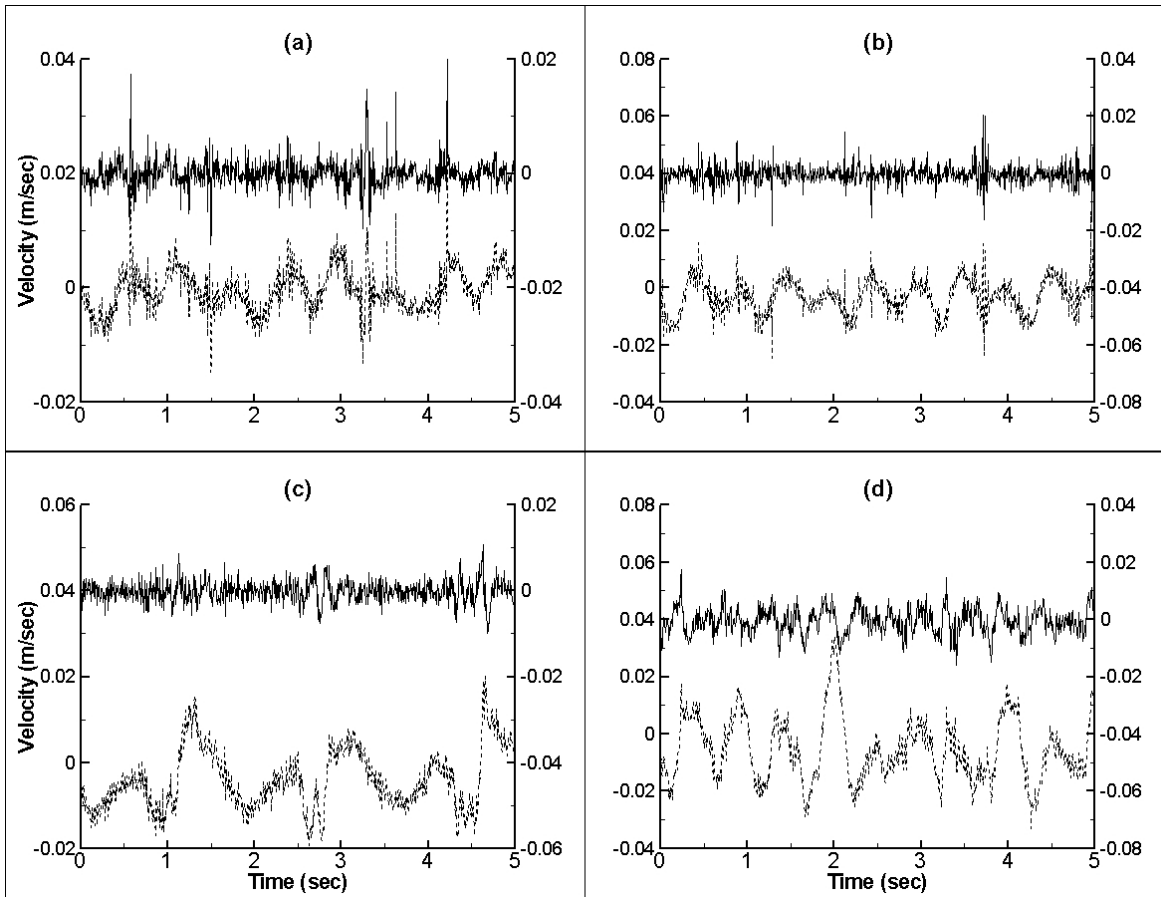
Appendix A5: Velocity series for across tank component “v” plunging breaking waves generated with a 12 cm stroke at depths of (a) 13.3 cm, (b) 27.3 cm and (c) 39.3 cm. Also shown by the dashed line is the water level for each series. The breaker occurred at 13.54 m from the flap.



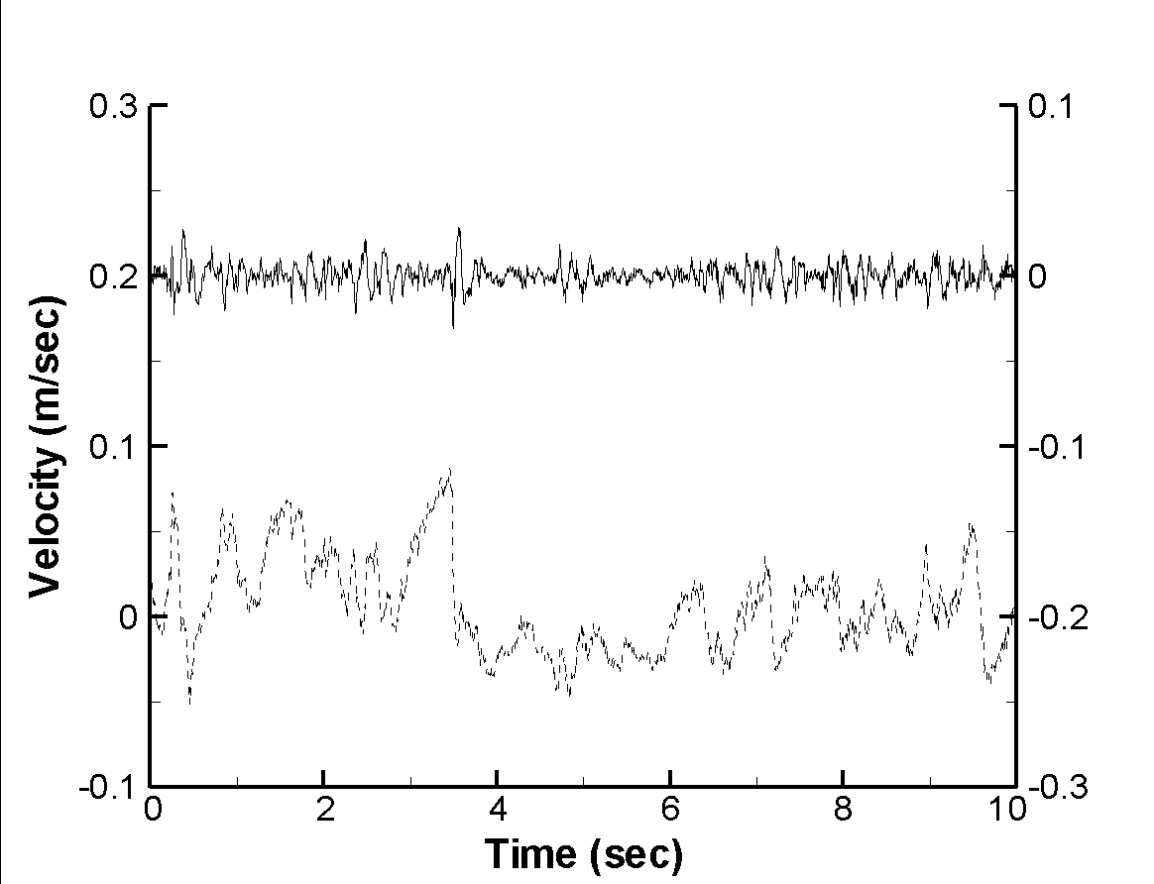
Appendix A6: Three component velocity spectra for the plunging breaking waves at a depth of 13.3 cm. The dominant frequencies of the system ($= 1/\Delta t$) are displayed. The Nyquist ($f/2$) frequency for the ADV sensor is $(200 \text{ Hz} / 2) = 100 \text{ Hz}$.



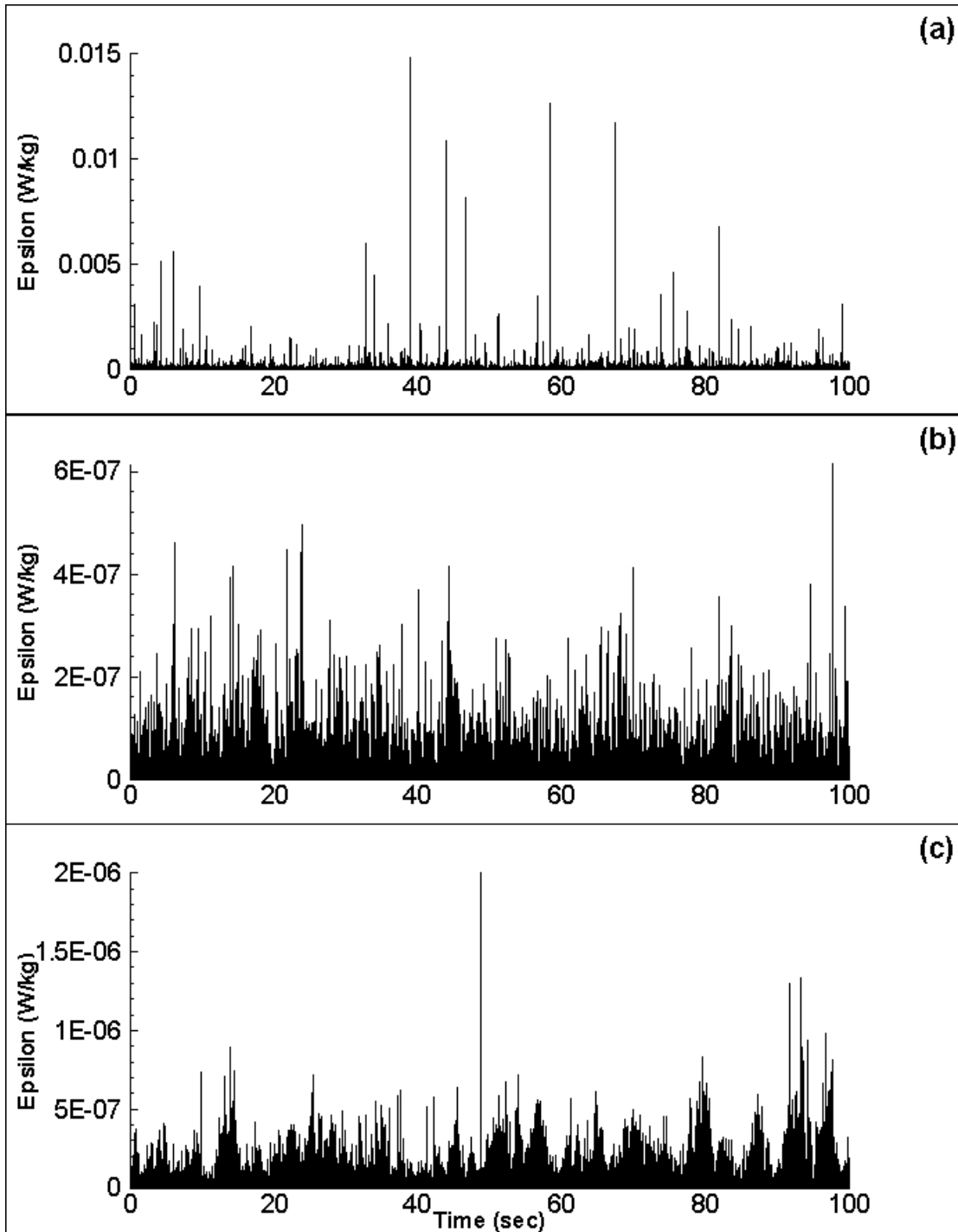
Appendix A7: Series for filtered across tank velocity “v” for (a) LF 7 cm stroke, (b) HF 7 cm stroke, (c) LF 12 cm stroke and (d) HF 12 cm stroke. Also shown (dashed) is the original velocity. Series are centered on their respective zeros.



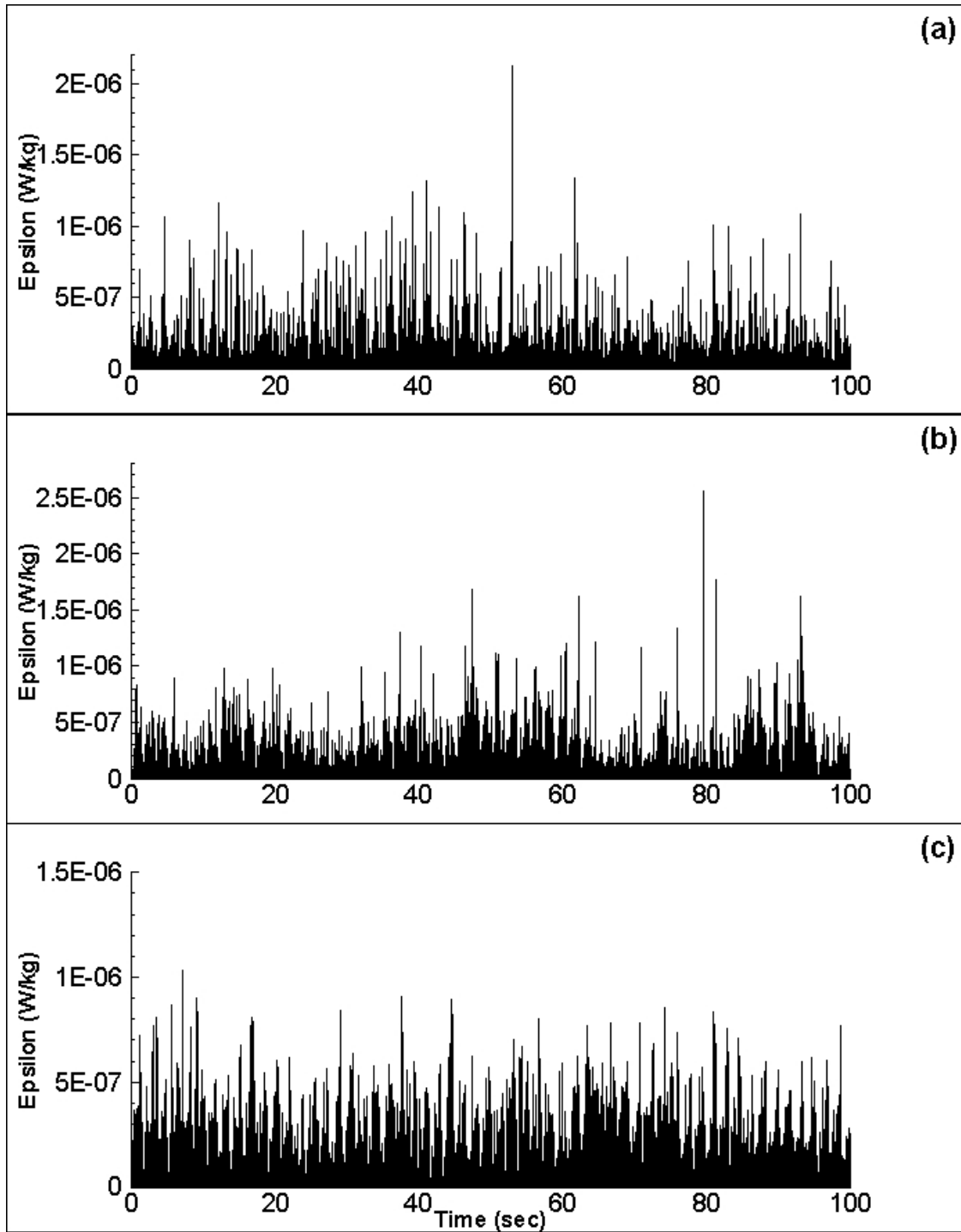
Appendix A8: Series for filtered across tank velocity “v” for the plunging breaker. Also shown (dashed) is the original velocity. Series are centered around their respective zeros.



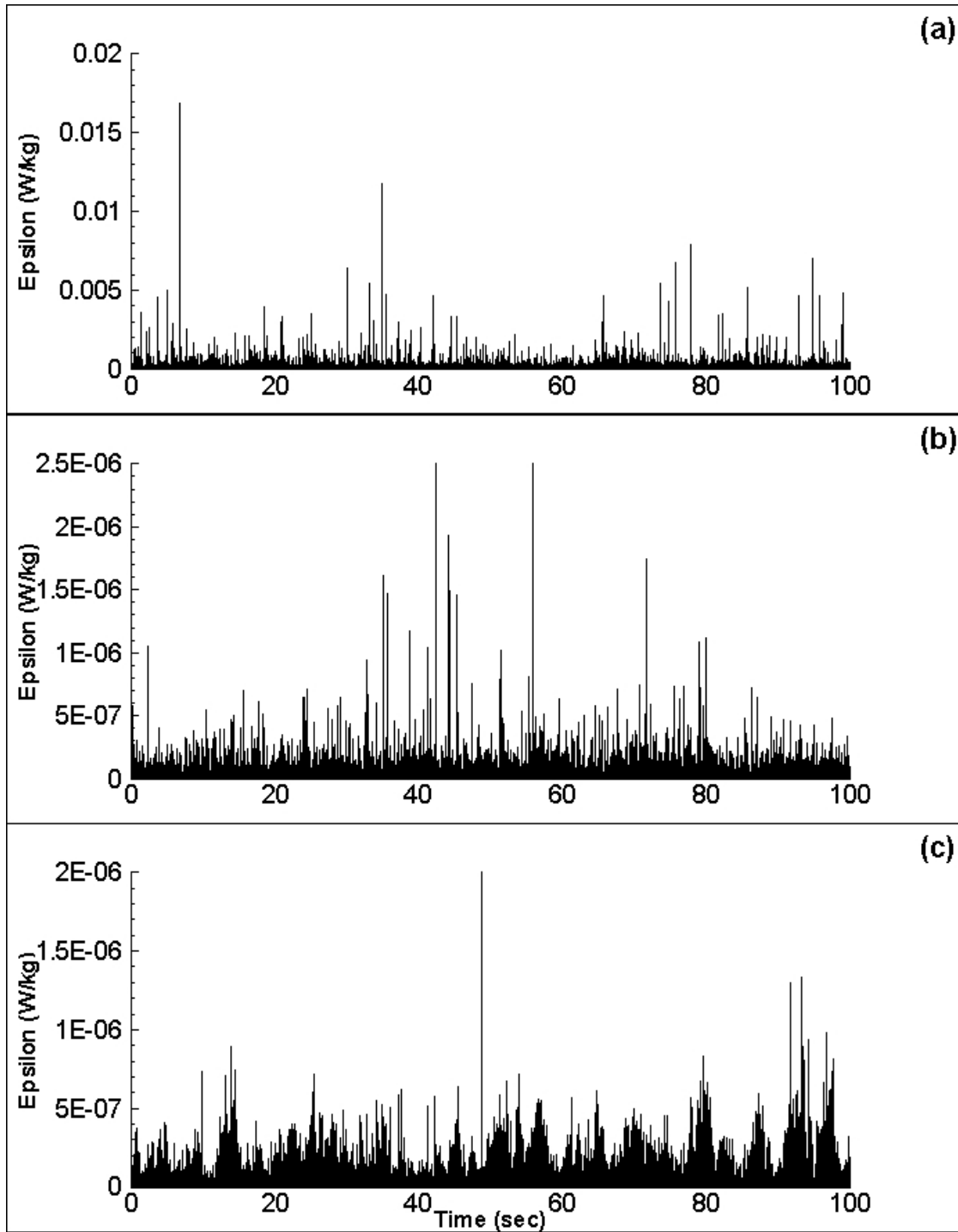
Appendix A9: Energy dissipation rates calculated over the regular wave low frequency (LF) 7 cm stroke data set for depth of (a) 10.7 cm, (b) 23.3 cm and (c) 33.3 cm.



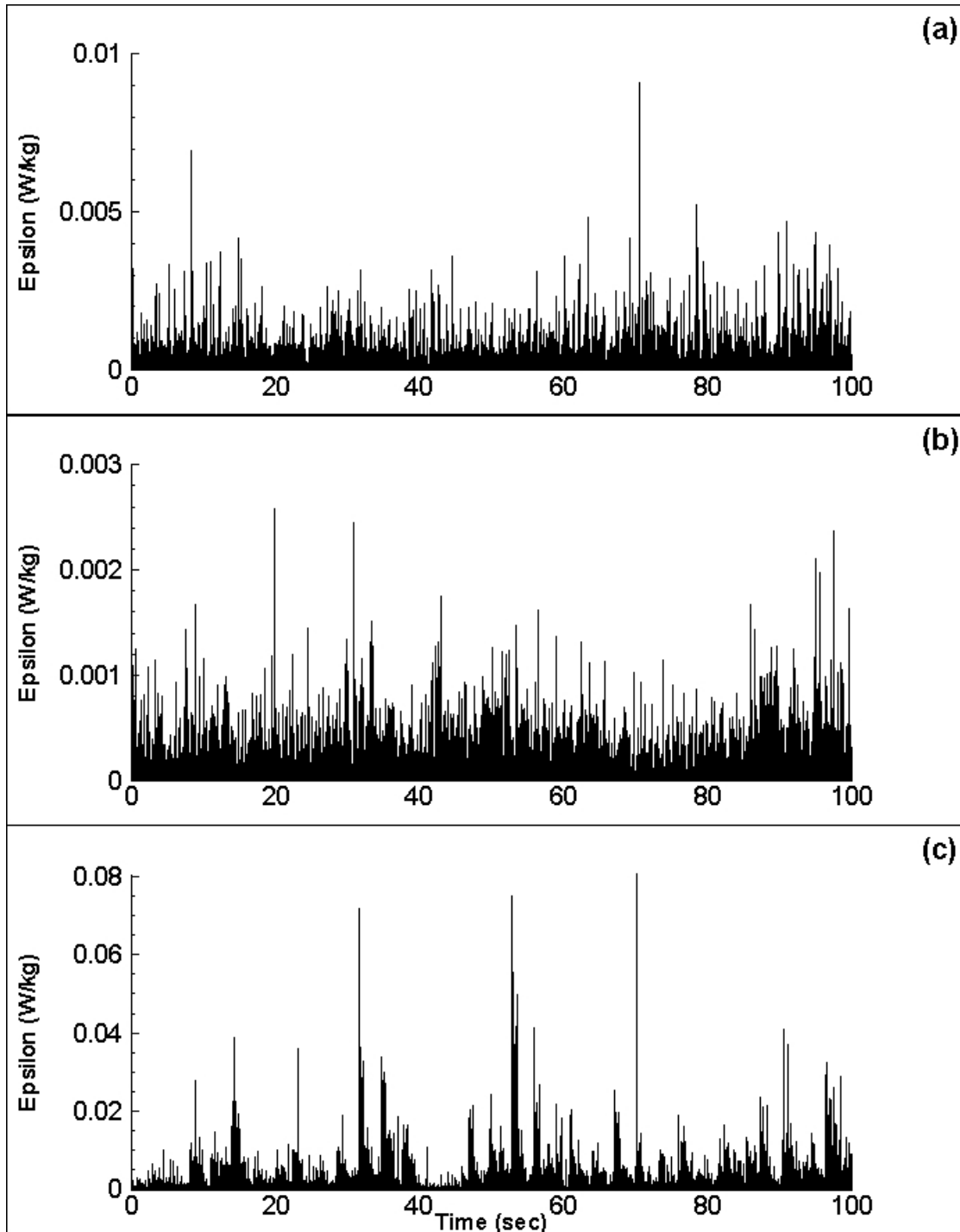
Appendix A10: Energy dissipation rates calculated over the regular wave low frequency (LF) 12 cm stroke data set for depths of (a) 13.3 cm, (b) 27.3 cm, and (c) 39.3 cm.



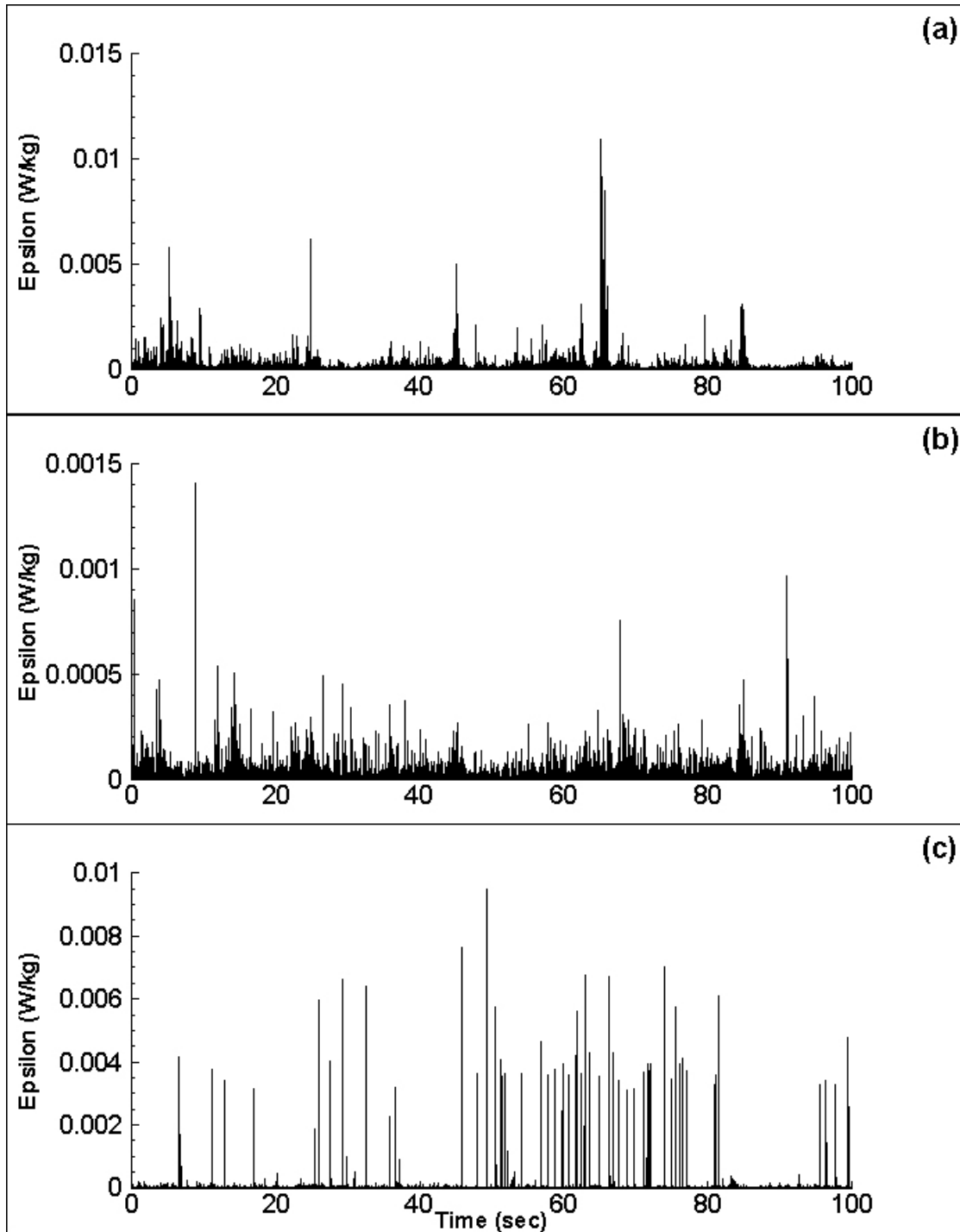
Appendix A11: Energy dissipation rates calculated over the regular wave high frequency (HF) 7 cm stroke data set for depth of (a) 10.7 cm, (b) 23.3 cm and (c) 33.3 cm.



Appendix A12: Energy dissipation rates calculated over the regular wave high frequency (HF) 12 cm stroke data set for depths of (a) 13.3 cm, (b) 27.3 cm, and (c) 39.3 cm.



Appendix A13: Energy dissipation rates calculated over the plunging breaker, 12 cm stroke data set for depth of (a) 6 cm, (b) 21.21 cm and (c) 41.49 cm.



**Appendix A14: Average temperature-response fluorometer results of ANS crude oil
Light Scattering (660nm)**

Description		Run #1	Run #2	Run #3	Average	Std. Dev.	% RSD
21°C	1000 ppb	48	40	58	49	9.0	19
	2500 ppb	88	97	102	96	7.1	7.4
	5000 ppb	208	198	215	207	8.6	4.1
	10000 ppb	401	433	474	436	36	8.3
	50000 ppb	1527	1537	1619	1561	50	3.2
12°C	1000 ppb	60	61	54	58	3.8	6.5
	2500 ppb	85	94	89	89	4.5	5.0
	5000 ppb	201	218	204	208	9.1	4.4
	10000 ppb	436	474	466	459	20	4.4
	50000 ppb	1678	1658	1645	1660	17	1.0
5°C	1000 ppb	43	42	52	46	5.4	12
	2500 ppb	92	82	92	89	5.8	6.5
	5000 ppb	198	186	201	195	7.9	4.0
	10000 ppb	423	407	432	421	13	3.0
	50000 ppb	1625	1700	1673	1666	38	2.3

Chlorophyll (ex470/em695)

Description		Run #1	Run #2	Run #3	Average	Std. Dev.	% RSD
21°C	1000 ppb	24	26	20	23	3.1	13
	2500 ppb	119	124	118	120	3.2	2.7
	5000 ppb	305	298	280	294	13	4.4
	10000 ppb	570	579	581	577	5.9	1.0
	50000 ppb	3440	3526	3530	3499	51	1.5
12°C	1000 ppb	28	30	21	26	4.7	18
	2500 ppb	168	187	182	179	10	5.5
	5000 ppb	381	403	394	393	11	2.8
	10000 ppb	766	759	763	763	3.5	0.5
	50000 ppb	3702	3787	3779	3756	47	1.2
5°C	1000 ppb	35	27	38	33	5.7	17
	2500 ppb	187	176	174	179	7.0	3.9
	5000 ppb	350	407	422	393	38	10
	10000 ppb	723	758	758	746	20	2.7
	50000 ppb	3786	3813	3836	3812	25	0.7

CDOM (ex370/em460)

Description		Run #1	Run #2	Run #3	Average	Std. Dev.	% RSD
21°C	1000 ppb	24	20	27	24	3.5	15
	2500 ppb	134	127	148	136	11	7.8
	5000 ppb	274	274	289	279	8.6	3.1
	10000 ppb	476	476	497	483	12	2.5
	50000 ppb	1508	1481	1525	1505	22	1.5
12°C	1000 ppb	20	24	20	21	2.3	11
	2500 ppb	162	162	160	161	1.2	0.7
	5000 ppb	279	285	284	283	3.2	1.1
	10000 ppb	467	456	461	461	5.5	1.2
	50000 ppb	1669	1650	1714	1678	33	2.0
5°C	1000 ppb	23	18	24	22	3.2	15
	2500 ppb	191	168	201	187	17	9.1
	5000 ppb	272	248	280	267	17	6.3
	10000 ppb	445	424	458	442	17	3.9
	50000 ppb	1661	1708	1691	1687	24	1.4

**Appendix A15: Average temperature-response fluoremeter results of MESA crude oil
Light Scattering (660nm)**

Description		Run #1	Run #2	Run #3	Average	Std. Dev.	% RSD
21°C	1000 ppb	18	25	22	22	3.5	16
	2500 ppb	65	75	71	70	5.0	7.2
	5000 ppb	157	154	155	155	1.5	1.0
	10000 ppb	325	306	332	321	13	4.2
	50000 ppb	1442	1421	1321	1395	65	4.6
12°C	1000 ppb	30	29	27	29	1.5	5.3
	2500 ppb	75	86	82	81	5.6	6.9
	5000 ppb	155	128	143	142	14	9.5
	10000 ppb	322	329	308	320	11	3.3
	50000 ppb	1558	1588	1571	1572	15	1.0
5°C	1000 ppb	31	31	24	29	3.9	14
	2500 ppb	68	62	61	64	3.7	5.8
	5000 ppb	114	126	128	123	7.5	6.1
	10000 ppb	333	346	346	342	7.3	2.1
	50000 ppb	1573	1522	1503	1533	36	2.3

Chlorophyll (ex470/em695)

Description		Run #1	Run #2	Run #3	Average	Std. Dev.	% RSD
21°C	1000 ppb	25	22	28	25	3.0	12
	2500 ppb	79	102	87	89	12	13
	5000 ppb	254	245	248	249	4.6	1.8
	10000 ppb	513	501	489	501	12	2.4
	50000 ppb	3384	3331	3307	3341	39	1.2
12°C	1000 ppb	30	41	32	34	5.9	17
	2500 ppb	135	109	134	126	15	12
	5000 ppb	240	295	266	267	28	10
	10000 ppb	578	609	590	592	16	2.6
	50000 ppb	3503	3620	3588	3570	60	1.7
5°C	1000 ppb	38	28	39	35	6.1	17
	2500 ppb	125	128	118	124	5.1	4.1
	5000 ppb	247	245	250	247	2.5	1.0
	10000 ppb	610	588	593	597	12	1.9
	50000 ppb	3601	3662	3399	3554	138	3.9

CDOM (ex370/em460)

Description		Run #1	Run #2	Run #3	Average	Std. Dev.	% RSD
21°C	1000 ppm	89	71	81	80	9.1	11
	2500 ppm	158	149	176	161	14	8.6
	5000 ppm	212	181	235	209	27	13
	10000 ppm	322	282	351	318	35	11
	50000 ppm	1394	1506	1436	1445	57	3.9
12°C	1000 ppm	103	107	119	110	8.3	7.6
	2500 ppm	162	192	207	187	23	12
	5000 ppm	249	236	255	247	9.7	3.9
	10000 ppm	458	447	453	453	5.5	1.2
	50000 ppm	1460	1441	1506	1469	33	2.3
5°C	1000 ppm	140	145	141	142	2.7	1.9
	2500 ppm	224	217	232	224	7.5	3.3
	5000 ppm	312	310	310	311	1.1	0.4
	10000 ppm	473	589	530	531	58	11
	50000 ppm	1421	1480	1520	1474	50	3.4

Appendix A16: Average background-subtracted turbidity-response fluorometer results of ANS Crude Oil

Light Scattering (660nm)

Description		Run #1	Run #2	Run #3	Average	Std. Dev.	% RSD
< 2 NTU	1000 ppb	48	43	50	47	3.6	7.7
	2500 ppb	82	77	87	82	5.0	6.1
	5000 ppb	162	145	178	162	17	10
	10000 ppb	351	334	367	351	17	4.7
	50000 ppb	1308	1274	1325	1302	26	2.0
40 NTU	1000 ppb	15	13	18	15	2.5	16
	2500 ppb	30	26	35	30	4.5	15
	5000 ppb	64	52	71	62	10	15
	10000 ppb	194	177	205	192	14	7.3
	50000 ppb	369	349	386	368	19	5.0
200 NTU	1000 ppb	12	10	14	12	2.0	17
	2500 ppb	24	20	26	23	3.1	13
	5000 ppb	50	39	58	49	10	19
	10000 ppb	209	189	221	206	16	7.8
	50000 ppb	420	396	433	416	19	4.5

Chlorophyll (ex470/em695)

Description		Run #1	Run #2	Run #3	Average	Std. Dev.	% RSD
< 2 NTU	1000 ppb	20	20	16	19	2.3	12
	2500 ppb	90	75	91	85	9.0	11
	5000 ppb	260	193	221	225	34	15
	10000 ppb	606	552	629	596	40	6.6
	50000 ppb	3670	3579	3697	3649	62	1.7
40 NTU	1000 ppb	21	25	29	25	4.0	16
	2500 ppb	121	105	103	110	9.9	9.0
	5000 ppb	221	199	201	207	12	5.9
	10000 ppb	346	319	409	358	46	13
	50000 ppb	1620	1635	1729	1661	59	3.6
200 NTU	1000 ppb	21	17	22	20	2.6	13
	2500 ppb	86	95	103	95	8.5	9.0
	5000 ppb	189	168	212	190	22	12
	10000 ppb	356	365	411	377	30	7.8
	50000 ppb	1531	1503	1453	1496	40	2.6

CDOM (ex370/em460)

Description		Run #1	Run #2	Run #3	Average	Std. Dev.	% RSD
< 2 NTU	1000 ppb	36	34	47	39	7.0	18
	2500 ppb	70	65	85	73	10	14
	5000 ppb	200	182	223	202	21	10
	10000 ppb	391	378	441	403	33	8.2
	50000 ppb	1163	1088	1194	1148	55	4.7
40 NTU	1000 ppb	17	12	16	15	2.6	18
	2500 ppb	40	30	40	37	5.8	16
	5000 ppb	77	64	80	74	8.5	12
	10000 ppb	200	180	213	198	17	8.4
	50000 ppb	455	418	473	449	28	6.2
200 NTU	1000 ppb	6	7	8	7	1.0	14
	2500 ppb	17	16	20	18	2.1	12
	5000 ppb	42	38	53	44	7.8	18
	10000 ppb	97	88	111	99	12	12
	50000 ppb	320	295	348	321	27	8.3

Appendix A17: Average background-subtracted turbidity-response fluorometer results of MESA Crude Oil

Light Scattering (660nm)

Description		Run #1	Run #2	Run #3	Average	Std. Dev.	% RSD
< 2 NTU	1000 ppb	43	53	50	49	5.1	11
	2500 ppb	73	78	70	74	4.0	5.5
	5000 ppb	146	154	159	153	6.6	4.3
	10000 ppb	413	407	415	412	4.2	1.0
	50000 ppb	1389	1409	1484	1427	50	3.5
40 NTU	1000 ppb	21	24	24	23	1.7	7.5
	2500 ppb	36	35	30	34	3.2	10
	5000 ppb	65	71	75	70	5.0	7.2
	10000 ppb	187	179	194	187	7.5	4.0
	50000 ppb	333	313	344	330	16	4.8
200 NTU	1000 ppb	23	32	28	28	4.5	16
	2500 ppb	34	39	39	37	2.9	7.7
	5000 ppb	66	63	61	63	2.5	4.0
	10000 ppb	204	196	219	206	12	5.7
	50000 ppb	414	399	446	420	24	5.7

Chlorophyll (ex470/em695)

Description		Run #1	Run #2	Run #3	Average	Std. Dev.	% RSD
< 2 NTU	1000 ppb	62	62	61	62	0.6	0.9
	2500 ppb	151	164	183	166	16	9.7
	5000 ppb	358	315	348	340	23	6.6
	10000 ppb	650	617	640	636	17	2.7
	50000 ppb	3296	3221	3133	3217	82	2.5
40 NTU	1000 ppb	73	57	83	71	13	18
	2500 ppb	96	75	107	93	16	18
	5000 ppb	133	109	147	130	19	15
	10000 ppb	256	225	280	254	28	11
	50000 ppb	1511	1463	1540	1505	39	2.6
200 NTU	1000 ppb	25	21	31	26	5.0	20
	2500 ppb	46	34	44	41	6.4	16
	5000 ppb	71	62	72	68	5.5	8.1
	10000 ppb	186	189	230	202	25	12
	50000 ppb	1349	1299	1367	1338	35	2.6

CDOM (ex370/em460)

Description		Run #1	Run #2	Run #3	Average	Std. Dev.	% RSD
< 2 NTU	1000 ppb	97	107	122	109	13	12
	2500 ppb	185	195	216	199	16	8.0
	5000 ppb	278	299	320	299	21	7.0
	10000 ppb	494	523	548	522	27	5.2
	50000 ppb	1514	1401	1400	1438	66	4.6
40 NTU	1000 ppb	27	31	36	31	4.5	14
	2500 ppb	54	42	45	47	6.2	13
	5000 ppb	88	77	82	82	5.5	6.7
	10000 ppb	204	192	217	204	13	6.1
	50000 ppb	428	385	414	409	22	5.4
200 NTU	1000 ppb	41	39	41	40	1.2	2.9
	2500 ppb	60	68	77	68	8.5	12
	5000 ppb	79	92	88	86	6.7	7.7
	10000 ppb	128	138	152	139	12	8.7
	50000 ppb	331	350	360	347	15	4.2